UNIVERSIDADE DE SÃO PAULO

Faculdade de Ciências Farmacêuticas

Programa de Pós-Graduação em Farmácia (Fisiopatologia e Toxicologia)

Área de Fisiopatologia

Application of CRISPR-Cas9 to interrogate novel gene functions in cutaneous melanoma

LARISSA SATIKO ALCANTARA SEKIMOTO MATSUYAMA

Tese apresentada à Faculdade de Ciências Farmacêuticas da Universidade de São Paulo para obtenção do título de DOUTOR EM CIÊNCIAS

Orientadora: Profa. Dra. Silvya Stuchi Maria-Engler

Co-orientadora: Profa. Dra. Patricia Abrão Possik

São Paulo

2021

UNIVERSIDADE DE SÃO PAULO

Faculdade de Ciências Farmacêuticas

Programa de Pós-Graduação em Farmácia (Fisiopatologia e Toxicologia)

Área de Fisiopatologia

Application of CRISPR-Cas9 to interrogate novel gene functions in cutaneous melanoma

LARISSA SATIKO ALCANTARA SEKIMOTO MATSUYAMA

Versão corrigida da Tese conforme resolução CoPGr 6018

Tese apresentada à Faculdade de Ciências Farmacêuticas da Universidade de São Paulo para obtenção do título de DOUTOR EM CIÊNCIAS

Orientadora: Profa. Dra. Silvya Stuchi Maria-Engler

Co-orientadora: Profa. Dra. Patricia Abrão Possik

São Paulo

2021

Ficha Catalográfica elaborada eletronicamente pelo autor, utilizando o programa desenvolvido pela Seção Técnica de Informática do ICMC/USP e adaptado para a Divisão de Biblioteca e Documentação do Conjunto das Químicas da USP

Bibliotecária responsável pela orientação de catalogação da publicação:
Marlene Aparecida Vieira - CRB - 8/5562

M434a

Matsuyama, Larissa Satiko Alcântara Sekimoto
Application of CRISPR-Cas9 to interrogate novel gene functions in cutaneous melanoma / Larissa Satiko Alcântara Sekimoto Matsuyama. - São Paulo, 2021.
155 p.

Tese (doutorado) - Faculdade de Ciências Farmacêuticas da Universidade de São Paulo. Departamento de Análises Clínicas e Toxicológicas.
Orientador: Maria-Engler, Silvya Stuchi
Coorientador: Possik, Patricia Abrão

1. Melanoma. 2. SIN3B. 3. IRF4. 4. CRISPR-Cas9. I. T. II. Maria-Engler, Silvya Stuchi, orientador. III. Possik, Patricia Abrão, coorientador.

Larissa Satiko Alcântara Sekimoto Matsuyama

Application of CRISPR-Cas9 to interrogate novel gene functions in cutaneous melanoma

Comissão Julgadora

da

Tese para obtenção do Título de Doutor

Prof. Dr.

Orientador/Presidente

_____

1° examinador

_____

2° examinador

_____

3° examinador

_____

4° examinador

São Paulo, _____ de _____ de 2021.

I would like to dedicate this thesis to my parents, Robilson and Celia, my brother Yuri, and my husband Bruno, for being my inspiration and always encouraging me to do my best at all times.

ACKNOWLEDGEMENTS

When I first started the whole process towards obtaining my PhD degree, I totally underestimated how challenging it would be, both personally and scientifically. Nonetheless, it was a fulfilling journey which allowed me to continue pursuing a scientific career. I would like to take this opportunity to thank everybody who supported me and contributed to this work.

First, I would like to thank my supervisor Silvya, for giving me the opportunity of concluding my PhD, also for your guidance and support throughout the years. I would also like to thank my co-supervisor Patricia, for all advice and patience when answering my endless questions. I began the CRISPR journey because of you.

To everyone in Skin Biology group, for your welcome and project discussions. Special thanks to Silvia Berlanga and Silvia Romano for advice on experimental work. Denisse, my IC Juliana and Daniele, who unfortunately already left the lab, for the laughter and friendship.

I would also like to say that I was lucky to have Dave as a mentor/co-supervisor during my sandwich PhD at Sanger. This thesis would not have been possible without Dave´s generosity and I truly appreciate him giving me the opportunity of staying is his laboratory for over a year, despite crazy pandemic situation. Thank you for putting your trust in me. Your kindness and dedication for science is really inspiring.

To everybody in Adam´s team for the amazing hospitality at Sanger. I was very fortunate to be surrounded by lovely people such as you all. Thanks to Alastair, Victoria, Manik, and Roy for all bioinformatic analyses and kindness answering my doubts. Thanks to Saskia, Jen, Andrea, and Vicky for making my stay in Cambridge so joyful. Thanks for all encouragement, also for sharing your knowledge and experience with me, especially Vicky for all discussions and many hours spent in cell culture. Also, many thanks to Sofia Chen, who allowed me to be part of her work and for her supervision during experiments. I am also grateful to all my collaborators. Thanks to Mariana Boroni and Natasha Jorge for analyses on TCGA data and David Fraser from Gene Editing team at Sanger, for sequencing analyses.

Finally, I would like to thank my big family, my grandparents, aunts, uncles, and cousins, for all celebrated achievements. Especially my mom, dad and my brother for constant love and support. Also, my husband Bruno, for sharing all frustrations, highs, and lows and for always being my inspiration. I wouldn’t be the person I am today without you. I respect and admire you all.

This study was financed in part by the Coordenação de Aperfeiçoamento de Pessoal de Nível Superior - Brasil (CAPES) - Finance Code 001, CAPES-PRINT #88887.372178/2019-00, FAPESP #2017/04926-6, CNPq, and the Wellcome Trust Sanger Institute.

“Nossas mentes possuem por natureza um insaciável desejo de saber a verdade”

Padre Cícero

RESUMO

MATSUYAMA, L. S. A. S. **Application of CRISPR-Cas9 to interrogate novel gene functions in cutaneous melanoma.** 2021. 155 p. Tese (Doutorado em Ciências) – Faculdade de Ciências Farmacêuticas, Universidade de São Paulo, São Paulo, 2021.

O melanoma representa 3% dos tipos de neoplasias cutâneas e é a maior causa das mortes por distúrbios de pele no mundo. A alta taxa de mortalidade associada à essa doença advém da alta capacidade de pacientes com melanoma desenvolverem metástases, e apresentarem recidiva após tratamento com inibidores da via de sinalização MAPK (como da proteína BRAF), comumente utilizados no tratamento de pacientes metastáticos. Assim, a investigação de genes envolvidos nos mecanismos de desenvolvimento do melanoma é primordial para novas estratégias terapêuticas mais efetivas. Dessa forma, descrevemos no presente trabalho dois projetos envolvendo os genes *SIN3B* e *IRF4* como possíveis biomarcadores para melanoma cutâneo. Em análises prévias de bioinformática realizados pelo nosso grupo, *SIN3B* foi identificado tendo maior expressão em melanomas metastáticos. Além disso, diversos estudos mostraram que o gene está envolvido na regulação da expressão gênica e transformação oncogênica. Dessa forma, descrevemos nessa tese alguns mecanismos pelos quais *SIN3B* pode influenciar no desenvolvimento do melanoma, através da caracterização funcional de células *SIN3B*-deletadas pela metodologia CRISPR-Cas9. Inicialmente, observamos aumento na expressão de *SIN3B* em melanomas metastáticos *BRAF*-mutados, onde notamos que a variante de *splicing* longa do gene (NM_001297595.1), era efetivamente prevalente em melanomas. Assim, desenhamos sequências de RNA guias entre os éxons 2 e 3 do gene *SIN3B* humano e, obtivemos três clones *knockout* e outros três clones controle (contendo plasmídeo vazio) em diferentes linhagens de melanoma (SKMEL28, A2058 e A375), para caracterização funcional. Observou-se que a ausência do gene não interferiu na proliferação das células tumorais, contudo, acarretou na diminuição de processos invasivos. Esses resultados foram averiguados através de ensaios em câmara de Boyden e análises de transcriptoma (sequenciamento de RNA total das células deletadas), onde notou-se diminuição das vias de migração e motilidade. Adicionalmente, um rastreamento de genes sinteticamente letais com *SIN3B* foi realizado com uma biblioteca de CRISPR capaz de silenciar todo o genoma. Esses resultados mostraram que os genes *USP7* e STK11, ambos pertencentes à via de sinalização de FoxO, são essenciais nas células *SIN3B* deletadas. Por fim, através de um projeto colaborativo com o *Wellcome Trust Sanger Institute*, análises prévias de sequenciamento de larga escala demonstraram que a deleção do gene *IRF4* era letal para células de melanoma. Dessa forma, realizamos o silenciamento de *IRF4* in vitro e notamos que a ausência do gene promove morte celular e apoptose, independentemente de *MYC* e *MITF*, conhecidos na literatura por serem alvos *downstream* do gene. Portanto, esses dados sugerem que *IRF4* tem um papel importante na sobrevivência de células de melanoma. Em conjunto, ambos trabalhos descritos nessa tese, demonstram como a metodologia CRISPR-Cas9 pode auxiliar no entendimento de processos importantes para a malignidade do melanoma e contribuir para estratégias terapêuticas mais efetivas para esse tumor.

Palavras chave: Melanoma, SIN3B, IRF4, CRISPR-Cas9.

ABSTRACT

MATSUYAMA, L. S. A. S. **Application of CRISPR-Cas9 to interrogate novel gene functions in cutaneous melanoma.** 2021. 155 p. Thesis (Doctor of Science) – Faculdade de Ciências Farmacêuticas, Universidade de São Paulo, São Paulo, 2021

Melanoma accounts for 3% of skin neoplasms and is the leading cause of death from skin disorders worldwide. The high mortality rate associated with this disease stems from the high capacity of melanoma patients to develop metastases and treatment relapse with inhibitors of the MAPK signaling pathway (such as BRAF inhibitors), commonly used in melanoma therapy. Thus, the investigation of genes involved in the mechanisms of melanoma development is essential for new and more effective therapeutic strategies. Hence, we describe in this thesis two projects involving the genes *SIN3B* and *IRF4* as possible biomarkers for cutaneous melanoma. Initially, through bioinformatics analyses performed by our group, an upregulation of *SIN3B* was found in metastatic melanomas. This result together with the understanding of *SIN3B* role in regulating gene expression and oncogenic transformation, prompted us to describe in this thesis some mechanisms by which SIN3B may influence melanoma development. We then sought to characterize the gene function using *SIN3B*-deleted cells, generated by the CRISPR-Cas9 methodology. Initially, we observed increased *SIN3B* expression in *BRAF*-mutant metastatic melanomas, where we noted that the long splicing variant of the gene (NM_001297595.1) was effectively prevalent in melanomas. Subsequently, we designed gRNAs between the exons 2 and 3 of the human *SIN3B* gene and engineered three knockout clones and three control clones (containing empty lentiCRISPRv2 plasmid) from different melanoma cell lines (SKMEL28, A2058, and A375). Through functional analyses, it was observed that the absence of the gene did not interfere in the proliferation of tumor cells; however, it led to a decrease in invasive properties. These results were verified by Boyden chamber assays and transcriptome analysis (total RNA sequencing of deleted cells), where a decrease in migration and motility pathways was observed. Additionally, a screening of synthetically lethal genes with *SIN3B* was performed with a genome wide CRISPR library. These results showed that *USP7* and *STK11* genes, which belong to the FoxO signaling pathway, were essential in *SIN3B*-depleted melanoma cells. Finally, through a collaborative project with the *Wellcome Trust Sanger Institute*, previous large-scale sequencing analyses demonstrated that deletion of the *IRF4* gene was lethal for melanoma cells. Accordingly, we performed *IRF4* silencing *in vitro* and noticed that the lack of *IRF4* promotes cell death and apoptosis, independently of *MYC* and *MITF*, known in the literature to be downstream targets of this gene. Therefore, these data suggest that *IRF4* plays a vital role in melanoma cell survival. Taken together, both works herein described in this thesis demonstrate how CRISPR-Cas9 can be applied to study the functions and mechanisms of genes involved in melanoma progression, collectively helping in the development of more effective therapeutic strategies for this tumor.

Keywords: Melanoma, SIN3B, IRF4, CRISPR-Cas9.

LIST OF FIGURES

LISTA OF TABLES

NOMENCLATURE

Acronyms / Abbreviations

BSA Bovine serum albumin

CAMs Cell adhesion molecules

cDNA Complementary DNA

CRISPR Clustered regularly interspaced short palindromic repeat

DEGs Differentially expressed genes

ddNTP Dideodynucleotide

DMEM Dulbecco´s Modified Eagle Medium

ECL Enhanced chemiluminescence system

ECM Extracellular matrix

EMT Epithelial-mesenchymal transition

FBS Fetal bovine serum

FDA US Food and Drug Administration

gDNA Genomic DNA

GO Gene ontology

GTEx Genotype-Tissue Expression

HCR Highly conserved region

HDAC Histone deacetylase

HDR Homology directed repair

HID Histone deacetylase interaction domain

INCA Brazilian National Cancer Institute

IRES Internal ribosomal entry site

KEGG Kyoto Encyclopedia of Genes and Genomes

MAGeCK Model-based analysis of genome-wide CRISPR-Cas9 knockout)

MAPK Mitogen-activated protein kinase

MMP Metaloproteinase

MOI Multiplicity of infection

NCBI National Center for Biotechnology Information

NGS Next-generation sequencing

NHEJ Non-homologous end joining

PAH Paired amphipathic alpha helix

PAM Photospacer adjacent motif

PBS Phosphate-buffered saline

PCR Polymerase chain reaction

PCA Principal component analysis

PI3K Phosphatidyl inositol 3-kinase

qPCR Quantitative polymerase chain reaction

RIN RNA integrity number

RSEM RNA-Seq by Expectation Maximization

RTK Receptor tyrosine kinase

sgRNA Single guide RNA

SNP Single nucleotide polymorphism

STRING Search Tool for Retrieval of Interacting Genes/Proteins

TCGA The Cancer Genome Atlas

UCSC University of California Santa Cruz

UV Ultraviolet

VGP Vertical growth phase

WGS Whole-genome sequencing

WES Whole-exome sequencing

WT Wild type

WTSS Whole transcriptome shotgun sequencing

CONTENTS

1. INTRODUCTION

1.1. Cutaneous melanoma

Cutaneous melanoma is the most aggressive type of skin cancer whose origin lies in the abnormal proliferation of melanocytes, neural crest-derived cells located within the basilar epidermis. Melanocytes are characterized by their ability to synthesize melanin, a pigment that gives the skin color and acts as a protective agent against ultraviolet (UV) radiation exposure.[2] This happens because the melanin is transferred from melanocytes to neighboring keratinocytes, where it absorbs and dissipates UV energy, protecting their nucleus from UV radiation-induced DNA damage.[3]Although skin cancer comprises 30% of all types of malignant tumors worldwide, melanoma has a low incidence, around 3% of skin neoplasms.[2] In 2020, the number of deaths due to melanoma in Brazil for men and women, respectively, was 1,159 and 819, whereas the estimate of new cases was 8,450, of which 4,200 cases were for men, 4,250 in women.[4] Still, melanoma accounts for 1,7% of all newly diagnosed cancers worldwide, and the incidence is increasing, especially in European-descent populations (Figure 1), remaining the deadliest skin disease due to its high invasiveness and, in more advanced cases, promoting metastasis, a fact that impairs its prognosis.[5]

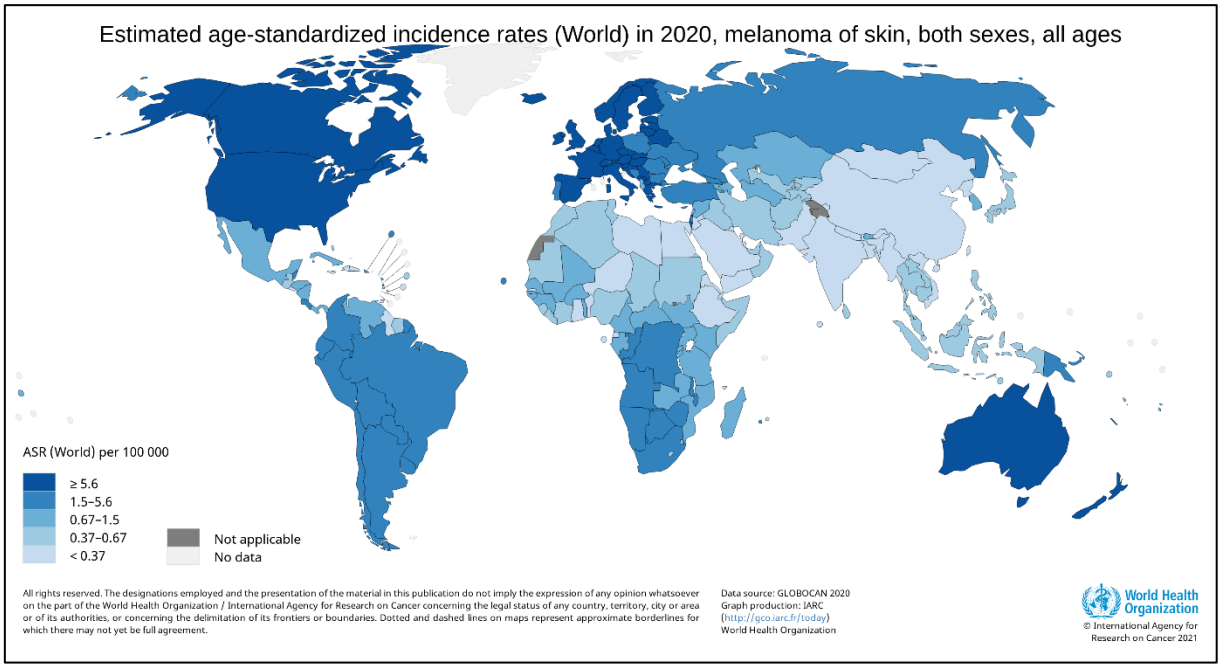

Figure 1. Incidence rates of melanoma worldwide. Data is shown with 2020 statistics. Melanoma incidence rates around the globe, both for males and females.

Source: Data extracted from GLOBOCAN 2020 and adapted from IARC.[6]

Melanoma is associated with various risk factors corresponding to either genetic predispositions or environmental stress, such as fair skin, presence of atypical nevi, number of moles, intermittent UV exposure, age, family history of skin cancer, and weakened immune system.[7; 8] To note, diagnosing melanoma in its early stages is crucial for the prognosis and survival of patients, as the 5-year survival rate for primary melanoma is 99% and declines rapidly for metastatic melanoma, accounting for only 27%.[9]

The transformation of melanocytes into melanoma stems from numerous genetic and environmental factors, usually resulting in sporadic somatic mutations. Generally, these mutations lead to mismatches of critical intracellular signaling pathways, such as cell cycle, apoptotic machinery, motility, and organization of the cytoskeleton, which may alter cell interactions with extracellular matrix and other neighboring stromal cells, culminating in the formation of a tumor microenvironment conducive to the eventual metastatic progression of melanoma (Figure 2).[10]

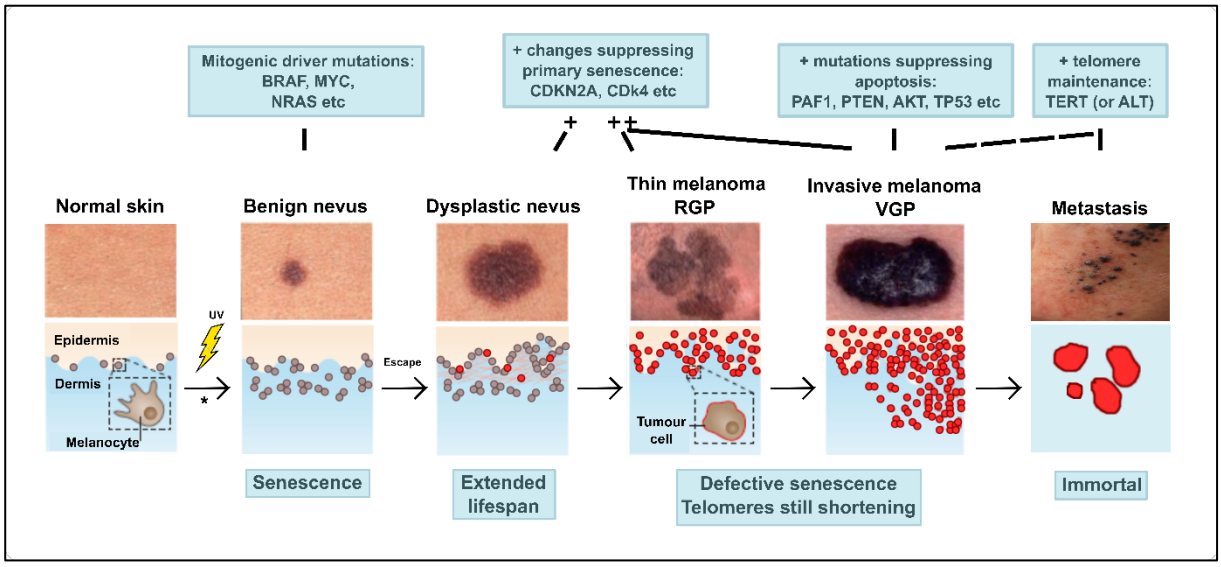

Figure 2. **Schematic representation of different genetic alterations which occur during melanoma progression.** The accumulation of genetic mutations in melanocytes (such as the initiator mutation BRAFV600E) activates oncogenes and inactivates tumor suppressor genes. The set of several mutations allow the initial proliferation of altered melanocytes, blood vessels growth, increased tumor invasion, immune response evasion, and eventual tumor metastasis.
Source: Adapted from Shain, A. H. et al.[11]

The standard Clark model describes melanoma progression, emphasizing the linear acquisition of phenotypic and genetic changes through a series of six steps, including the disrupted growth of melanocytes, formation of nevi lesions, and, subsequently, development of dysplasia (which may arise from new lesions or preexisting nevi), hyperplasia, invasion, and

metastasis to other organs.[12] Initially, abnormal activation of the MAPK (mitogen-activated protein kinase) pathway occurs due to benign moles harboring the *BRAFV600E* mutation. Once the oncogene-induced senescence is surpassed through the inactivation of *CDKN2A* and other cell cycle checkpoints, the proliferation of tumoral cells is stimulated. Then, the radial growth of melanoma cells spreads progressively by activating the human reverse transcriptase (*hTERT*), leading to the final stage of melanoma progression, which consists of growing deep in the dermis (vertical growth phase – VGP) owing to apoptosis repression.[13] This last phase outlines a high tumor mutational burden and increased copy number alterations.

While the classic Clark model was prevailing, a deeper understanding of melanoma biology has been attained over the past few years. Multiple melanoma subtypes were associated with different precursor legions, therefore either emerging *de novo* or from pre-existing nevi. Approximately 25 – 33% of cutaneous melanomas in intermittent sun-exposed areas arise from nevi, usually possessing *BRAFV600E* and *PTEN* mutations. Conversely, non-nevi-associated melanomas stem from chronically sun-damaged body sites, such as in the head and neck, and have more *NF1* and *TP53* mutations.[11; 14] Hence, even if *BRAF* is mutated in up to 80% of benign nevi, it is not sufficient for melanoma evolution, implying that melanoma tumors progress through the acquisition of other mutations and adapting many critical biological pathways, favoring tumor invasion and surrounding infiltration. These features attest to the heterogeneous nature of melanoma and will be discussed in the following topics.

1.2. Genetics of melanoma and signaling pathways

Melanoma displays one of the highest numbers of somatic mutations over all types of cancers, probably due to the UV-induced mutagenesis producing the C>T signature, [15; 16]and the understanding of melanoma mutational landscape has vastly evolved based on improving next-generation sequencing (NGS) and large-scale expression analyses of tumors. These platforms allowed the genomic profiling of the disease, which contributed to melanoma therapeutics. [17] Whole-exome sequence analysis of primary and metastatic melanoma samples from The Cancer Genome Atlas (TCGA) acknowledged the classification of four melanoma genomic subtypes: *BRAF*-mutant, *NRAS*-mutant, *NF1*-mutant, and triple-wild-type. Deregulation of these genes are regarded as driver alterations in melanoma development.[18; 19]

The most prevalent mutation is in the *BRAF* proto-oncogene, which occurs in 33-65% of cutaneous melanomas, predominantly in superficial spreading melanoma subtype. A valine to a glutamate point mutation at residue 600 (*BRAFV600E*) is found in almost 90% of *BRAF*-mutated tumors, followed by the less common mutation V600K (substitution of a valine for a lysine).[20; 21] The recurrent BRAFV600E mutation constitutively activates the central RAS/RAF/MEK/ERK (MAPK) kinase pathway promoting cell proliferation, survival of melanoma tumor cells, and evasion of cellular senescence and apoptosis.[22; 23; 24; 25; 26]

The second most common mutation is in the GTPase *NRAS*, a member of the RAS signaling proteins. *NRAS* is mutated in about 15-30% of melanomas, primarily switching glutamine to either arginine or lysine in codon 61 (Q61R/K/L). This mutation results in altered GTPase activity [27], keeping the malignant transformation by persistently activating both MAPK and PI3K (phosphatidylinositol 3-kinase) pathways (Figure 3), usually conferring thicker and aggressive melanoma tumors.[28] The latter PI3K pathway activation is involved in several functions within the cell, regulating cell cycle progression, aberrant growth of neoplastic cells, survival, and migration[29]. Additionally, the tumor suppressor gene *NF1* is the third key driver of melanoma and inhibits downstream *RAS* signaling. Chronically sun-exposed skin or wild-type (WT) melanomas for *BRAF* and NRAS often present *NF1* mutations (10-15%) [30; 31]. Hence, *NF1* loss-of-function also promotes MAPK and PI3K pathways. Lastly, few cutaneous melanomas and most mucosal and acral melanomas lack mutations in *BRAF, NRAS,* or *NF1,* defining a heterogeneous subgroup of triple wild type mutant tumors, which frequently harbor mutations in the receptor tyrosine kinase *KIT.* These mutations are commonly found in 39 % of mucosal and 36 % of acral, instead of 28 % of cutaneous melanomas. [32; 33] Altogether, *BRAF, NRAS, NF1,* and triple wild type deregulations represent necessary driver alterations in melanoma development. Exploring additional molecular variations could help elucidate the biological heterogeneity of melanoma and characterization of invasive and metastatic subtypes. Consequently, identification of other predictive biomarkers may benefit patients since, to date, only *BRAF* mutations have been included in clinical practice.[17]

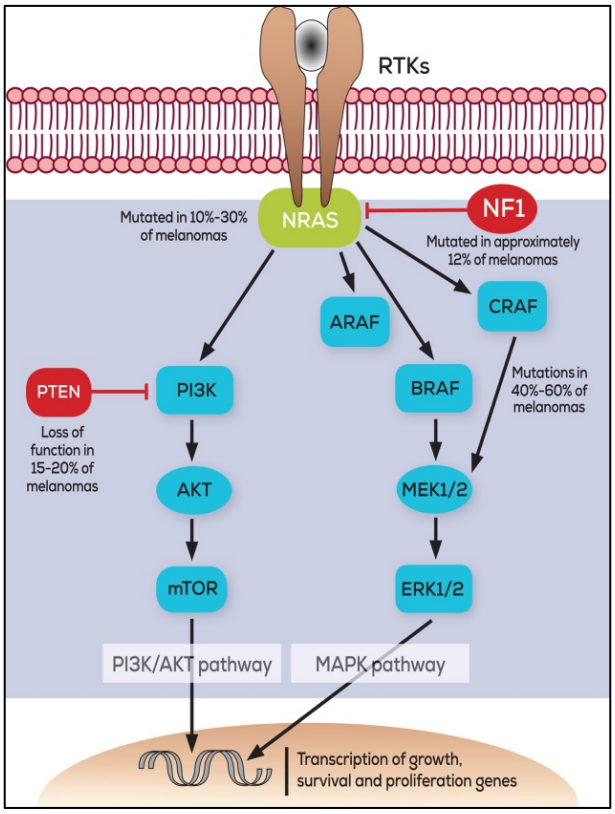

Figure 3. **Essential signaling pathways in cutaneous melanoma.** The binding of receptor tyrosine kinases (RTKs) stimulates MAPK downstream activation of *RAF, MEK, ERK* kinases and promotes PI3K/AKT activation through *PI3K*s, *AKT,* and *mTOR* kinases. Each pathway leads to phosphorylation and transcription of genes linked to cell growth, survival, and proliferation.
Source: Adapted from Lim, S. Y. et. al. [34]

1.3. Current melanoma treatments and therapy resistance phenomenon

Melanoma mortality is decreasing globally given several recently approved therapies for advanced-stage disease. However, therapeutic options for melanoma routinely depend on tumor location, stage, and genetic modifications. Surgical excision is primarily recommended for early staged melanomas, and systemic therapy has been the pillar treatment for most metastatic patients.[35; 36]

Initially, chemotherapy was the most predominant therapy for advanced melanoma and remains as palliative care of refractory and relapsed disease because of its cytotoxic activity against tumor cells.[37] Since its approval by the US Food and Drug Administration (FDA) in 1975, the alkylating agent dacarbazine has become the standard regimen for inoperable melanoma. The drug promotes methylation of nucleic acids or direct DNA damage, resulting in cell death. Nevertheless, administration of either dacarbazine or temozolomide, another alkylating agent, generated minimal responses of 10 to 25% of the cases and a low impact on

overall survival.[38] Only in the 1990s, progress in the mechanisms of immunological responses to melanoma was assessed with the FDA approval of the non-selective forms of immunotherapy, such as high doses of interleukin-2, which elicited tumor-infiltrating T-cells proliferation and instigation of lymphokine-activated killer cells to lyse tumor cells. However, the complete response of only 6% of advanced patients was achieved, with high toxicity and low effectiveness, urging novel therapies.[39]

The revolution of melanoma therapeutics came after the pivotal discovery of approximately half of melanomas retaining *BRAF* mutations [21], enabling studies on targeted therapy through the development of BRAF selective inhibitors. Vemurafenib was the first molecularly targeted drug, authorized by the FDA in 2011, inducing inhibition of mutated BRAFV600E kinase and reducing MAPK signaling activity.[40; 41; 42] Early investigations indicated promising results, with 75% of patients achieving a partial response and increased survival for more than seven months.[43; 44]

Another BRAF inhibitor was developed soon after that. In 2013, dabrafenib was approved with a response rate of 59% in BRAFV600E melanomas and 13% for BRAFV600 mutants. [45; 46; 47]Considering the importance of the BRAF mutation in melanoma development, the use of oncogene-directed therapy, especially with BRAF inhibitors such as Vemurafenib and Dabrafenib, has become an efficient study strategy and therapeutic alternative. However, despite the initial efficacy, after a few months of treatment with BRAF inhibitors, patients present an aggressive recurrence of melanoma due to the development of resistance, culminating in death (Figure 4).[48]

Additionally, it can be observed that acquired resistance strongly influences tumor invasion and proliferation. Recent data support this finding, as they demonstrate that melanoma cells with acquired resistance to Vemurafenib treatment have tremendous invasive potential compared to sensitive ones, partially due to their high expression of matrix metalloproteinases (MMPs).[49] Thus, it is remarkable how studies of resistance pathways, aiming at more effective therapies against melanoma, are still needed since melanoma may not respond to the chemotherapeutic agents of choice.

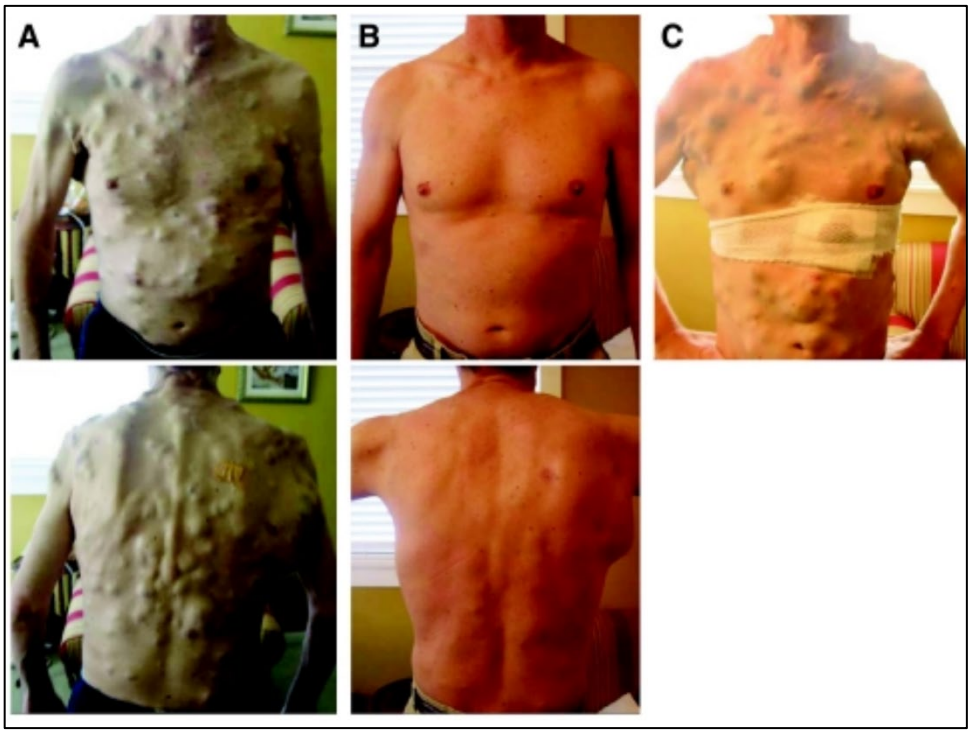

Figure 4. **Images of a 38-year-old patient with subcutaneous metastases of *BRAF*-mutant melanoma.** A) Image was taken before treatment with BRAF inhibitor (Vemurafenib – PLX4032). B) After fifteen weeks of treatment. C) Recurrence of the disease after twenty-three weeks of therapy, indicating acquired resistance to the treatment.
Source: Wagle, N. et al, 2011.[50]

The resistance phenomenon is often related to some mechanisms as follows: reactivation of MAPK pathway due to *RAS* and *ERK* mutations and elevated expression of *CRAF*, modification in *ERK1/2* regulated cell cycle events, and activation of alternative pathways, for instance, the PI3K/AKT/mTOR.[43; 48; 51; 52] Therefore, recent ongoing researches aimed to overcome resistance, and some practical reported strategies intended to develop new inhibitors targeting downstream effectors of driver oncogenes, such as *MEK*, or combinatorial inhibition of both *BRAF* and *MEK*. Trametinib is a non-ATP competitive *MEK1/2* inhibitor, which binds to the allosteric binding site adjacent to the ATP site, preventing *MEK* activation.[53] It was accepted in 2013 as a monotherapy for BRAFV600E-mutant metastatic melanomas, improving clinical response rate compared to patients treated with chemotherapy.[54] In 2014, FDA approved the combined therapy of Trametinib and Dabrafenib, causing increased survival (around 11 months), significantly higher than a single administration of Dabrafenib.[43] Hence, this indicates that the future of melanoma therapeutics resides in combined therapies, directed to either the commonly altered melanoma pathways MAPK and PI3K or simultaneous treatment with targeted-inhibitors and immunotherapeutic drugs.

Despite dual therapy with BRAF and MEK inhibitors triggering a better overall response rate in melanoma patients, this effect is transient, and resistance to these drugs is frequent. Long-term tumor remissions can be accomplished through immune checkpoint inhibitors, leading to increased patient survival. However, a low response rate remains predominant. Therefore, there has been a growing interest in combining targeted therapy and immunotherapy for advanced melanoma patients because of the complementary strengths of both treatments, which could contribute to durable responses in clinics.[55; 56]

Over the past few decades, extensive studies promoted a better knowledge of the host immune system and its role in tumor biology to identify and eliminate foreign cancer cells. Recently, immunotherapy emerged as the breakthrough treatment of advanced melanoma, with modern immunotherapeutic approaches focusing on T-cells therapies, cytokine, vaccines, and immune checkpoint inhibitors.[40; 57; 58] The latter immune checkpoints are composed of several inhibitors that block regulatory pathways, which generally allow evasion of immune-mediated destruction of tumors, thereby strengthening the immune response mechanisms.[59]

So far, three drugs have been accepted by the FDA, showing a positive impact on patients survival rates, especially when combined: Ipilimumab (approved in 2011), a monoclonal antibody antagonist to the cytotoxic T lymphocyte-associated protein 4 (CTLA-4), Pembrolizumab and Nivolumab (approved in 2014), both antagonists to the programmed cell death protein 1 (PD1).[60] These monoclonal antibodies designed to block CTLA-4 and PD-1 reactivate the antitumor responses of the immune system.

Ipilimumab is a monoclonal antibody that up-regulates T-cell proliferation and activation through blocking CTLA-4, often overexpressed in melanoma.[61] A trial with 676 patients in late melanoma stages demonstrated that Ipilimumab alone conferred a median overall survival of 10 months. Nevertheless, other clinical trials indicated toxicity upon treatment, with 15-35% of patients acquiring adverse reactions.[62] Conversely, PD-1 blockade with Pembrolizumab and Nivolumab showed response rates ranging from 20-40% in phase I clinical trials due to blockade of tumor cells recognition by T-lymphocytes, enabling evasion of host's native antitumor responses.[63; 64] Despite initial treatment efficacy with anti-CTLA-4 and anti-PD1, recent reports reveal patients' resistance to immunotherapies. Current argued mechanisms behind this phenomenon are slight changes in protein expression or lower production of antigenic epitopes.[65] To improve patients outcomes, several clinical studies were conducted to assess combinatorial regimens containing immune checkpoint blockers and

conventional therapies, including targeted inhibitors.[40] Consequently, much work is still needed to address melanoma treatment limitations, and future research could focus on establishing new biomarkers and understanding the mechanisms behind resistance to current therapies. A timeline of approved therapies for advanced melanoma is presented in Figure 5.

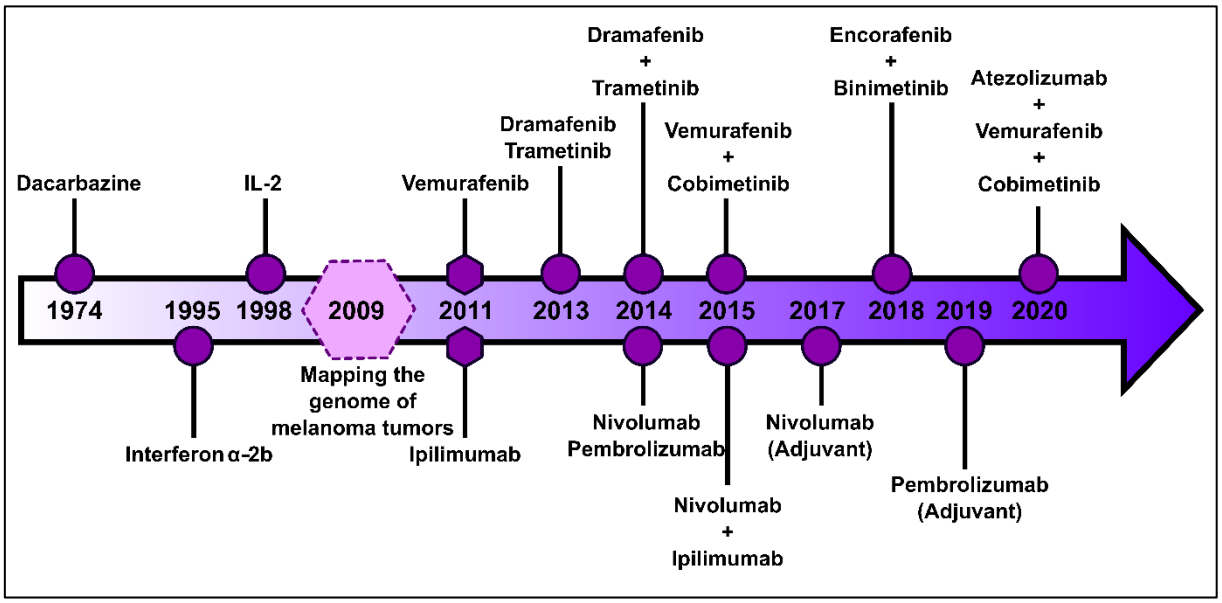

Figure 5. **Timeline of FDA-approved targeted and immunotherapeutic drugs.** Initially, non-selective chemotherapy and immunotherapy were employed for advanced melanomas. However, the Cancer Genome Atlas Project began to map the genome of melanoma tumors in 2009, which made it possible to design novel drugs for immunotherapy, targeted therapy, or combinatorial therapeutic regimens.

1.4. Next generation sequencing (NGS) applied for cancer biology

The breakthrough of DNA sequencing was developed in 1977 by Sanger [66], whose method determined nucleotides order in single-stranded DNA molecules by the complementary synthesis of polynucleotide chains. This technique selectively incorporates radiolabelled ddNTPs (dideoxynucleotides) that act as specific chain-terminating inhibitors of DNA polymerase, resulting in fragments of different lengths, since ddNTPs impair further DNA extension.[67] Sanger sequencing dominated genomic research for many years and secured significant achievements, including the completion of human genome sequence in 2003 [68], which revealed critical details regarding how genes function, aiding to identification of somatic mutations, single-gene diseases, and providing a new basis for cancer research.[69; 70] Nevertheless, faster and affordable sequencing technologies were needed to profile the molecular landscape of cancer, so prediction of disease outcome and discovery of new targets for optimal therapies could be possible.

This demand led to the advent of next-generation sequencing (NGS), offering high-throughput and parallel sequencing reactions. This technology can be used for whole-genome sequencing (WGS), whole-exome sequencing (WES), and whole transcriptome shotgun sequencing (WTSS), also known as RNA sequencing. Altogether, these approaches provide valuable data on tumor biology, combined with bioinformatics tools. WGS and WES provide complex information on genomic cancer alterations, consisting of point mutations, small insertions, deletions, copy number alterations, and variations compared with normal samples. Alternatively, transcriptome sequencing quantifies gene expression profiles, recognizes alternative splicing and RNA editing.[69; 71]

NGS mechanisms comprise shotgun sequencing of randomly fragmented genomic DNA (gDNA) or cDNA reverse transcribed from RNA. Afterward, adapter sequences are added to either gDNA or cDNA to construct library templates, and library amplification occurs. All nucleotide incorporation is checked through luminescence detection, and NGS generates millions of short sequences reads. The workflow begins with converting sequencing signals to short reads of nucleotide sequences, followed by quality assessment of NGS reads and aligning them to the reference genome. After that, variant identification and annotations are assessed along with data visualization. Finally, data filtration of identified alterations accompanies validation of sequencing results, and all data is combined into a single bioinformatic output to answer the biological questions of interest. [72; 73]

NGS data analysis is highly compute-intensive and requires bioinformatics skills to analyze, integrate and interpret all data. Thus, integrated data visualization platforms are essential for obtaining a complete whole-genome cancer profile and determining genomic changes contributing to malignancies. This idea prompted the development of projects which connect different omics approaches across several tumor types with clinical outcomes, such as the leading large public databases The Cancer Genome Atlas (TCGA) and the International Cancer Genome Consortium (ICGC). TCGA and ICGC were respectively launched in 2005 and 2008 and, within both consortia, hundreds of tumors were evaluated on a genome-wide scale. More specifically, the TCGA-SKCM provisional dataset comprises 478 primary and metastatic cutaneous melanoma tumors with details of RNA sequencing, DNA methylation, miRNA, and single nucleotide polymorphisms (SNP). This study disclosed the four subtypes *BRAF*-mutant, *NRAS*-mutant, *NF1*-mutant, and triple wild-type melanomas, previously discussed on early topics in this thesis, that identified point-mutations such as in *BRAF*, establishing melanoma targeted therapies. In summary, the emergence of these public

repositories ratifies the importance of NGS to comprehensively characterize altered molecular events present in cancers, including point mutations, aberrant methylation, gene expression patterns, and DNA copy number changes.[74; 75; 76; 77]

1.5. CRISPR-Cas9 as a tool and its mechanisms

The human genome comprises billions of DNA bases and holds all information to build and maintain an organism. Therefore, modulating or enabling precise modifications in the genome is essential for understanding gene function in normal and disease conditions, and its biological mechanisms. In this context, CRISPR-Cas9 technology has revolutionized genome engineering for being reasonably inexpensive and conferring high editing efficiency in diverse organisms.

CRISPR stands for the clustered regularly interspaced short palindromic repeat DNA sequences, and the CRISPR-Cas9 system is a prokaryotic adaptative immune mechanism found in several bacteria and most archaea, responsible for the cleavage of exogenous viral DNA during phage infection. After a viral challenge, DNA fragments of invading phages, called spacer sequences, are integrated into the CRISPR repeat-spacer array of the host genome,[78] conferring a genetic memory of phage invasion, helping to detect and destroy invaders in future new infections.[79; 80]

There are currently six types of CRISPR systems, and each contains the cluster of CRISPR-associated (Cas) genes (encoding Cas proteins), non-coding RNAs, and repeats, interspaced by foreign DNA targets (spacers), constituting the CRISPR RNA array (crRNA).[81] The most characterized is type II, which consists of the Cas9 DNA endonuclease from *Streptococcus pyogenes* and a non-coding transactivating helper (tracrRNA) that hybridizes with the crRNA.[82; 83]

In general, this hybrid structure, which can be combined to build a chimeric sgRNA to simplify the system later for use in mammalian cells, directs the Cas9 nuclease to the target DNA containing a 20-nucleotide sequence and adjacent 5' - NGG conserved motif (PAM) to promote a double-strand break three base pairs before PAM (Figure 6).[79] After the break, the target locus goes through one of the two major DNA repair pathways: NHEJ (Non-Homologous End Joining) or HDR (Homology Directed Repair). In the absence of a repair template, the NHEJ pathway is activated, resulting in random nucleotide insertions and/or deletions (indels)

or substitutions at the cleavage site. NHEJ is typically the pathway used for gene inactivation since indels in a coding exon can frequently lead to frameshift mutations or premature termination codons, resulting in gene loss of function.[84] However, when a donor template is present, the HDR pathway is initiated. The repair appears at a substantially lower frequency than NHEJ, and the mechanism is in the form of homologous arms flanking the inserted sequence or single-stranded DNA oligonucleotides. This machinery performs precise gene modifications, such as gene knock-in, deletion, correction, or mutagenesis.[85]

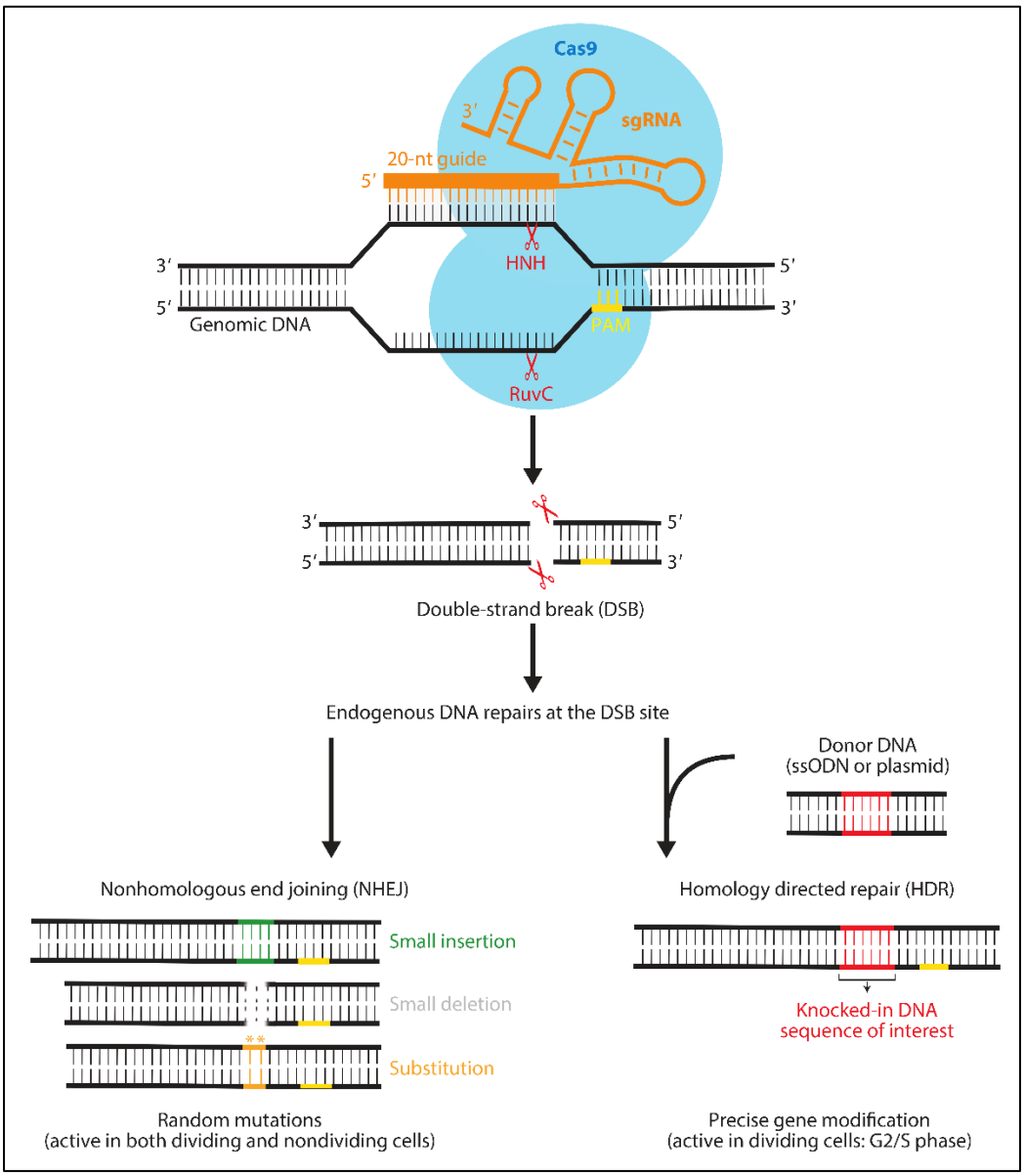

Figure 6. **CRISPR-Cas9 mechanism for genome engineering.** A chimeric sgRNA directs the Cas9 endonuclease to the target DNA, through a 20-nucleotide sequence, generating double-strand break. Then, NHEJ or HDR repair mechanisms generate desired gene modifications. Abbreviations: CRISPR RNA (crRNA), photospacer adjacent motif (PAM), single-guide RNA (sgRNA) and transactivating CRISPR RNA (tracrRNA).

Source: Adapted from Jiang, F., Doudna, J. A.[83]

Hence, the CRISPR-Cas9 machinery can precisely modify the genome of mammalian cells and living organisms, interrogating gene functions and regulatory elements, such as enhancers, which regulate the transcription of distance genes. Lately, the method has been optimized significantly to reduce off-target binding, for instance, using two mutant Cas9, each cutting opposite strands of DNA [86], or to improve Cas9 specificity by mitigating the helicase activity to disrupt off-target sites.[87; 88] Additionally, new applications have been developed, including transcriptional inactivation through the CRISPR interference method (CRISPRi) or activation (CRISPRa) using, respectively, an enzymatically inactive dCas9 fused with a transcriptional repressor to knockdown a gene, or dCas9 with an activation mediator, increasing transcription.[89; 90; 91] However, since completing the human genome, one of the most noteworthy CRISPR-Cas9 accomplishments involved large-scale functional screenings to identify a significant number of genes that influence a specific phenotype in an unbiased way, an approach that will be discussed in the subsequent section.[92]

1.6. Pooled CRISPR screenings

The optimization of CRISPR-Cas9 paved the way for large-scale functional screens, which determine genotype-phenotype interactions. Generally, CRISPR screens are presented in one of the two formats: arrayed, where sgRNAs are individually introduced in different culture wells (i.e., single perturbation per well), or pooled, with a library of sgRNAs targeting multiple genes applied at once into a population of cells, before phenotype-based selection.[93; 94] Usually, pooled screens are more advantageous than the arrayed format because they are cost-effective, with no requirement for liquid handling using robotics, and the first studies employing pooled genome-wide CRISPR screens were published in 2014.[95; 96]

Their workflow (Figure 7) typically initiates with designing a library of multiple sgRNAs targeting different genes, synthesizing the oligonucleotides in a pool of guides, and packaging the plasmid library into lentivirus, to further transduce in a single population. Cas9 can be introduced concomitantly with the sgRNA, or cells could be modified to stably express Cas9 prior to library transduction.[97] Viruses are put at a low multiplicity of infection (MOI, 0,1 to 0,3) to ensure each cell receives only a single perturbation. Finally, selection pressure is applied, and the frequency of each sgRNA is counted through NGS (next-generation sequencing). Computational analysis, namely MAGeCK (Model-based Analysis of Genome-wide CRISPR-Cas9 Knockout)[98] or BAGEL (Bayesian of Gene Essentiality)[99] can be used to

determine the abundance of enriched or depleted sgRNAs between control and phenotyped cells, thereby spotting the most significant gene hits responsible for the observed phenotype.[93; 100]

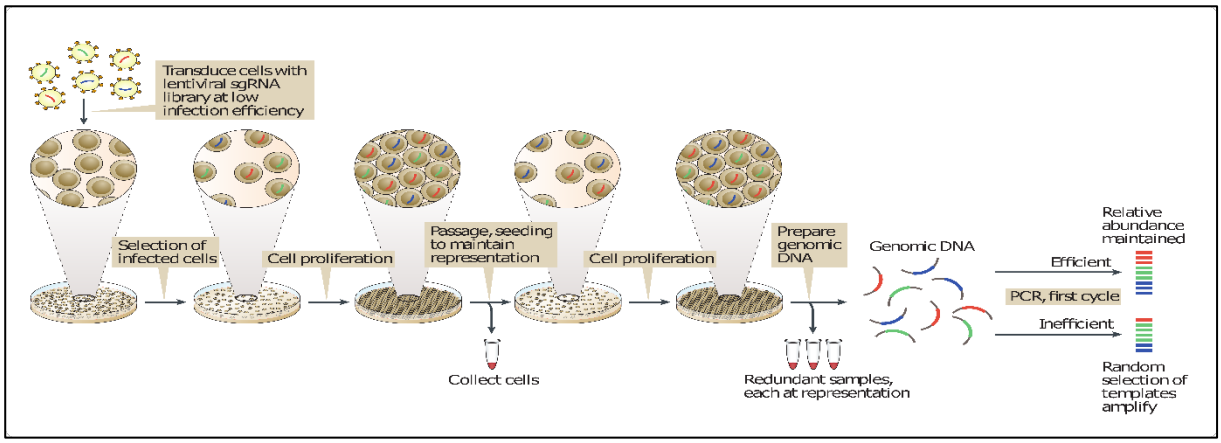

Figure 7. **Overview of pooled CRISPR-Cas9 screening.** First, a sgRNA library is prepared and, when the plasmid library does not encode the endonuclease Cas9, cells must be previously engineered to express Cas9. Then, library transduction occurs, generating a heterogeneous population with diverse genetic perturbations. A selection pressure, which could be antibiotic selection, is applied, and cells are kept in culture. Genomic DNA is extracted, followed by PCR amplification of sgRNAs and NGS. Analysis identifies depleted or enriched sgRNAs of gene hits.
Source: Adapted from Doench, J. G.[92]

There are two main CRISPR-Cas9 screening strategies used to identify novel protein functions due to altering gene expression: enrichment and depletion screens. The first approach relies on a gene loss conferring growth advantage after exposure to selection stress, such as drug treatment. The selective pressure is strong enough, so most cells die; thus, only a tiny fraction of surviving and drug-resistant cells is enriched.[101] Contrarily, depletion screens can pinpoint genes causing decreased cell fitness (i.e., essential genes)[102; 103] and synthetic lethal interactions, in which one mutated or depleted gene alone does not affect cell viability, but a combination of mutations or loss-of-function in different genes leads to cell death.[104; 105]

Altogether, pooled CRISPR screens have greatly progressed in diverse phenotypic assays to allow associating the role of the genome in normal and disease states. However, despite great utility, these screens may provide some challenges for data analysis, especially related to variability in sgRNA efficiency, resulting in a limited selection of genes with large effects[106] or excessive Cas9-mediated cutting in high copy number regions[107], leading to false-positive results. Thus, overcoming false positive or false negative results is crucial. Through proper experimental design, such as increasing number of replicates or cell lines and especially maintaining library representation throughout the screening procedure, data reproducibility

could be improved to provide a valid hit list.[108] Additionally, the validation of the perturbations or their gene targets can be assessed when testing lead candidates in multiple cellular models, rescreening cells with a different library, or rescuing the phenotype by, for example, introducing expressing vectors encoding cDNA with silent mutations to generate a silencing-resistant version of the gene hits.[93]

1.7. Outline of this thesis

This work comprises two different chapters, both under the scope of cutaneous melanoma research. The first is the main project focused on the role of the *SIN3B* gene in melanoma. Results describe a differential expression of *SIN3B* during the disease progression using a comprehensive panel of human melanoma cell lines, the associated pathways which may contribute to invasive properties, and ultimately, the *SIN3B* synthetic lethal partners in metastatic melanomas. Conversely, the second chapter outlines a small collaborative project I participated during my sandwich Ph.D at the Wellcome Trust Sanger Institute (Cambridge, United Kingdom) funded both by CAPES-PRINT and Sanger Institute, related to *IRF4* upregulation in melanoma cells and how they could be dependent on this transcription factor. This thesis is a collaboration with the University of São Paulo (São Paulo, Brazil), the Brazilian National Cancer Institute (Rio de Janeiro, Brazil), and the Wellcome Trust Sanger Institute (São Paulo, Brazil).

CHAPTER I: CHROMATIN-ASSOCIATED PROTEIN SIN3B ROLE IN CUTANEOUS MELANOMA PROGRESSION

2. INTRODUCTION

2.1. The SIN3/HDAC core complex

SIN3 (SWI-independent 3) was firstly identified in 1987 by two groups through genetic screening, aiming to elucidate the mating-type switching in *Saccharomyces cerevisiae*,[109; 110], and recognized as a global transcriptional regulator in 1992, by its capacity to both positively and more often negatively regulate gene transcription.[111] This protein is highly conserved from yeast to humans and has two alternatively spliced isoforms in mammals: *SIN3A* and *SIN3B*. Both paralogs maintained 63% sequence similarity at the protein level, with SIN3B lacking an amino acid tail before the PAH1 domain, and were initially discovered as MAD1 or MXI1 binding partners, antagonizing MYC signaling to control the cell cycle.[112; 113; 114; 115]

SIN3 is a scaffolding protein with no intrinsic DNA-binding activity. Yet, it supports the SIN3/histone deacetylase (HDAC) core complexes, recruited by sequence-specific transcription factors to promoter sites, resulting in deacetylation of histones H3 and H4, and transcriptional silencing.[116; 117; 118] Hence, SIN3 cooperates with HDAC for its repressor activity. Several studies described that the core SIN3/HDAC complex comprises seven proteins: HDAC1, HDAC2, RBAP46, RBAP48, SAP30, SAP18, and SDS3. As previously discussed, the deacetylase histones HDAC1 and HDAC2 compact chromatin and silence gene expression[118], whereas other proteins provide both stability and support for the complex. More specifically, the retinoblastoma-associated proteins RBAP46 and RBAP48 interestingly interact with histones H4 and H2A and help stabilize the interaction of the SIN3/HDAC complex with histone H4, while the SIN3-associated proteins SAP19 and SAP30 preserve the complex association with HDAC. In addition, SDS3 is necessary for the integrity and catalytic activity of the SIN3/HDAC core complex.[119; 120; 121] To date, a variety of other additional interactors were reported, which include SAP180, SAP130, SAP25, ING1/2, and KDM5A, working concomitantly or independently to repress gene transcription through the demethylation of histones.[113; 122] As a result, the whole complex encompasses various biological

processes, such as cell cycle progression, genomic stability, embryonic development, and, when in the presence of abnormal recruitment of this complex or alteration of its enzymatic activity, the implication in oncogenic transformation.

Structurally (Figure 8), SIN3 alone contains four paired amphipathic alpha-helices (PAHs) domains, forming helix-hoop-helix dimerization motifs equally found in the MYC family of DNA-binding transcription factors, [123] one histone deacetylase interaction domain (HID), and one highly conserved region (HCR). Structural works using nuclear magnetic resonance and X-ray diffraction techniques revealed that PAH1 and PAH2 function as independent domains [124], with high similarity (45% identical) but recognizing different proteins.[125] Also, both are preserved domains for interactions with many transcription factors [126]. However, the regions from PAH3, PAH4, HID, and HCR serve as scaffold structures to assemble other subunits of the SIN3/HDAC co-repressor complex.[112]

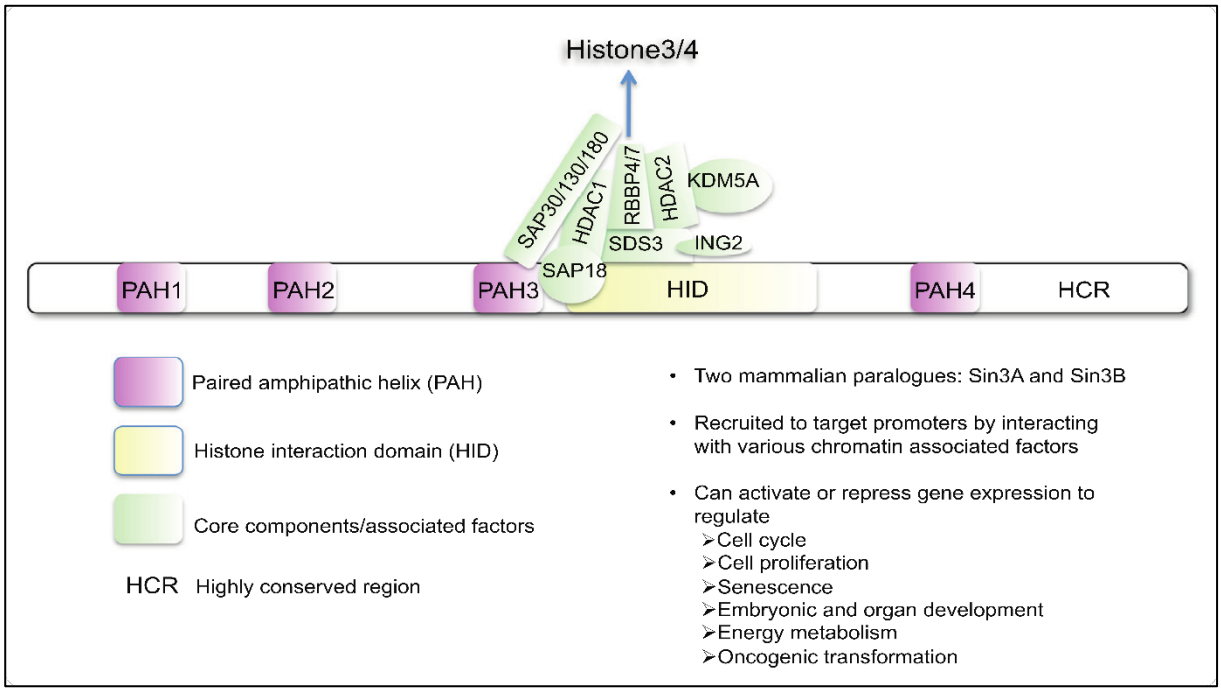

Figure 8. **Schematic representation of the SIN3/HDAC core complex structure and its functions**. SIN3 has six conserved domains, which include four alpha-helix domains (PAH), a histone interacting domain (HID), and a conserved region (HCR).
Source: Bansal et. al.[127]

2.2. *SIN3B* as a tumor supressor or oncogene

Recently, many studies have demonstrated different roles played by the SIN3 complex, from regular cellular events, such as growth, differentiation, senescence, to oncogenic transformations.[128] In mammals, accumulating evidence shows that the two paralogs SIN3A and SIN3B are not functionally redundant. Both proteins have all six conserved domains described earlier and interact with transcription factors in common, like p53, Mad-1, KLF, REST and ESET but present some distinct functions.[113; 129; 130] One of the proposed explanations for this variability is that PAH1 and PAH2 domains of each protein present differences in their sequences, promoting distinctive binding interfaces and protein-protein interactions.[124]

The human *SIN3B* gene, the target of this work, contains five protein-coding variants (five mRNA transcripts), as shown in Figure 9, generated through splicing events (removal of introns and joining of exons, sequences encoding proteins). These transcripts encode different proteins that have or do not have PAH and HID domains, which can play different roles.[131]

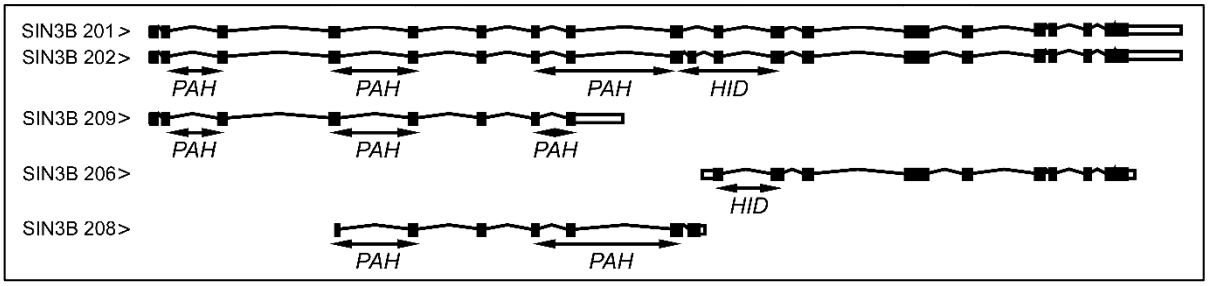

Figure 9. Schematic representation of human SIN3B protein -coding transcripts containing PAH and HID domains. The SIN3B 201 (NM_001297595.1), SIN3B 202 (NM_015260.3), and SIN3B 206 (NM_001297597.1) variants hold the HID domains, whereas the SIN3B 208 and SIN3B 209, which annotated accession numbers from the NCBI (National Center for Biotechnology Information), possess only PAH domains.
Source: Adapted from Faherty, N. et al, 2016.[131]

A previous study carried out by Grandinetti and collaborators demonstrated that *SIN3B* upregulation in fibroblasts led to oncogene-induced senescence, and decreased *SIN3B* expression is associated with tumor progression *in vivo*.[132] These results are related to those presented by DiMauro et al., where *SIN3B* inactivation prevented cell senescence in pre-neoplastic pancreatic lesions.[133] Another complementary study presented by Rielland showed that *SIN3B* silencing led to a delay in the progression of pancreatic tumors.[134] In addition to influencing carcinogenesis, another vital role of *SIN3B* is in controlling cell cycle progression. *SIN3B* expression leads to the repression of genes responsible for cell division through histone

deacetylation and chromatin compaction, keeping cells in the G0/G1 phase.[135] Another distinctive report evidenced that stable knockdown of *SIN3B* in breast cancer cells caused a significant decrease in transwell invasion and the number of invasive colonies.[136]

It is known that senescent cells are non-dividing cells still capable of synthesizing and secreting various factors such as cytokines, proteases, growth factors that together create a senescence-associated secretory phenotype (SASP). Research from Cantor et al. showed that contrarily to what was expected, with senescence acting as a barrier to tumor progression, the deletion of *SIN3B* triggered a decrease in tumor progression and increased survival in mice with pancreatic ductal adenocarcinoma. In this study, the hypothesis raised was that SASP promoted pancreatic cancer progression by recruiting immune cells and generating an inflammatory microenvironment.[137]

Therefore, the function of *SIN3B* as a tumor suppressor or oncogene is still open for debate and seems to be cancer dependent. Even though no studies of *SIN3B* in melanoma are present in the literature, previous analyses by our research group (Oliveira, et.al.)[138], with an initial screening in a bioinformatics platform, show an upregulation of *SIN3B* in melanomas, indicating a possible molecular role in the disease development.[138] Thus, the investigation of the *SIN3B* involvement in melanoma progression may be of great importance for developing novel effective therapies.

3. CHAPTER AIMS

This extensive SIN3B project aims to explore the role of *SIN3B* on the biology of human melanomas by:

- Evaluating *SIN3B* expression in different cohorts of normal skin, primary and metastatic melanomas, and correlating high and low *SIN3B* expression with patient's outcome on survival;
- Assessing the differential expression, at mRNA and protein levels, of SIN3B variants in a panel of human melanoma cell lines and melanocytes;
- Generating *SIN3B* depleted cells using CRISPR-Cas9 to gain insights on gene function and cellular dependencies;
- Investigating genes and pathways differentially modulated by *SIN3B* deletion using RNA sequencing;
- Performing a genome-wide CRISPR dropout screen to identify *SIN3B* synthetic lethal partners and their common pathways.

4. MATERIALS AND METHODS

4.1. Cell culture

Primary melanocytes were isolated from donated foreskin samples at the University of São Paulo Hospital (CEP/HU-USP 943/09, SISNEP CAAE 0062.0.198.000-9) as approved by the local ethics committee (CEP/FCF-USP 534). They were isolated and cultivated according to the protocol previously described by our group.[139]

A panel of melanoma cell lines harboring different mutations (mutational landscape shown in Table 1) were used.[138; 140] SKMEL28, SKMEL29, UACC62, A2058, and their resistant counterparts cells (cells resistant to BRAF inhibitor Vemurafenib), as well as SKMEL103, SKMEL147, SKMEL173, A2058, and UACC257 cells were routinely grown in Dulbecco's modified Eagle's (DMEM) medium supplemented with 10% fetal bovine serum (FBS, Gibco). Conversely, A375 and WM164 melanoma cells were grown in RPMI medium supplemented with 10% FBS. Other WM9, WM35, and WM793 cells were cultivated in a 4:1 mixture (v/v) of MCDB153 and Leibovitz's L-15 with 2% of FBS, insulin 5 µg/mL and $CaCl_2$ 1,6 mM. All media contained antibiotics (100 U/ml of penicillin and 100 µg/ml of streptomycin), and all cells were incubated at 37°C, 5% CO2. *BRAF*-resistant cells were generated during treatment with increasing Vemurafenib (BRAF inhibitor, Zelboraf, PLX4032/RG7204, Daiichi Sankyo/Roche, Japan) doses for 4-6 weeks until colonies were isolated. They were cultivated in with medium containing the inhibitor at the following concentrations: 3 µM for WM164R, 4,5 µM for A375R and 6 µM for SKMEL28R, SKMEL29R, and UACC62R.

All cultures were regularly tested and confirmed negative for *Mycoplasma spp.* infection. PCR (polymerase chain reaction) with specific primers for *Mycoplasma* detection were used (sense - 5' GGC GAA TGG GTG AGT AAC ACG 3' and antisense - 5' CGG ATA ACG GTT GCG ACC TAT 3'). In addition, all cells were authenticated and confirmed to have STR profiles (short-tandem repeat profiling) equivalent to those published in the literature.

Table 1. Melanoma cell lines and their respective mutational profiles, regarding the two major mutated genes *BRAF* and *NRAS*

		Mutational profiles	
Cell line	**Disease**	**NRAS**	**BRAF**
WM35	Primary (RGP)	WT	p.V600E (heterozygous)
WM793	Primary (VGP)	WT	p.V600E (heterozygous)
SKMEL28P	Metastatic	WT	p.V600E (homozygous)
SKMEL28R	metastatic	WT	p.V600E (homozygous)
SKMEL29P	metastatic	WT	p.V600E (homozygous)
SKMEL29R	metastatic	WT	p.V600E (homozygous)
UACC62P	metastatic	WT	p.V600E (homozygous)
UACC62R	metastatic	WT	p.V600E (homozygous)
A375P	metastatic	WT	p.V600E (homozygous)
A375R	metastatic	WT	p.V600E (homozygous)
WM164P	metastatic	WT	p.V600E (heterozygous)
WM164R	metastatic	WT	p.V600E (heterozygous)
UACC257	metastatic	WT	p.V600E (heterozygous)
WM9	metastatic	WT	p.V600E (heterozygous)
A2058	metastatic	WT	p.V600E (heterozygous)
SKMEL103	metastatic	p.Q61R	WT
SKMEL147	metastatic	p.Q61R	WT
SKMEL173	metastatic	p.Q61K	WT

* Abbreviations: P (parental), R (resistant), WT (wild type), p.Q61R (substitution at position 61of glutamine Q to arginine R), p.Q61K (substitution at position 61 from glutamine Q to lysine K), p.V600E (substitution of valine V for glutamic acid E), RGP (radial growth phase), and VGP (vertical growth phase).

4.2. Assessing *SIN3B* variants mRNA and protein levels

4.2.1. Total RNA isolation

Total RNA was extracted from both melanoma cells and primary melanocytes using the RNeasy Plus Mini Kit (Qiagen, Hilden, Germany), following the manufacturer´s instructions. The density and purity of RNA were checked by measuring the 260/280 nm ratio through an ultraviolet light spectrophotometer (Nanodrop). The RNA quality was tested by Agilent Bioanalyzer, which generates an RNA integrity number (RIN), and only samples with a threshold RIN ≥ 8 were utilized in this project.

4.2.2. Reverse Transcription for complementary DNA (cDNA) synthesis

Reverse transcription was performed with the High-Capacity cDNA Reverse Transcription kit (#4368814, Applied Biosystems, CA, USA). 2 µg of each total RNA sample was added to 4 µl of RT Random primers, 4 µl of 10X RT Buffer, 1.6 µl of 25X 100 mM dNTP, 2 µl of transcriptase enzyme and 8.4 µl of nuclease-free water (i.e., 20µL of reaction for every 2 µg of RNA). This mixture was incubated in a thermocycler, in one step each of 25°C for 10 minutes, 37°C for 120 minutes, 85°C for 5 minutes and stored at 4°C. Finally, each cDNA produced was stored at -20°C before usage.

4.2.3. Semi-quantitative RT-PCR for determining the presence of different *SIN3B* transcripts

The cDNA sequences of each *SIN3B* splice variant were obtained using the Ensembl website (www.ensembl.org) to design specific primers for each transcript through the OligoPerfect primer designer tool (Thermo Fisher Scientific, Massachusetts, USA) [141]. All primers were screened for hairpins, dimer formation and target specificity by BLASTN against nr databank. Initially, each sequence was submitted to alignment by the Clustal Omega program[142; 143], and to better visualize the differences of type and number of nucleotides among the aligned sequences, the Clustal alignment was imported by the Jalview program (https://www.jalview.org/). Unique regions of each transcript were placed in the OligoPerfect tool, and primers for each isoform were obtained. Thus, the cDNAs from the splice variants were PCR-amplified using the previously designed primers (Table 2) and analyzed on 1% agarose gels. Table 3 presents the cycle conditions for the fragments' amplification

Table 2. Primer sequences of each *SIN3B* splice variant

Transcript	%GC	Sense	Pimer length (bp)	Tm (°C)	Sequence	Amplicon size (bp)
SIN3B 201	54.55	*forward*	22	60.96	CAAGGAGGTACTGAACGACACC	262
	66.67	*reverse*	18	62.75	GATCACCTCCGACGTGCC	
SIN3B 202	45.45	*forward*	22	60.17	AGCTTGACCATTGGACACTTCT	353
	66.67	*reverse*	18	62.75	GATCACCTCCGACGTGCC	
SIN3B 206	30.77	*forward*	26	60.87	AAAGCGTAATCCACATTTTAAGAATG	386
	47.62	*reverse*	21	60.12	TACCTGCACCAAGAGGAAATG	
SIN3B 208	55.56	*forward*	18	61.57	TCAGCAAACTCTGGCCCA	243
	57.89	*reverse*	19	60.75	GAGGAACTTGCAGATCCGG	
SIN3B 209	60.28	*forward*	19	60.28	TGAGCAGCTGACTTCCCAG	684
	59.85	*reverse*	21	59.85	TGGTCACAAAAACAATCACCAA	

Table 3. PCR steps and conditions for the amplification of different SIN3B transcripts

	Initial denaturation	Denaturation	Annealing	Extension	Final extension
Temperature	98°C	98°C	64°C	72°C	72°C
Time	2 minutes	15 seconds	30 seconds	2 minutes	10 minutes
Cycles	1	25			1

4.2.4. Gene expression analysis by qPCR

Quantitative PCR (qPCR) reactions to analyze differential *SIN3B* mRNA expression were carried out with two primers: Hs01006373_m1 and Hs01006369_m1 (Figure 10). Human *SIN3B* has five protein-coding transcripts containing histone deacetylase interacting domains (HID) and paired amphipathic helices (PAH). Hence, these two primers were used to quantify the variants' expression, i.e., those containing PAH domains (Hs01006369_m1, Applied Biosystems, CA, USA) and those with HID domains (Hs01006373_m1, Applied Biosystems, CA, USA). This allowed us to infer whether there were quantitative differences in mRNA levels

of the *SIN3B* splicing variants. A primer for the housekeeping gene *ACTB* (beta-actin, Hs01060665_g1, Applied Biosystems, CA, USA) was also used for normalizing the interest gene. All primers were from Taqman® assays (Thermo Fisher Scientific, Massachusetts, USA). Real-time PCR was performed using the StepOne Plus Real-Time PCR System (Applied Biosystems, CA, USA) in Prof. Jorge Luiz de Mello Sampaio's laboratory (Faculty of Pharmaceutical Sciences, University of São Paulo). Experiments were conducted in biological triplicates, each with its respective technical triplicate, under the following qPCR conditions: a cycle of 50°C for 2 minutes, initial denaturation with one cycle of 95°C and 40 cycles with denaturation at 95°C for 15 seconds and primer annealing and extension at 60°C for 60 seconds. Additionally, a pool of cDNAs from all cells was employed to determine primers' efficiency in qPCR reactions. All primers' amplification efficiency was around 96% to 106%.

Data were generated by the StepOne software 2.0 (Applied Biosystems). Relative *SIN3B* mRNA levels in melanoma cell lines were calculated using melanocytes as control cells. Analyses were assessed through the comparative Ct (cycle threshold) method, also known as the $2^{-\Delta\Delta Ct}$ [144]. This method assumes that PCR efficiency of both target gene (*SIN3B*) and internal gene control (*ACTB*) is close to one, and it is represented by the following equation:

$$Fold\ change = 2^{-\Delta\Delta Ct}$$

$$2^{-\Delta\Delta Ct} = [(C_T\ SIN3B - C_T\ ACTB)melanoma\ cells - (C_T\ SIN3B - C_T\ ACTB)melanocytes$$

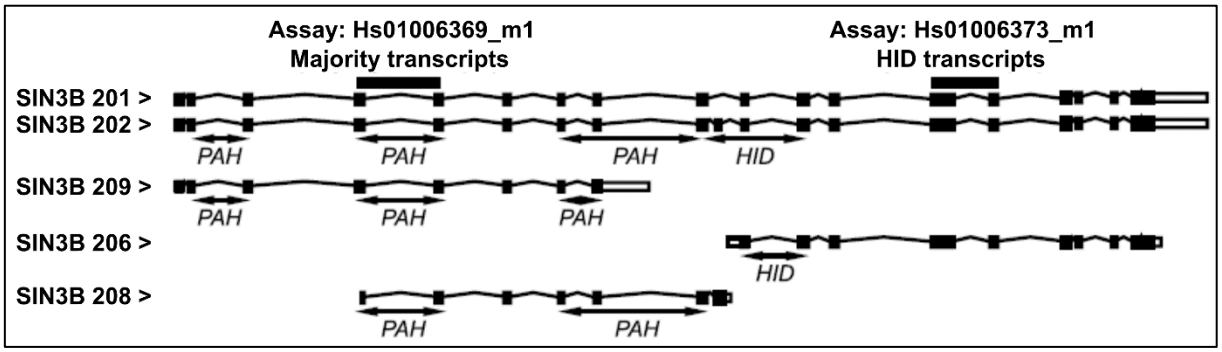

Figure 10. Schematic of specific human transcripts measured by two different *SIN3B* qPCR gene expression assays. Human *SIN3B* is alternatively spliced to produce different protein-coding transcripts containing PAH and HID domains. *SIN3B* expression was analyzed using the Hs01006373_m1 and Hs01006369_m1primers.
Source: Adapted from Faherty, N. et al, 2016.[131]

4.2.5. Protein extraction and Western Blotting

Protein isolation:

SIN3B protein expression was investigated in parental and resistant melanoma cells and primary melanocytes. Cells were washed twice with ice-cold PBS (phosphate-buffered saline) and lysed with 1X RIPA buffer (50 mM Tris pH 8.0, 150 mM NaCl, 0.5% sodium deoxycholate, 1.0% NP-40, 0.1% SDS and 1mM of EDTA), with 1:10 (v/v) of protease inhibitor cocktail (complete protease inhibitor cocktail, Sigma,), 1:100 (v/v) of phosphatase inhibitor (Sigma), pepstatin (1mg/mL), leupeptin (1mg/mL), aprotinin (1mg/mL), 1mM sodium orthovanadate, 25mM sodium fluoride and 1mM PMSF. The volume of lysis solution was dependent on cell number/plate. Cells were incubated on ice for 5-10 minutes, then scraped and transferred to Eppendorfs. Samples were centrifuged at 14,000g for 30 minutes at 4°C. The supernatant was transferred to fresh Eppendorfs and stored at -80°C. Protein lysates were quantified using the Pierce™ BCA Protein Assay Kit (#23225, Thermo Fisher Scientific, Massachusetts, USA), as instructed by the manufacturer's protocol.

Immunoblot analysis:

20 µg of total protein was subjected to 4-20% polyacrylamide (#4561094, Mini-PROTEAN TGX, Biorad, California, USA) gradient gel electrophoresis and subsequently transferred to PVDF membranes. The membranes were blocked with 3% bovine serum albumin (BSA) dissolved in Tween 20 TBS buffer (50 mM Tris-HCl pH 7.6, 150 mM NaCl, and 0.1% Tween 20) for 1 hour at room temperature. Primary antibodies were incubated overnight at 4°C on a shaker. The antibodies used were for SIN3B (1:200, Santa Cruz Biotechnology – sc13145, mouse) and beta-actin (1:1000, Abcam – ab8227, rabbit). After that, membranes were incubated with secondary antibodies at room temperature for 1 hour. Finally, protein bands were detected by ECL (enhanced chemiluminescence system, #WBLUF0100, Millipore, Massachusetts, USA) before reading on ImageQuant™ LAS 4000. The blots were quantified using the ImageJ program (NIH - National Institute of Health).

4.3. Generation of isogenic control and *SIN3B* knockout clones

4.3.1. Designing *SIN3B* gRNAs

Different guides were designed in the first conserved functional PAH domain, located between exons 2 and 3 of the human *SIN3B* gene. The cDNA sequence corresponding to the domain was obtained from the Ensembl database (www.ensembl.org) and inserted in the online platform CRISPR Design (www.crispr.mit.edu). Three different gRNAs with the highest score for on-target activity and at least three mismatches for any off-target of predicted coding genes in the genome were selected. The following oligonucleotides (forward and reverse) were synthesized for cloning as described in Table 4.

Table 4. Oligonucleotides for generating *SIN3B*-depleted melanoma cell lines

	Guide	Sense	Sequence
GUIDE 1	CTCCAGGAGTATCGATGCTC **TGG**	*forward*	CACCGCTCCAGGAGTATCGATGCTC
		reverse	AAACGAGCATCGATACTCCTGGAGC
GUIDE 2	GACCAGGTGAAGATCCGCTT **TGG**	*forward*	CACCGACCAGGTGAAGATCCGCTT
		reverse	AAACAAGCGGATCTTCCACCTGGTC
GUIDE 3	AGAAGACGCCCTCACCTATC **TGG**	*forward*	CACCGAGAAGACGCCCTCACCTATC
		reverse	AAACGATAGGTGAGGGCGTCTTCTC

4.3.2. Cloning of *SIN3B* gRNAs

Synthesized gRNAs (OligoPerfect primer designer tool, Thermo Fisher Scientific, Massachusetts, USA) were resuspended in nuclease-free water to a final concentration of 100 µM, 1 µL of each forward and reverse oligonucleotides were added to a mixture with 7 µL of water and 1 µL of T4 DNA ligase buffer (#M0202S, NEB, New England Biolabs, Massachusetts, USA). The reaction was incubated for 30 minutes at 37°C, followed by 5 minutes at 95°C and a gradual reduction in temperature, at a 5°C per minute ratio up to 25°C.

Annealed oligonucleotides were cloned into the linearized lentiCRISPRv2 empty backbone (#52961, Addgene, Massachusetts, USA), a lentiviral vector-based CRISPR-Cas9 delivery[145], through a mixture of 1 µL of the annealed oligonucleotides (1:100 dilution), 2 µL of buffer for T4 ligase, 2 µL of T4 ligase and 15 µL of water, incubating at 4°C overnight. Previous digestion of the lentiCRISPRv2 plasmid was carried out with the BsmBI enzyme (#R0739, NEB, New England Biolabs, Massachusetts, USA) at 55°C for 2 hours. Competent bacterial cells of *Escherichia coli* XL1-Blue were transformed by heat shock, and the clones expanded. DNA from four colonies was sent for Sanger sequencing (hU6-F 5'-GAGGGCCTATTTCCCATGATT-3' sequencing primer) at the Human Genome and Stem Cell Research Center (University of São Paulo, https://genoma.ib.usp.br/en) to confirm proper gRNAs insertion (Figure 11).

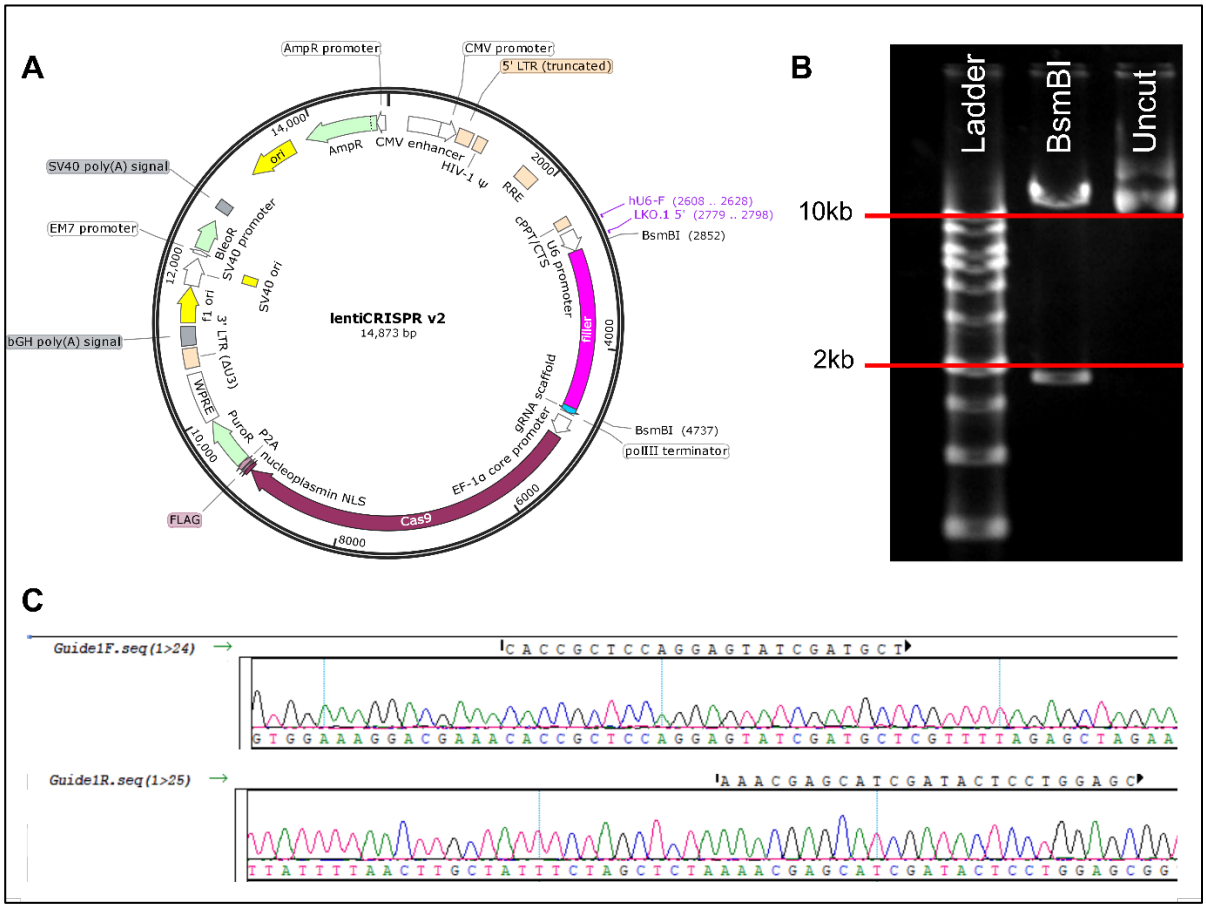

Figure 11. **Cloning *SIN3B* gRNAs into lenticrisprv2 empty backbone. A)** Plasmid map showing the empty lenticrisprv2 backbone. The *SIN3B* gRNAs were ligated downstream of the U6 promoter into the gRNA scaffold. **B)** Product sizes of vector digestion with BsmBI enzyme on an 1% agarose gel. A filler of approximately 1,8kb was removed. **C)** Schematic of Sanger sequencing results for one of the *SIN3B* gRNAs. It is possible to notice that the oligonucleotides (forward and reverse sequences) are present within the cloned plasmid. Similar results were found for the other two *SIN3B* gRNAs.
Source: Adapted from Addgene[146]

4.3.3. Pooled or single-cell clones post CRISPR editing

A common approach to understanding a gene function is to probe the phenotype of a cell in which a particular gene is lost. This can be achieved by CRISPR-Cas9, as previously discussed in earlier sections. Nevertheless, typically only a minority of cells are successfully edited, and a pooled cell population with variable modifications is generated after CRISPR-mediated repair mechanisms. Thus, this mixed population possesses several genetic and phenotypic alterations prior to single-cell isolation. Consequently, producing multiple knockout clones in independent cell lines and control clones derived under similar conditions could be a proper strategy to address unexpected results due to population heterogeneity and clonal variability.[147; 148]

Delivery of CRISPR-Cas9 to the cells is commonly conducted via viral or chemical vectors. Virus-mediated transduction transfers plasmid DNA into host cells using viruses (very often lentiviruses), which penetrate the nuclear envelope during cell division. Hence, with this approach, the CRISPR machinery is integrated into the host genome. Conversely, chemical transfection uses lipid vesicles that encapsulate the plasmid DNA to be introduced to the cells through endocytosis.[149; 150] Therefore, chemical transfection of the CRISPR components is effective for proliferative and easy-to-transfect cells and may lead to more minor off-target effects, commonly associated with constitutive Cas9 expression in stably-transduced cells.[151]

Therefore, we employed in this project both transduction and transfection of the CRISPR machinery into high *SIN3B*-expressing melanoma cell lines and addressed the advantages of selecting single CRISPR-edited clones to evaluate the effects of loss of *SIN3B* function in melanomas. The protocols are described in the following sections.

4.3.3.1. First protocol: Polyclonal generation of *SIN3B*-depleted melanoma cells

Lentivirus production:

This first protocol was used before successfully generating isogenic *SIN3B* knockout clones, as will be discussed in the following sections. All values given are related to lentivirus production in a 10cm dish (Table 5). All lentivirus worked as approved by the local ethics committee, n°7.125/20).

HEK293FT cells were cultured in DMEM supplemented with 10% heat-inactivated FBS (Gibco), 0,1 mM MEM non-essential amino acids, 1mM sodium pyruvate, and 2 mM L-glutamine, at 37°C, 5% CO_2, in a humidified incubator. These exponentially growing cells were seeded at a density of 4,5. 10^6 /10cm dish, and the following day, the medium was aspirated and replaced with 9mL DMEM containing chloroquine (final concentration of 25 µM) prior to transfection. Cells were transfected by calcium phosphate-DNA precipitation method[152].This protocol introduces plasmid DNA to cultures via a precipitate that attaches to the cell surface. This precipitate is produced due to slowly mixing a HEPES-buffered saline solution with another containing calcium chloride and DNA.

Transfer vector lentiCRISPRv2 (#52961, Addgene, Massachusetts, USA) with or without *SIN3B* gRNAs, packaging plasmids (pRSV rev, pMDLg/pRRE, and pHCMV-G, kindly donated by Professor Marisol Soengas, SNIO, Spain), and a reporter plasmid for GFP (green fluorescent protein) detection (pEGFP) were added to 500 µL of 0.25M calcium chloride solution. Subsequently, 500 µl of 2X HEPES (HBS) buffer (280 mM NaCl, 1.5 mM Na2HPO4, and 50 mM HEPES, pH 7.0) was introduced dropwise to the transfection mixture while being vortexed. HEK293FT cells were incubated with the combination of medium, 25 µM chloroquine, and transfection blend for six hours, and the cultures were replaced with 9mL of new complete medium. After 48 hours, virus supernatant was collected and filtered with a 0.45 µm low protein-binding filter (#SLHP033RS, Merck Millipore, Massachusetts, USA). Aliquots were stored at - 80°C and frozen for at least 2 hours before being used in experiments.

Table 5. Composition of lentiviral transfection complex

Reagent	Volume / Amount
DMEM complete medium	9 mL
lentiCRISPRv2 (empty vector or clones with *SIN3B* gRNAs)	8 µg
pRSV rev	3 µg
pMDLg/pRRE	3 µg
pHCMV-G	3 µg
0.25M calcium chloride solution	500 µL
2X HEPES (HBS) buffer	500 µL

Lentivirus stable transduction:

The lentiCRISPRv2 plasmid expressing Cas9, gRNAs, and puromycin resistance was packaged into a lentivirus (Section 4.3.3, previous topic). Hence, for lentiviral transduction, metastatic human melanoma cells with high *SIN3B* were selected (WM164P, Section 4.1). Approximately 10^5 of each cell line was seeded in 6-well plates, and after 24 hours, transduced with 1:6 (v/v) of virus and medium ratio, containing 10 µg/ml of polybrene. In both cases, cells with no lentivirus were plated in parallel as controls for antibiotic selection. After 48 hours post-transduction, 2 µg/ml puromycin was added (#ant-pr-1, InvivoGen, California, USA). Complete death in the control plate confirmed successful puromycin selection. All melanoma cells were continuously cultured in puromycin to ensure high Cas9 activity. *SIN3B* knockout was confirmed through protein detection (Section 4.2.5).

4.3.3.2. Second protocol: Generation of isogenic *SIN3B* depleted cells

Three metastatic melanoma cell lines (SKMEL28, A375, and A2058) were cultivated in 6-well plates at a density of 10^5 cells/well. The next day, cells were transiently transfected with 2.5 µg of empty lentiCRISPRv2 plasmid, as a control, or 2.5 µg of the vector with Guide 2 (Section 4.3.1), using 1:3 (v/v) DNA/lipofectamine ratio (#15338100, Lipofectamine LTX, Thermo Fisher Scientific, Massachusetts, USA), according to the protocol provided by the manufacturer. For each condition, transfections were performed in triplicate. After 24 hours post-transfection, cells were selected with a medium containing 2 µg/ml puromycin for 72 hours. All cells were kept in puromycin and diluted to 400 cells/10cm dish so that isolated colonies were formed, and each clone subcultured in T75 flasks for expansion. *SIN3B* knockout was confirmed through Western Blotting (Section 4.2.5) and next-generation sequencing.

4.3.4. Next generation sequencing to identify targeted modifications

This protocol describes the process of identifying the insertion-deletion (indel) variants generated by the *SIN3B* gRNA-mediated double-strand break. A two-step PCR approach was applied to amplify amplicons surrounding the putative Cas9 cut site. Results were analyzed through the MiSEQ 150pb paired-ending platform (Illumina, Foster City, CA, USA).

David Fraser from the Gene Editing Team at Wellcome Trust Sanger Institute kindly performed each step, and a schematic representation is shown in Figure 12. Briefly, all *SIN3B* knockout and control clones were harvested, and genomic DNA was isolated using Gentra Puregene Cell Kit (#1048146, Qiagen, Hilden, Germany) according to the manufacture´s protocol. Libraries were made with a two-step PCR protocol. First, the target genomic site was amplified with KAPA PCR Reaction Mix (Roche), and the locus-specific primers (F: forward and R: reverse):

F: 5'-GGAACCCATCTTCTGGACCC-3’
R: 5'-AATCCCCCACAAAGCTCCACA-3'

Indexing of the PCR product (Table 6) was performed using a pair of primers containing Illumina append sequences (adaptor sequences in red):

F: 5'-ACACTCTTTCCCTACACGACGCTCTTCCGATCTTTCCCCTCAGGGACCCC-3'
R: 5'-TCGGCATTCCTGCTGAACCGCTCTTCCGATCTGTCCCCTGAGGTGGAGAG-3’

Samples were sequenced on MiSEQ (Illumina, Foster City, CA, USA) at the DNA pipelines operations center located at the Wellcome Trust Sanger Institute. Following sequencing reads were aligned to reference SIN3B genomic DNA sequence and examined for the presence of CRISPR-mediated indels.

Table 6. Summary of PCR conditions for targeted site amplification and addition of sequencing adaptors

Initial denaturation	**Denaturation**	**Annealing**	**Extension**	**Denaturation**	**Annealing**	**Extension**	**Extension**
95°C 3 minutes	98°C 20 seconds	68°C 15 seconds	72°C 30 seconds	98°C 20 seconds	60°C 15 seconds	72°C 30 seconds	72°C 1 minutes
1	8			23			1

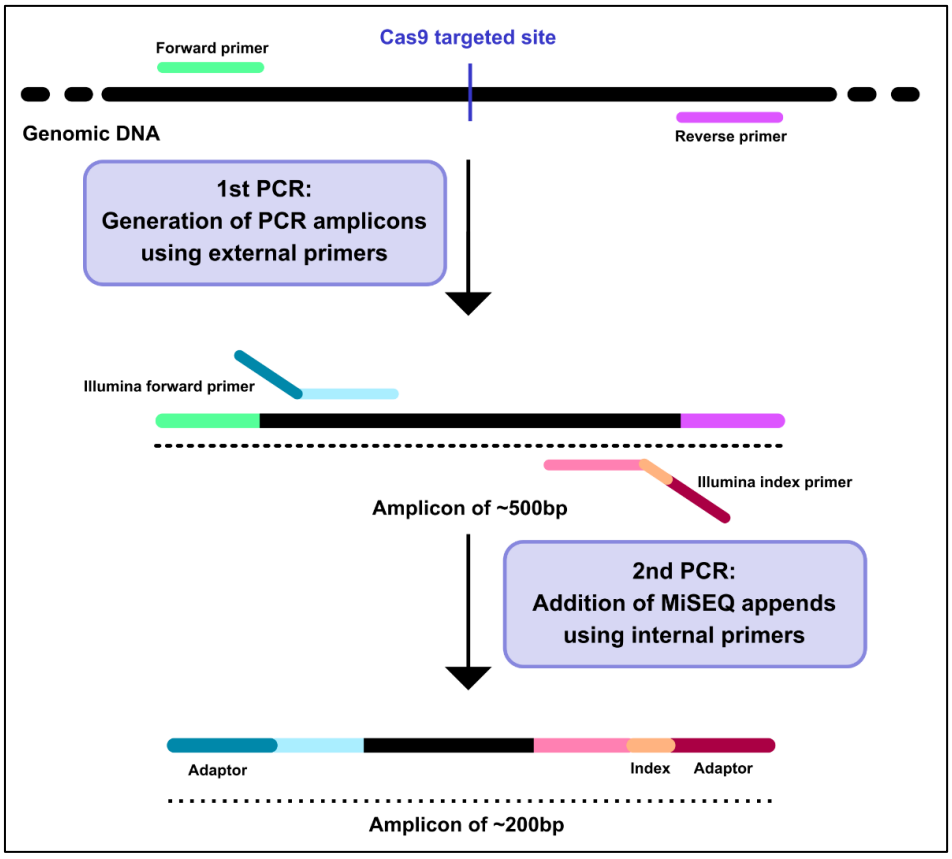

Figure 12. Illustration of the two-step polymerase chain reaction (PCR) approach, and high-throughput sequencing to identify insertions or deletions of nucleotides in *SIN3B* knockout melanoma clones. The first PCR reaction provides the targeted DNA region, generating an amplicon used for a second PCR, to add sequencing adaptor sequences and indexes, allowing multiplexing of samples.

4.4. Functional analyses

4.4.1. Protein expression analysis of resistance and epithelial-mesenchymal transition markers

Initial analysis on protein expression of epithelial-mesenchymal transition and resistance markers was applied in the heterogeneous population of cells post-CRISPR-based *SIN3B* knockout. In addition, the expression of *BMI1*, a known repressor of *SIN3B*, whose upregulation induces increased tumor invasion, and resistance was also evaluated.[133; 153] All samples were run under reducing conditions, as previously described in Section 4.2.5. Staining was conducted with the primary antibodies for *AXL* (1:500, ab77773, Abcam, 98 KDa), *MITF* (1:500, ab12039, Abcam, 59 KDa), *ERK* (1:1000, #9102, Cell Signaling, 42-44 KDa), *p-ERK* (1: 1000, #9101, Cell Signaling, 42-44 KDa), Vimentin (1:1000, #5741, Cell Signaling, 57 KDa), *BMI1* (1:1000, 05-367, Millipore, 40-44 KDa), E-cadherin (1:1000, #5296, Cell

Signaling,, 135KDa), *N-cadherin* (1:1000, #13116, Cell Signaling, 140 KDa) and *Beta-actin* (1:2000, Abcam - ab8227, 42 KDa). Protein bands were detected by ECL enhanced chemiluminescence system (#WBLUF0100, Millipore, Massachusetts, USA).

4.4.2. Cell growth assays

SIN3B knockout and control cells were seeded in biological triplicates in 24-well plates at a density of 1.10^4 cells per well. Cells were counted after 24, 72, 120, and 168 hours using a hemocytometer stained with 0,4% trypan blue dye solution (#T6146, Sigma-Aldrich, St. Louis, MO, USA). Total cell number was recorded and plotted on GraphPad Prism.

4.4.3. Clonogenic assays

A375 (400 cells/dish), A2058 (600 cells/dish), SKMEL28 (600 cells/dish) and WM164 (600 cells/dish) melanoma cells were plated in 35 mm dishes (Corning). The medium was replenished every 2-3 days, and after 14 days, all cultures were washed with PBS, fixed, and stained with a crystal violet solution containing methanol (0,5% crystal blue, 50% methanol, and 49,5% Milli-Q water). A scanner imaged plates, and the number of colonies was determined from ImageJ software (http://rsbweb.nih.gov/ij/).

4.4.4. Boyden chamber migration and invasion assays

The Transwell polycarbonate membranes coated with Matrigel (8 µm inserts, #354480, Corning, New York, USA) or without Matrigel (8 µm inserts, #353097, Corning, New York, USA) were used respectively for invasion and migration analyses. In summary, both control and *SIN3B* depleted cells were harvested, and 1.10^5 cells in FBS-free medium were introduced to each insert. High concentration serum media (20% FBS) were added to the outside (bottom) of the well to encourage migration or invasion. The 24-well plates were incubated at 37°C for 24 hours. Migrated or invaded cells were fixed in 95% ice-cold methanol and stained with Giemsa solution (1:10 dilution in deionized water, #GS500, Sigma, Missouri, USA) for 1 hour. Cells were imaged under an inverted microscope, and ten independent fields were used for quantification using ImageJ software (http://rsbweb.nih.gov/ij/).

4.4.5. Statistical analysis

Data are presented as means ± standard deviation, and Graphpad Prism software was used for plotting graphs and performing statistical analysis. For a two-group comparison, a two-tailed unpaired t-test or one-way ANOVA with Tukey-Kramer multiple comparisons was employed. Results were considered statistically significant with $p<0.05$. Significant differences between groups (control and *SIN3B* knockout) were designated by *** and ### $p<0.001$, ** and ## $p<0.01$, * and # $p<0.05$.

4.5. Bioinformatics analyses

4.5.1. Analysis of human melanoma tumor samples from the Cancer Genome Atlas (TCGA)

Bioinformatics analyses were performed using the TCGA (The Cancer Genome Atlas) dataset of the NIH (National Institute of Health) containing samples from patients with melanoma. Briefly, RNA sequencing data from 448 melanoma samples (TCGA PanCancer Atlas, SKCM – Skin Cutaneous Melanoma), sequenced through Illumina platform (Illumina HiSeq) and previously normalized (RSEM values), were extracted from the public site cBioPortal (https://www.cbioportal.org/), hosted by the Memorial Sloan Kettering Cancer Center[154]. In addition, clinical details such as patients' age and disease stage were also acquired through the same portal. According to the American Joint Committee on Cancer classification, graphs were generated to assess SIN3B gene expression among patients with different melanoma stages. All samples were sorted based on the median of expression values, using R computing environment (version 4.0.3, http://www.R-project.org), with tidyverse, ggplot2 and RColorBrewer packages.

Conversely, UCSC Xena was used (http://xena.ucsc.edu/), to compare the expression of *SIN3B* and its transcripts in normal and tumor tissue samples. It consists of an open-access portal for the scientific community that uses the TCGA and GDC (Genomic Data Commons) databases to relate genomic data with phenotypic variables.[155] Similarly, expression of the *SIN3B* variants in primary and metastatic melanomas was also assessed with TCGA data, in collaboration with Mariana Boroni, from the Brazilian National Institute of Cancer (INCA). Finally, a doctoral student Roy Rabbie, from Dr. David Adams' group at the Wellcome Trust

Sanger Institute (Cambridge, United Kingdom) produced Kaplan-Meier survival curves through samples from patients with metastatic melanoma, discriminating between groups with high or low *SIN3B* levels. Log-rank statistical test was performed with p-value = 0.021.

4.5.2. Transcriptome sequencing and data analysis

Total RNA was extracted from control (transfected with empty lentiCRISPRv2 plasmid) and *SIN3B* knockout clones (containing *SIN3B* sgRNA) of three different melanoma cell lines (SKMEL28, A375, and A2058) as described in Section 4.2.1. Multiplex sequencing libraries were generated from TruSeq Stranded total RNA (Illumina), pooled, and sequenced across multiple lanes on NovaSeq 6000 (Illumina). Paired-end 100 bp reads were aligned and mapped to the CRCh38 reference genome with STAR (via Canapps version 2.5.0).[156] Read counting was performed using htseq-count from the HTSeq package. Differential gene expression analysis was handled with DESeq2 (version 1.30.1)[157] in R (version 4.0.3). After Benjamin-Hochberg correction, genes with an adjusted p-value of < 0.01 and $\log_2$ fold change ≥ 1 or ≤ -1 were considered significantly differentially expressed. Gene Ontology (GO) enrichment analysis was executed to find common GO terms of the differentially expressed genes, applying Gostats (version 2.56.0). For KEGG (Kyoto Encyclopedia of Genes and Genomes) pathway analysis, enriched pathways were visualized by pathview package (version 1.30.1).[158] List of differentially expressed genes is present in Appendix A.1.

4.6. Genome-wide CRISPR-Cas9 screening in *SIN3B* isogenic melanoma clones

4.6.1. Lentivirus production

HEK293T cells were employed for the lentivirus production of either the genome-wide library or transfer vectors used in the Cas9 activity test. These cells were cultured in an IMDM medium (#12-722F, Lonza, Basel, Switzerland) supplemented with 10% FBS and incubated at 37°C, 5% CO_2. Cells were seeded at 18.10^6 cells per T150 flask for 24 hours before transfection. After that, the medium was replaced with 12,6 mL Opti-MEM™ (#31985062,Gibco, Thermo Fisher, Massachusetts, USA). The transfer vector and packaging plasmids (pMD2.G, #12259 and psPax2, #12260, Addgene, Massachusetts, USA) were diluted in 7,4 mL Opti-MEM™. Next, PLUS™ reagent (#15338100, Thermo Fisher, Massachusetts)

was added to the mixture, and after 5 minutes, Lipofectamine™ LTX (#15338100, Thermo Fisher, Massachusetts, USA) was introduced to the solution. The lipofectamine-DNA complex was assembled for 30 minutes, then carefully moved to the cultures dropwise. Virus supernatant was collected after 30 hours, filtered utilizing a 0,45 µm filter (# SLHO033RS, Merck/Millipore, Massachusetts, USA), and kept at -80°C prior to usage.

Table 7. Composition of reagents for lentivirus production in T150flasks

Reagent	Volume / Amount
OptiMem	7.4 ml
Transfer vector	7.4 ug
psPax2	18.26 ug
pMD2.G	3.95 ug
PLUS reagent	29.6 ul
Lipofectamine LTX	88.8 ul

4.6.2. Assessment of Cas9 activity

Cas9-expressing cells are necessary to perform a CRISPR screening effectively. Therefore, control and *SIN3B* knockout clones from the easily transducible A375 cells were used to assess Cas9 activity since they already carry the endonuclease expression due to the previous transfection lentiCRISPRv2 plasmid (Section 4.3.2). Two vectors were employed to test clonal Cas9 efficiency: one expressing BFP and GFP (control, #67979, Addgene, Massachusetts, USA) and another expressing BFP, GFP, and a gRNA targeting GFP (reporter, #67980, Massachusetts, USA).

The clones (1.10^5 cells/well seeded in 6-well plates) were transduced in suspension with 200 µL lentivirus (8 µg/mL polybrene), carrying either the control or reporter vector. A completely fresh medium was introduced the following morning. After 48 hours, cells were detached and fixed with 100 µL of 4% paraformaldehyde (#F8775, Sigma, Missouri, USA) for 15 minutes. Afterward, cells were washed with PBS and analyzed using flow cytometry (BD Fortessa II) with BD FACSDiva™ software. Expression of BFP was detected using 405 nm excitation and 450/50 filter, whereas BFP was collected with 488 nm of excitation wavelength and 530/20 bandpass filter. Data analysis was conducted using FlowJo v.10, and Cas9 activity

was measured by the percentage of BFP+/GFP- cells, considering that the GFP gRNA switched off GFP expression. A minimum Cas9 activity of 90%was required for all clones.

4.6.3. Genome-wide library titration

The Neo-IRES gRNA library was kindly provided by David Adams from the Wellcome Trust Sanger Institute. This library was modified from Kosuke Yusa´s genome-wide library to acquire neomycin resistance and an internal ribosomal entry site (IRES) downstream the neomycin gene, to separate two coding regions. This library contains 101,090 gRNAs targeting 18,009 genes from the human genome (backbone in Figure 13). The idea was to use an unbiased approach to identify synthetic lethal partners with the *SIN3B* gene on a genome-wide scale.

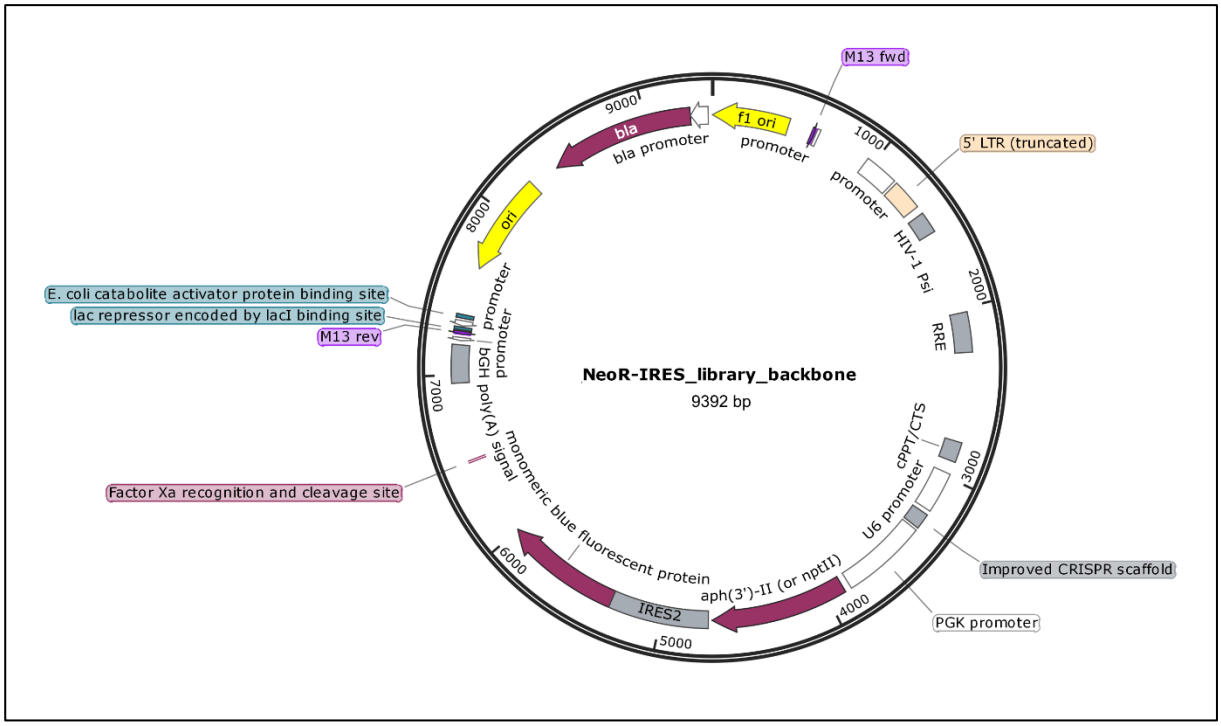

Figure 13. Map of the NeoR-IRES library backbone. This plasmid contains a neomycin resistance gene and BFP (blue fluorescent protein) marker for virus titration.

The library was packaged into lentivirus as described in Section 4.6.1. A375 Cas9 expressing cells (control and *SIN3B* knockout clones) were transduced with an MOI (multiplicity of infection) of 0,3 to secure each cell carrying a single gRNA[159], infected in suspension, and seeded in 6-well plates (1.10^5 cells/ well, 80% confluence). Polybrene at a final concentration of 8 µg/mL was included in each well. The library virus was titrated as indicated in Figure 14. After 48 hours, cells were fixed with 4% paraformaldehyde for 15 minutes and analyzed by flow cytometry (BD Fortessa II). Data analysis was carried on FlowJo v.10, and a

graph of the percentage of BFP positive cells versus volume of the virus was used to calculate the amount of library virus corresponding to an MOI of 0,3.

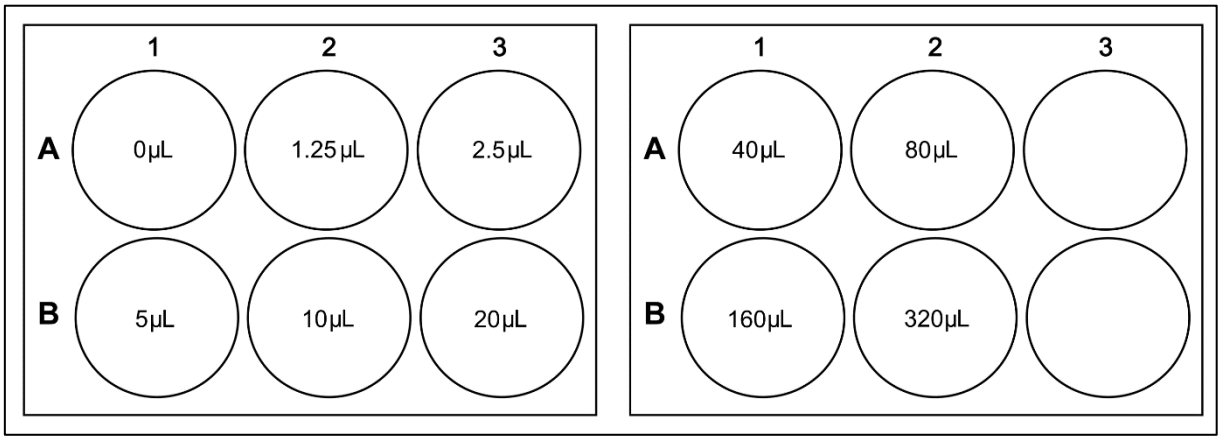

Figure 14. Schematic representation of library virus titration. Dilutions of cell-virus suspensions were added in 6-well plates. Virus volumes are indicate in each well.

4.6.4. CRISPR-Cas9 genome-wide screening in A375 melanoma clones

Each A375 Cas9-expressing clone (from two control clones or three *SIN3B* knockout clones) was cultivated before transduction with the genome-wide library, and three separate transduction replicates were set up (totalizing 15 replicates for all clones). For each replicate, 30 million cells were infected in suspension in three separate T150 flasks with the NeoR-IRES genome-wide library virus, at an MOI of 0,3. The next day, the medium was replaced for all flasks, and one T150 flask containing cells from each replicate was fixed with 4% paraformaldehyde. BFP expression was analyzed by flow cytometry (Section 4.6.3) to measure transduction rate. After 48 hours, successfully transduced cells were selected with neomycin at 1mg/mL (G418, geneticin, #10131027, Thermo Fisher, Massachusetts, USA) for five days and expanded in a 3-layer multi-flask (#353143, Falcon®, Corning, New York, USA) for two weeks. A library representation of at least 100x was maintained at all times (i.e., 100 cells per sgRNA). 15 million cells were harvested per replicate, and pellets were stored at -80°C until DNA extraction. A timeline of the screening is depicted in Figure 15.

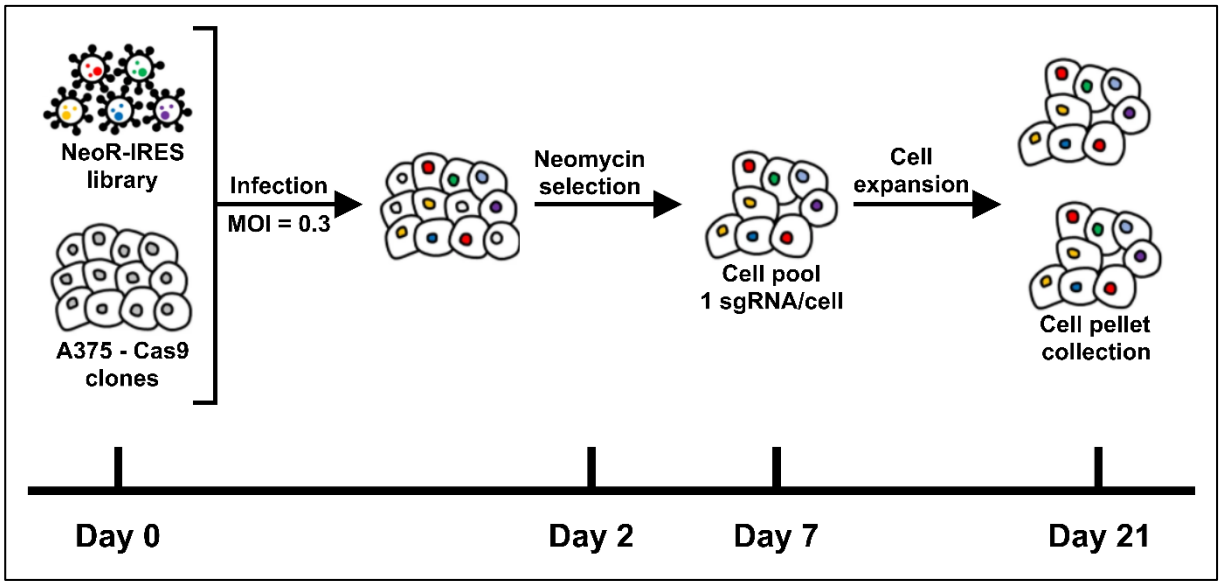

Figure 15. **Screening approach to identify *SIN3B* synthetic lethal targets.** A375 melanoma clones (control transfected with empty lentiCRISPRv2 vector or *SIN3B* knockout cells containing sgRNA for the gene) express Cas9. These clones were infected in suspension with the NeoR-IRES lentiviral library at an MOI of approximately 0,3. Transduced cells were selected with neomycin, followed by progressive expansion of cell cultures, totalizing 21 days of screening. The synthetic lethal candidates are those genes specifically essential in *SIN3B* knockout cells.
Source: Adapted from Wei, L. et.al.[160]

4.6.5. First round of PCR and product purification

Genomic DNA was isolated from pellets of 15 million cells for each screen replicate, using the Blood & Cell Culture DNA Maxi (#13362, Qiagen, Hilden, Germany). The first round of PCR was performed to amplify the gRNAs within each screen sample after the screening and the NeoR-IRES library plasmid to use as control later for sequencing analysis. Table 8 details all primers used for the amplification.

Table 8. Primer sequences used in first round of PCR

Primer Name	Sequence (5' – 3')
Neo PCR1 F'	ACACTCTTTCCCTACACGACGCTCTTCCGATCTCTTGTGGAAAGGACGAAACA
Neo PCR1 R'	TCGGCATTCCTGCTGAACCGCTCTTCCGATCTTATCTTGTTCAATGGCCGATC

Approximately 6,6 pg genomic DNA (gDNA) is presented in one cell.[161] Our library has approximately 100,000 gRNAs. Considering a 100x screening representation, we aimed at cultivating 10 million cells per replicate to maintain library representation. Thus, 66 µg of genomic DNA was required per replicate for PCR reactions. Typically, 2 µg gDNA is used per reaction, so we performed 33 PCR reactions for every sample. The same PCR conditions were

used for sequencing the library from plasmid DNA, except changing for 10 reactions and 15 ng DNA/reaction. The number of cycles and reagents used in PCR reactions are presented, respectively, in Table 9 and Table 10.

Table 9. First-round PCR steps for gRNA amplification

	Initial denaturation	**Denaturation**	**Annealing**	**Extension**	**Final extension**
Temperature	98°C	98°C	61°C	72°C	72°C
Time	30 seconds	10 seconds	15 seconds	20 seconds	2 minutes
Cycles	1	28			1

Table 10. Reagents for first round PCR reactions

Reagent	**Volume / Amount per reaction**
Genomic DNA	2 µg
2X Q5 Hot Start High-Fidelity Mix (New England Biolabs)	25 uL
Primer mix (10 µM for both forward and reverse)	1 uL
Nuclease-free water	Up to 50 uL

PCR products were run on a 2% agarose gel (200 V for 30 minutes) to ensure successful amplification (Figure 16). Finally, PCR products were purified using QIAquick PCR Purification Kit (# 28104, Qiagen, Hilden, Germany), according to the manufacturer´s protocol, and quantified using a fluorometer (Qubit, Thermo Fisher Scientific, Massachusetts, USA). Each product was diluted to 40 pg/µL in nuclease-free water.

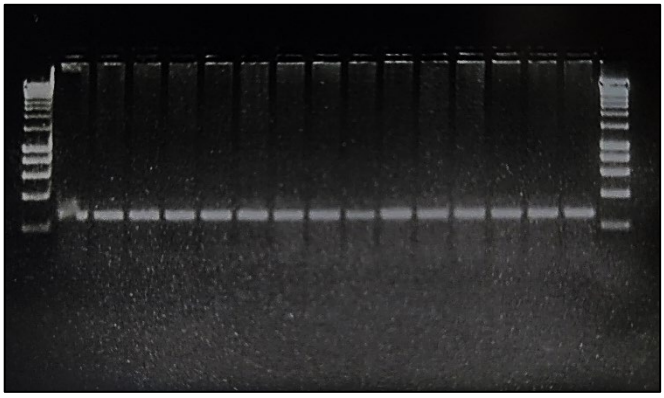

Figure 16. PCR products analysis by gel electrophoresis. gRNAs from 15 samples (control and *SIN3B* knockout clones screened in triplicate) were amplified by PCR reactions. Unique bands (approximately 300 bp) confirmed successful amplification.

4.6.6. Second round of PCR and product purification

The second round of PCR was completed to add sequencing tags to the first-round PCR products. Unique reverse primers (which are the sequencing tags) were added per sample. Thus, from our 15 samples, each one had a unique reverse tag primer. All primers are included in Table 11, and second-round PCR mixture and thermocycler conditions are presented, respectively, in Table 12 and Table 13.

Table 11. Primers' list for second-round PCR reactions

Primer Name	Sequence (5' – 3')
PE 1.0 F'	AATGATACGGCGACCACCGAGATCTACACTCTTTCCCTACACGACGCTCTTCCGATCT
iPCRtag 1	CAAGCAGAAGACGGCATACGAGATAACGTGATGAGATCGGTCTCGGCATTCCTGCTGAACCGC TCTTCCGATC
iPCRtag 2	CAAGCAGAAGACGGCATACGAGATAAACATCGGAGATCGGTCTCGGCATTCCTGCTGAACCGC TCTTCCGATC
iPCRtag 3	CAAGCAGAAGACGGCATACGAGATATGCCTAAGAGATCGGTCTCGGCATTCCTGCTGAACCGC TCTTCCGATC
iPCRtag 4	CAAGCAGAAGACGGCATACGAGATAGTGGTCAGAGATCGGTCTCGGCATTCCTGCTGAACCGC TCTTCCGATC
iPCRtag 5	CAAGCAGAAGACGGCATACGAGATACCACTGTGAGATCGGTCTCGGCATTCCTGCTGAACCGCT CTTCCGATC
iPCRtag 6	CAAGCAGAAGACGGCATACGAGATACATTGGCGAGATCGGTCTCGGCATTCCTGCTGAACCGC TCTTCCGATC
iPCRtag 7	CAAGCAGAAGACGGCATACGAGATCAGATCTGGAGATCGGTCTCGGCATTCCTGCTGAACCGC TCTTCCGATC
iPCRtag 8	CAAGCAGAAGACGGCATACGAGATCATCAAGTGAGATCGGTCTCGGCATTCCTGCTGAACCGC TCTTCCGATC
iPCRtag 9	CAAGCAGAAGACGGCATACGAGATCGCTGATCGAGATCGGTCTCGGCATTCCTGCTGAACCGCT CTTCCGATC
iPCRtag 10	CAAGCAGAAGACGGCATACGAGATACAAGCTAGAGATCGGTCTCGGCATTCCTGCTGAACCGC TCTTCCGATC
iPCRtag 11	CAAGCAGAAGACGGCATACGAGATCTGTAGCCGAGATCGGTCTCGGCATTCCTGCTGAACCGCT CTTCCGATC
iPCRtag 12	CAAGCAGAAGACGGCATACGAGATAGTACAAGGAGATCGGTCTCGGCATTCCTGCTGAACCGC TCTTCCGATC
iPCRtag 13	CAAGCAGAAGACGGCATACGAGATAACAACCAGAGATCGGTCTCGGCATTCCTGCTGAACCGC TCTTCCGATC
iPCRtag 14	CAAGCAGAAGACGGCATACGAGATAACCGAGAGAGATCGGTCTCGGCATTCCTGCTGAACCGC TCTTCCGATC
iPCRtag 15	CAAGCAGAAGACGGCATACGAGATAACGCTTAGAGATCGGTCTCGGCATTCCTGCTGAACCGC TCTTCCGATC

Table 12. Second-round PCR steps to include sequencing tags

	Initial denaturation	Denaturation	Annealing	Extension	Final extension
Temperature	98°C	98°C	66°C	72°C	72°C
Time	30 seconds	10 seconds	15 seconds	20 seconds	5 minutes
Cycles	1	8			1

Table 13. Reagents for second-round PCR reactions

Reagent	Volume / Amount per reaction
First-round PCR product (40 pg/µL dilution)	5 µL (200 pg)
2X KAPA HiFi HotStart Ready Mix (#KK2601, Kapa Biosystems, Basel,Switzerland)	25 uL
Primer mix (5 µM for both forward and reverse)	2 uL (1 µL forward and 1 µL reverse tag)
Nuclease-free water	18 uL

Approximately 31,5 µL of the post-PCR mixture (at a concentration of 2 ng/µL) was added to the AMPure SPRI beads solution (#A63880, Beckman Coulter, California, USA) at a ratio of 0,8:1 PCR product/beads, and incubated for 5 minutes at room temperature. All tubes were placed on a magnetic rack for 5 minutes to attach beads and the supernatant was discarded. Samples were washed twice with 200 µL of 80% ethanol for 30 seconds. Then, tubes were removed from the magnet and 35 µL of nuclease-free water eluted DNA. Tubes were placed back on magnet for 3 minutes and purified DNAs were transferred to clean microtubes. Ultimately, the Bioanalyzer automated electrophoresis system (Agilent) was used to attest correct amplification bands (300 bp) of clean DNA samples. All DNAs were kept as -20°C prior to sequencing.

4.6.7. Sequencing and data analysis

Single-end (19 bp) sequencing was performed on Illumina HiSeq 2500 (with the primer 5'-TCTTCCGATCTCTTGTGGAAAGGACGAAACACCG-3'). Fifteen samples (technical screen triplicate from two control clones and three *SIN3B* knockout clones) were multiplexed and run in four lanes. The NeoR-IRES genome-wide library was sequenced separately in another lane. After sequencing, reads were aligned to the gRNAs present in the library using a pipeline developed by the Wellcome Trust Sanger Institute sequencing support

facilities. Victoria Offord from David Adam´s group at Sanger kindly performed all analyses. List of enriched and depleted genes is disponible in Appendix A.2.

5. RESULTS AND DISCUSSION

5.1. *SIN3B* expression analyses using public databases

UCSC (University of California Santa Cruz) Xena (http://xena.ucsc.edu) is a high-performance visualization analysis tool containing large public databases, such as TCGA for cancer samples and GTEx (Genotype-Tissue Expression) that includes normal tissues. This platform allows researchers to interpret cancer genomics interactively, facilitating analysis of the numerous high-throughput sequencing results currently available. In gene expression analysis, comparison with normal and cancer samples is incredibly challenging due to differences in sample processing among the datasets. Therefore, both TCGA and GTEx resources were processed under the same bioinformatics pipeline in this platform, reducing batch effects which could potentially hinder analyses of interest.[162]

Hence, the web-based Xena browser was used to verify whether *SIN3B* levels are differentiated between normal skin and cutaneous melanoma, as shown in Figure 17. Expression values were normalized by the DESeq2 method, based on the ratio of counts for a gene in each sample to the geometric mean of each gene across all samples.[163]

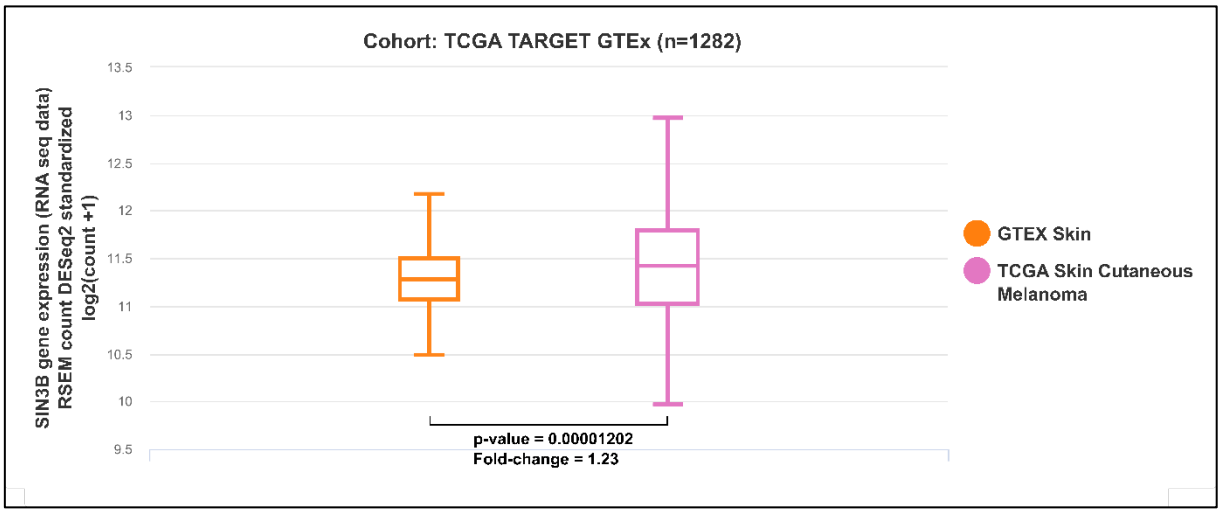

Figure 17. Result of SIN3B expression between normal skin (GTEx) and melanoma tumors (TCGA). Data were generated by the Xena browser portal and normalized by the DESeq2 package. The Welch test was employed, obtaining a p-value of 0.00001202. Thus, it is possible to observe an increase of *SIN3B* expression in cutaneous melanomas.
Source: Adapted from UCSC Xena.[164]

An increase of *SIN3B* levels in cutaneous melanoma samples was noted (p-value=0.00001202). Interestingly, considering that the human *SIN3B* gene possesses five

protein-coding splice variants (previously presented in Figure 9, Section 2.2), expression data of all different transcripts (Figure 18), including *SIN3B* protein-coding isoforms, indicates a high upregulation of the long variant 201 (NCBI accession number NM_001297595.1 or ENST00000248054.10 Ensembl reference number). These findings suggest that all *SIN3B* protein domains might be required for the gene function in melanomas. However, an improved understanding of *SIN3B* domains and its containing complexes in melanomas is still necessary.

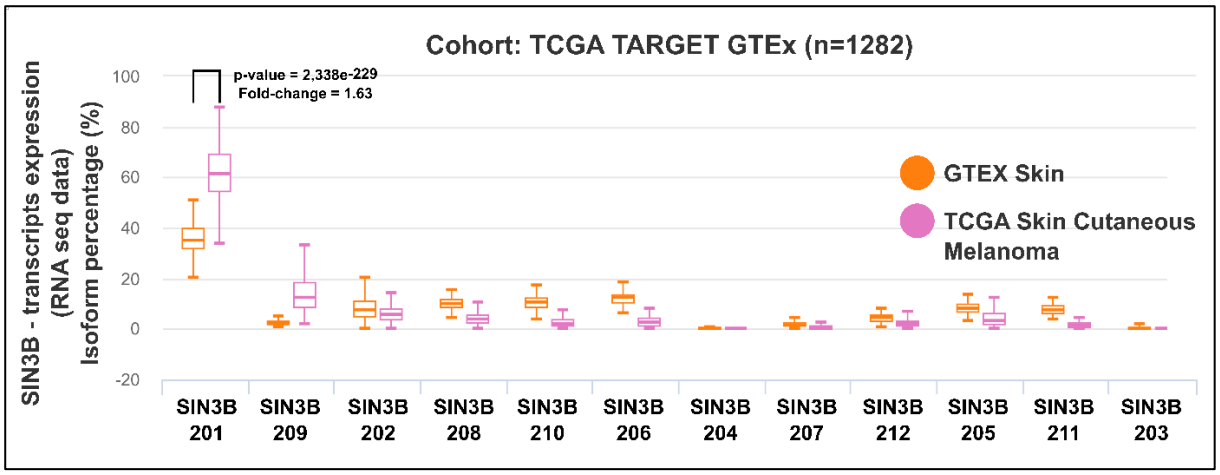

Figure 18. Analysis of all SIN3B transcripts levels in normal skin samples (GTEx) and cutaneous melanoma (TCGA). The lengthly transcript SIN3B 201, highlighted in red, with accession number NM_001297595.1 or ENST00000248054.10, presented the highest expression value in melanoma compared to other transcripts. In addition, there was a significant differential expression between normal and tumor tissue, whose p-value obtained was $p = 2{,}338e^{-229}$.

Source: Adapted from UCSC Xena.[164]

Similar results were detected in collaboration with Mariana Boroni's team at the Brazilian National Cancer Institute (INCA) through analysis of the TCGA dataset (Figure 19). A high abundance of the long variant 201 (NM_001297595.1) was perceived in both primary and metastatic melanomas, with no significant difference between the two groups. In fact, *SIN3B* expression was equally distributed among different melanoma stages (Figure 20), characterized by the American Joint Committee on Cancer (AJCC)[165; 166], indicating that *SIN3B* could be a typical signature of advanced-stage lesions and regulate the early stages of melanoma development since significant *SIN3B* upregulation was found comparing normal skin with metastatic melanomas.[167; 168]

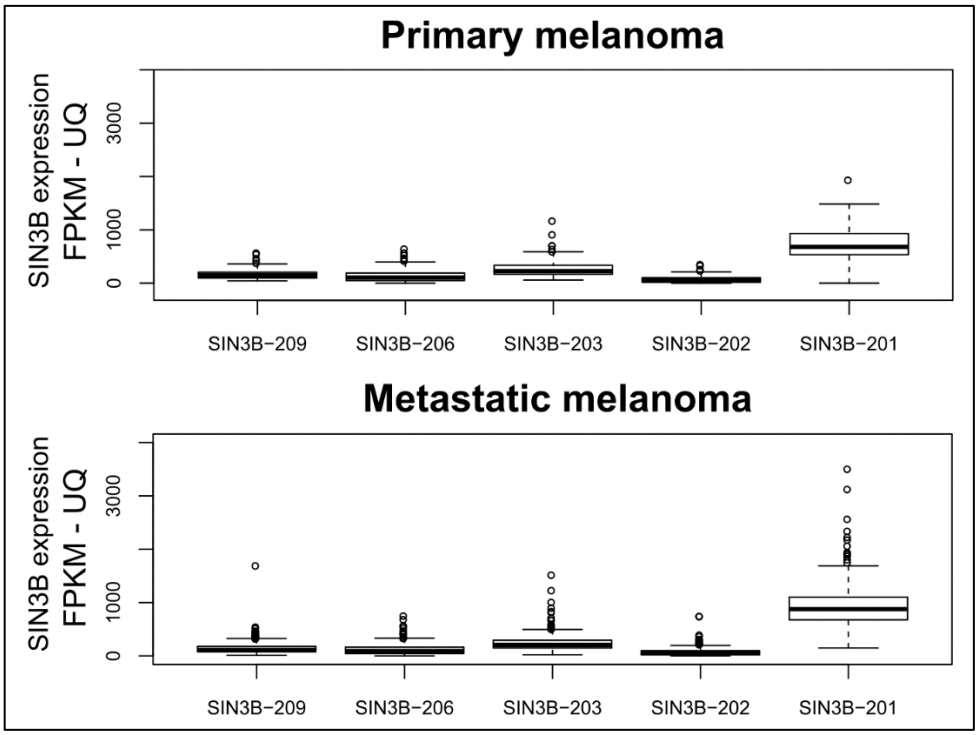

Figure 19. **Expression of *SIN3B* transcripts in primary and metastatic melanoma tumor samples using the TCGA database.** A higher abundance of the long isoform 201 is noted compared to the other *SIN3B* splice variants. Data were normalized for both sequencing depth and genome size (fragments per kilobase of transcript per million – FPKM) and by the upper quartile method. An unpaired t-test attested a p-value=$4.42.10^{-6}$ in primary melanomas and p-value=$8.56.10^{-5}$ for metastatic melanomas.

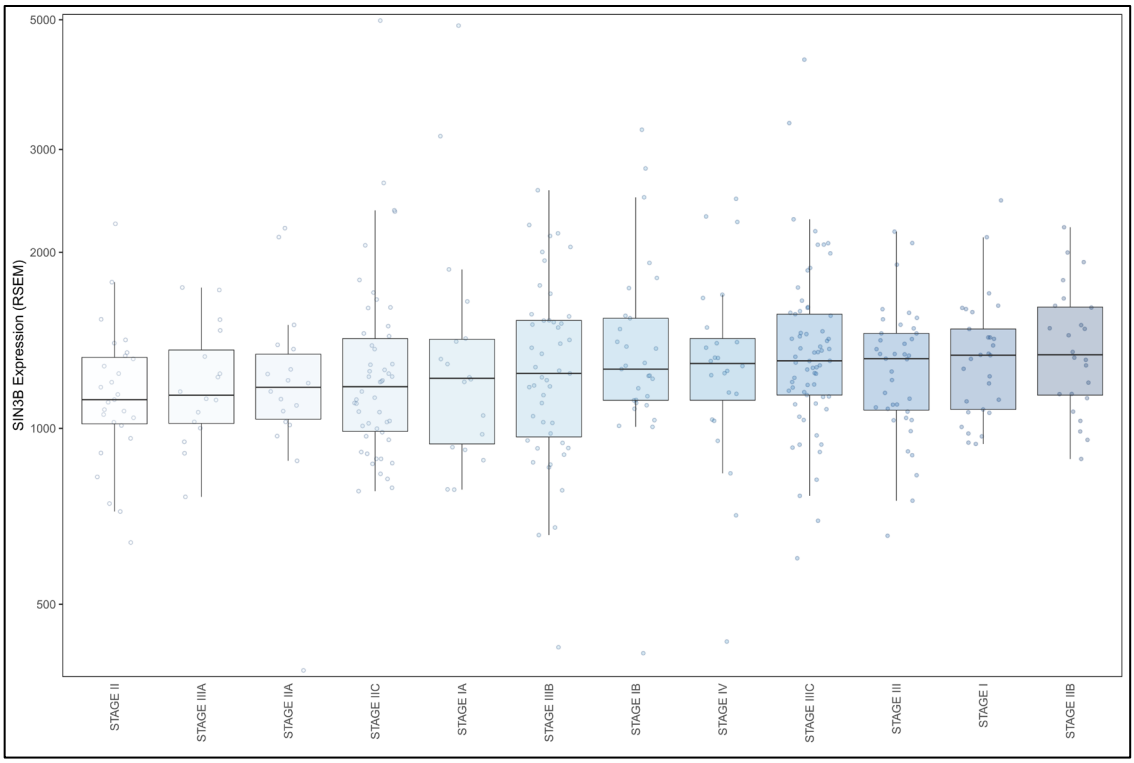

Figure 20. ***SIN3B* expression across different melanoma stages.** An equal *SIN3B* expression was observed during melanoma staging. Data was normalized by the upper quartile method.

Another exploratory analysis of great clinical relevance is to estimate overall survival of melanoma patients harboring high or low *SIN3B* expression, since a Kaplan-Meier curve aids to the understanding of a gene association with disease prognosis. To date, several treatments are based on the identification of altered proteins in tumors, endorsing a production of target-directed molecules for specific protein inactivation. In this context, the evaluation of *SIN3B* on patient's outcome could suggest its possible role as a melanoma biomarker.

Therefore, the overall survival data of melanoma patients containing high or low *SIN3B* expression was appraised, as exhibited in Figure 21. Remarkably, high levels of *SIN3B* corroborate for worse response and survival. This demonstrates that a possible contribution of *SIN3B i*n tumorigenesis. Currently, many articles fail to document recurrent mutations within the *SIN3B* gene in different tumors. However, researches show its modulated expression in different malignancies .[169] Thus, SIN3B could have a clinical function in cutaneous melanomas, which was still not described in the literature. Moving forward, unbiased studies on identifying specific *SIN3B* interaction partners or downstream mediators could support the investigation of melanoma physiological processes and the generation of novel therapeutic strategies for melanoma treatment.

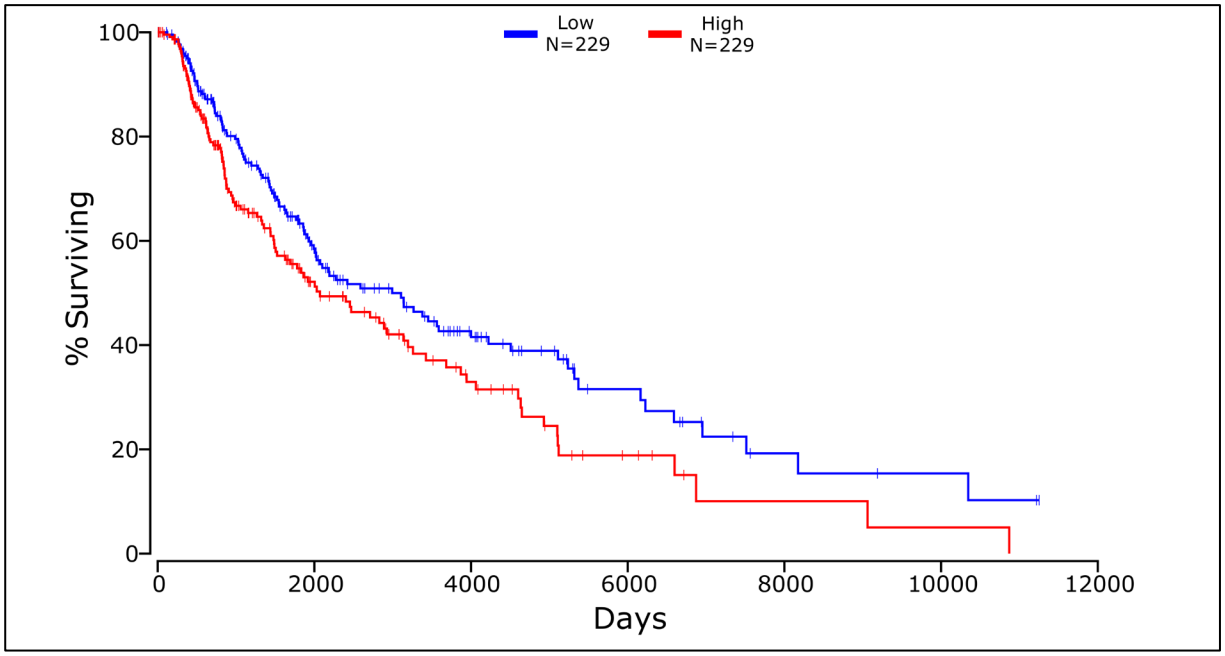

Figure 21. Kaplan-Meier survival curve of melanoma patients presenting high or low *SIN3B* expression. High *SIN3B* expression is associated with a poor overall survival in melanoma patients. The univariate Kaplan – Meier survival plot was generated using the statistical log-rant test, with p value = 0.021.

5.2. *SIN3B* is highly expressed in metastatic melanomas

The initial expression analysis of the *SIN3B* protein-coding transcripts in normal melanocytes, primary and metastatic melanoma cell lines, was determined with semi-quantitative RT-PCR reactions (Section 4.2.3). The idea was to qualitatively detect which *SIN3B* variants were present in melanoma cells so designing sgRNAs to generate *SIN3B* knockout cells could be achievable. Results are present in Figure 22.

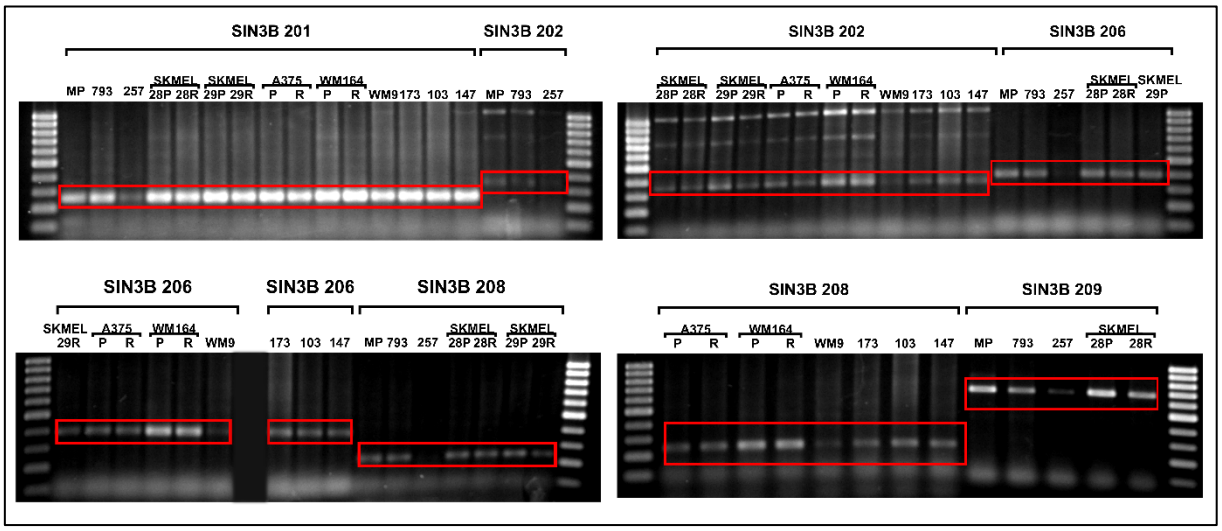

Figure 22. Expression of *SIN3B* splice variants across normal melanocytes and melanoma cells. Normal melanocytes (MP), WM793 (793) primary melanoma cells and other metastatic melanoma cell lines parental (P) or resistant to *BRAF* inhibitor (R) are presented. Bands were extracted from the agarose gel and submitted to sequencing (result not shown). Each band corresponds to the expected transcripts (result not shown). Red rectangles indicate the expected amplicon sizes of each transcript.

All *SIN3B* protein-coding variants were expressed across melanoma cells. Nevertheless, this result does not allow us to infer whether there are quantitative differences in the expression of the transcripts. This happens because, in a conventional RT-PCR reaction, several cycles of amplification are commonly used. Thus, when running the PCR products on agarose gel, the signal is already saturated. Since one of the main goals of the present work was to generate complete homozygous deletion for *SIN3B* using the CRISPR/Cas9 methodology, designing proper sgRNAs targeting common exons (coding regions of the genome) to all *SIN3B* splice variants is crucial for loss of gene function. Thus, it is necessary to determine which transcripts of *SIN3B* are expressed in melanomas. Accordingly, qPCR and western blot analyses were carried out to address this issue.

A real-time PCR (also known as qPCR) is a technique that combines DNA amplification and detection into a single step due to a fluorescent dye bonded to the amplified

gene product during PCR reactions. PCR amplification curves display the accumulation of fluorescent emission at each reaction cycle. Generally, greater amounts of target DNA render a faster advent of fluorescent signals. Hence, qPCR is an excellent method to obtain quantitative data on gene expression.[170] Consequently, mRNA expression of *SIN3B* transcripts (Figure 23) was conducted with two primers: Hs01006373_m1 targeting HID-containing variants and Hs01006369_m1 for the majority of the *SIN3B* variants. A primer for the housekeeping gene *ACTB* (beta-actin, Hs01060665_g1) was also used for normalizing *SIN3B* expression values.

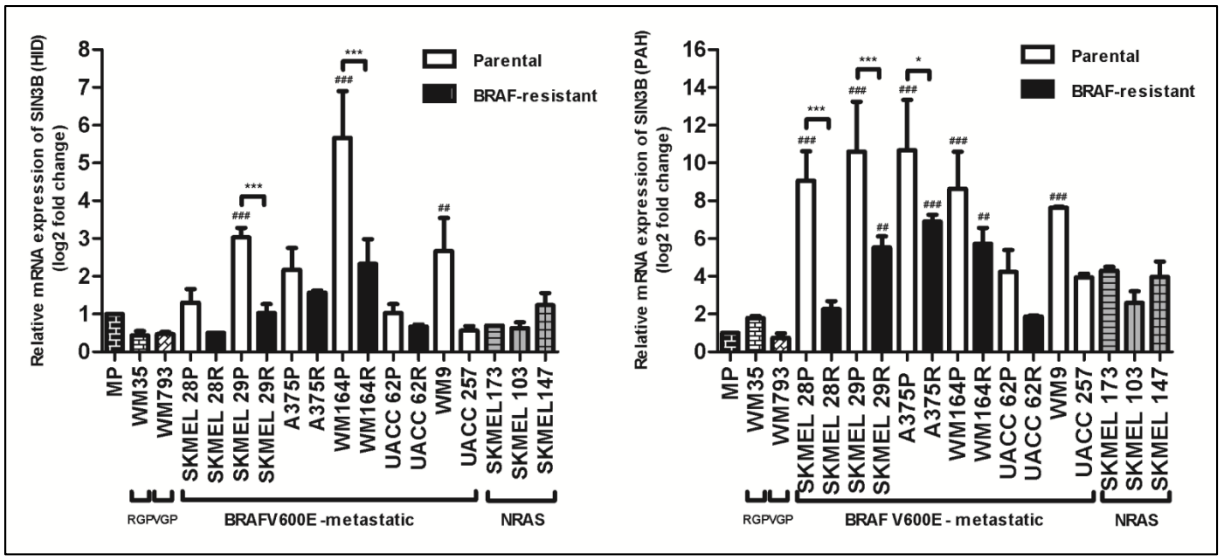

Figure 23. Expression of *SIN3B* splice variants in a panel of melanoma cell lines, including parental and *BRAF*-resistant cells. On the left side is the relative expression of the human *SIN3B* protein-coding transcripts that contain HID (histone deacetylase interacting domain) domain, normalized by the *ACTB* gene. On the right side is the expression of most *SIN3B* transcripts, which present PAH (paired amphipathic helix) domains. The expression values of all cell lines were normalized to those of normal melanocytes (MP). One-way ANOVA test with Tukey pair-to-pair comparisons was carried out. P-values of * represent $p<0.05$, ** and ## $p<0.01$, *** and ### $p<0.001$. Statistical comparison between melanoma cell lines and melanocytes are represented by # and between parental e *BRAF*-resistant cells by *.

Results presented above for both primers indicated that metastatic melanoma cells bearing $BRAF^{V600E}$ mutations showed increased *SIN3B* expression compared to melanocytes and even primary melanomas. Our analysis correlates with those presented by Di Mauro and colleagues, which revealed an upregulation of *SIN3B* upon $BRAF^{V600E}$ oncogenic activation. Indeed, the expression of activated $BRAF^{V600E}$ was sufficient to promote higher protein and mRNA levels of *SIN3B* in primary mouse embryonic fibroblasts.[133] Notably, our findings also exhibited a decrease in *SIN3B* expression in melanoma cells resistant to *BRAF*-inhibitor (Vemurafenib, Zelboraf, PLX4032/RG7204, Daiichi Sankyo/Roche, Japan). Taken together, the modulation of *SIN3B* expression in melanomas allows us to suggest a role for *SIN3B* both as a marker of malignant transformation and resistance to *BRAF* inhibitor.

However, each primer indicated even higher upregulation of PAH-containing transcripts of the human *SIN3B* genome relative to HID-variants. Both functional domains have been previously characterized as docking sites for *SIN3B* interactors. In particular, PAH domains are known flexible interfaces for interactions with several transcription factors, participating in a plethora of mechanisms and pathways, both in normal and tumoral conditions.[112; 126; 128] Thus, consistent with the importance of the PAH domains for the gene function, we could argue that PAH-containing variants (notably *SIN3B* 201, *SIN3B* 202, *SIN3B* 208, and *SIN3B* 209 reference numbers from Ensembl) are required and more altered in cutaneous melanoma, especially in BRAF-mutated metastatic melanomas. Therefore, their increased expression could contribute to the disease progression.

After exploring mRNA expression of the *SIN3B* transcripts, western blotting analysis for protein expression of human *SIN3B* gene (Santa Cruz Biotechnology, sc-13145) was assessed in different melanoma cell lines (also normal melanocytes used as control cells), results are presented in Figure 24.

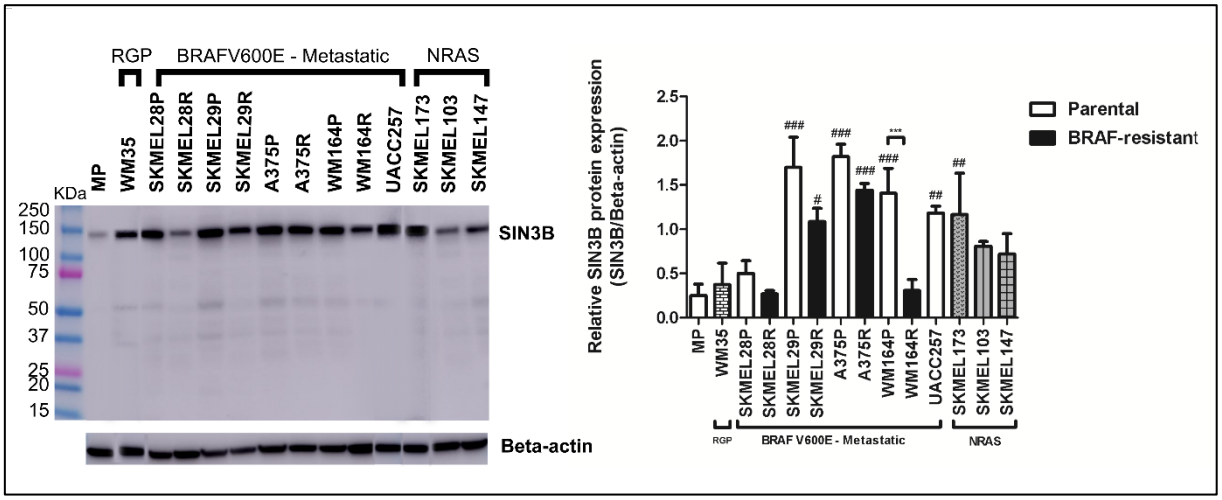

Figure 24. ***SIN3B* protein expression in a panel of melanoma cell lines.** A band of approximately 130 KDa was observed. This size corresponds to the long isoforms of *SIN3B* (either SIN3B 201, NM_001297595.1 or *SIN3B* 202, NM_015260.3). Beta-actin (42 KDa) was used as a normalizer for relative expression calculations. The graph represents the quantification of the relative *SIN3B* protein expression, for three-independent experiments. One-way ANOVA with Tukey-Kramer multiple comparisons was employed for statistical analysis. ##represents a p-value<0.01, *** and ### p-value<0.001.

Comparably with the results displayed by qPCR, the *BRAF*-mutant metastatic melanoma cells showed the highest *SIN3B* protein expression values. In addition, *BRAF*-resistant cells also unveiled a downregulation of *SIN3B* protein levels. Nonetheless, the immunoblot indicated only one protein band, whose predicted size was approximately 130

KDa. Among the five possible protein-coding variants of *SIN3B*, only two presented a molecular weight close to 130 KDa: *SIN3B* 201 (130 KDa, NM_001297595.1) and *SIN3B* 202 (133 KDa, NM_015260.3). Predicted protein sizes of both variants could be found in the Uniprot online portal (https://www.uniprot.org/).[143]

Considering that the immunogen from the *SIN3B* antibody (Santa Cruz Biotechnology, sc-13145) recognizes the second alpha-helix domain of the gene (PAH2), the results obtained from the qPCR assay (using the primer targeting most of the transcripts) and that the two long transcripts cited previously differ in only one small exon (exon 10, as observed from Ensembl website), the SDS-PAGE gel would hardly have the resolution to separate both bands. In summary, all data demonstrate an expression of only the long *SIN3B* splice variants in human melanoma cell lines. Conversely, these findings correlate with the bioinformatic analyses discussed in Section 5.1, where the *SIN3B* 201 transcript (NM_001297595.1) was prevalent in melanoma patients. Thus, all pieces of evidence suggest a correlation of *SIN3B* 201 isoform levels with the progression of human melanomas and a worse overall prognosis for advanced-stage melanoma patients.

5.3. Functional analyses in isogenic *SIN3B* knockout cells

5.3.1. Inconsistent phenotypic changes with pooled *SIN3B*-knockout melanoma cells

gRNAs against the *SIN3B* long splice variant effectively expressed in metastatic melanoma cells (harboring $BRAF^{V600E}$ mutation) were designed according to the description in Section 4.3.1. All gRNA sequences are located in the first PAH functional domain of *SIN3B* (PAH1), between exons 2 and 3, increasing the odds of generating mutants with complete loss of gene function.

Therefore, three oligonucleotides with a high score and minimal off-target activity were selected (Table 4). These sequences were cloned into the lentiCRISPRv2 vector (Addgene, #52961), and every generated construct was transfected in HEK293FT cells for lentivirus production. After 24 hours, a noticeable GFP fluorescence (Figure 25) was presented in all cultures, indicating a successful transfection.

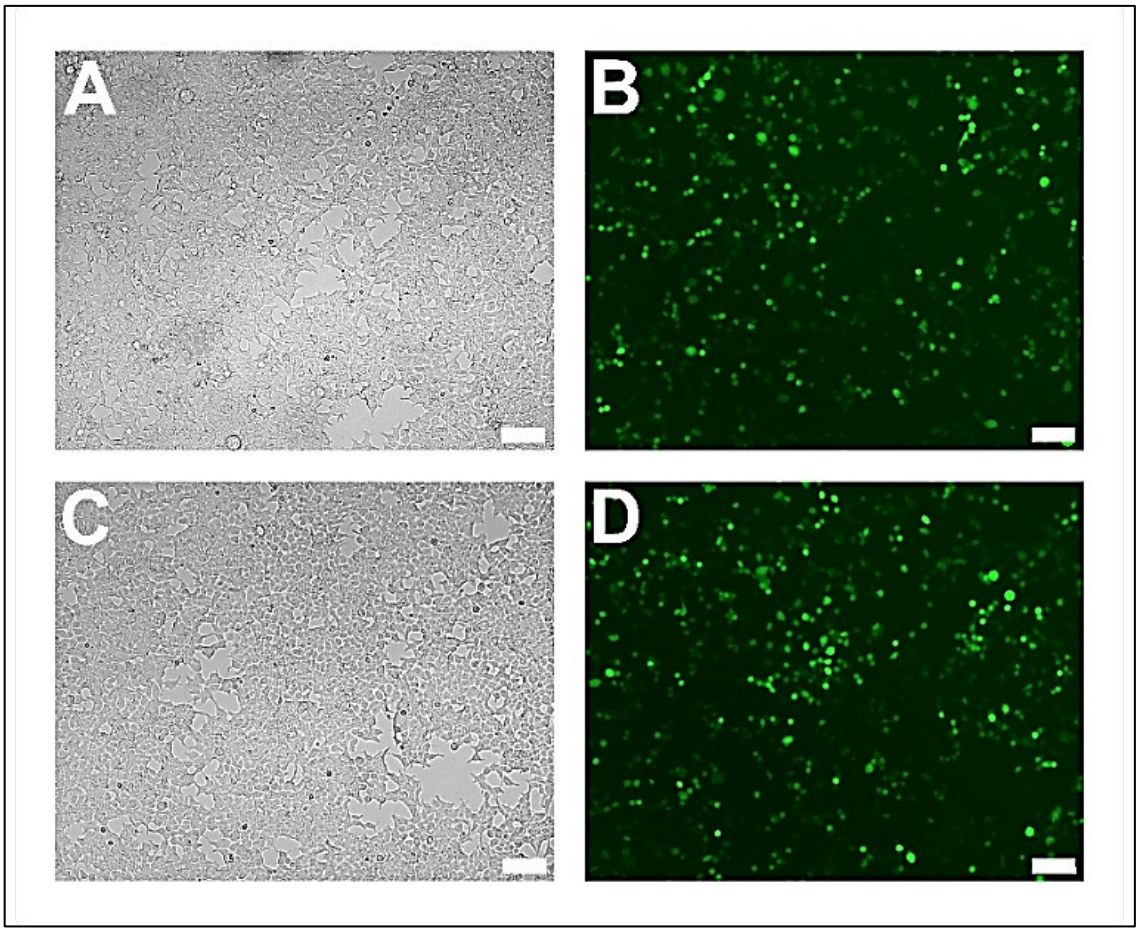

Figure 25. Representative brightfield and fluorescence images of HEK293FT cells after 24 hours of transfection with empty gRNA-cloned lentiCRISPRv2 plasmid. A) HEK293FT cells transfected with empty lentiCRISPRv2 vector (control). B) A fluorescence image indicates good transfection efficiency of the empty vector. C) Brightfield image of HEK293FT cells with a construct containing *SIN3B* gRNA (Guide 1). D) Fluorescence imaging. It is also noted that many cells were transfected. This high rate of GFP-positive cells was also observed for transfections of the other constructs (with Guide 2 and Guide 3, result not shown). Scale bar: 100 μm.

Subsequently, supernatants containing the virus (empty lentiCRISPRv2, lentiCRISPRv2-Guide 1, lentiCRISPRv2-Guide 2, or lentiCRISPRv2-Guide 3 constructs) were collected for lentiviral transduction in metastatic melanoma cells (Section 4.3.3). As previously described, these cells retained expressive *SIN3B* upregulation. Thus, WM164P (parental) metastatic melanomas, hereafter denominated WM164 cells, were initially used for transduction. After 48 hours of lentiviral infection, cells were selected with a complete medium containing puromycin (2μg/mL) for 72 hours. Validation of knockouts was performed through immunoblot analysis, estimating *SIN3B* protein expression (Santa Cruz Biotechnology, sc-13145) of control cells (with empty lentiCRISPRv2 vector) and transduced cells holding gRNA-constructs (lentiCRISPRv2- Guide 1, lentiCRISPRv2-Guide 2, or lentiCRISPRv2-

Guide 3). Experiments were conducted in triplicate (20 µg of total protein per well), and both blot and protein quantification are presented in Figure 26.

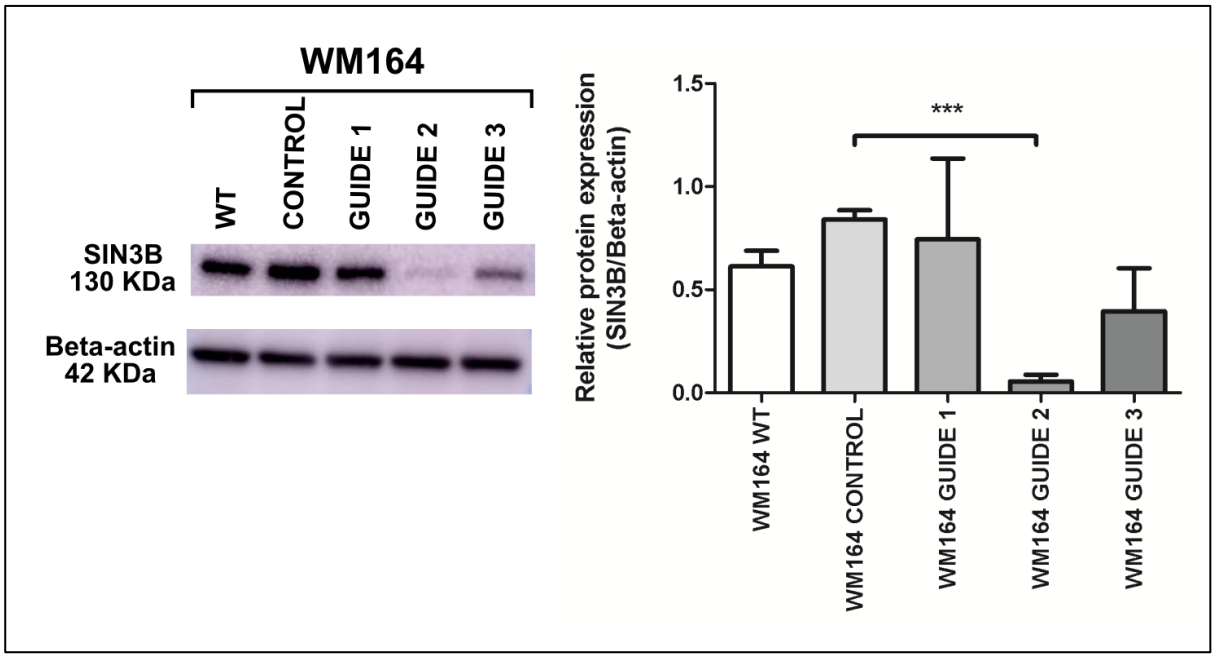

Figure 26. Western blot confirming the CRISPR-mediated deletion of *SIN3B* in WM164 metastatic melanoma cells. Untransduced (wild type – WT) and control cells (infected with the empty plasmid) showed similar *SIN3B* expression. However, only cells transduced with Guide 2 showed an expressive decrease in SIN3B. Quantitatively, approximately 98% of reduced *SIN3B* protein levels were noted. An unpaired t-test attested significant results, with a *** p-value<0.001.

Western blot analysis remains as the gold standard approach to verify that a protein of interest was ablated. According to Figure 26, it is remarkable how only Guide 2 was efficient in reducing *SIN3B* expression post-CRISPR-mediated mutagenesis, but cells kept a residual protein expression. It is worth remembering that the CRISPR/Cas9 methodology frequently introduces short frameshift mutations on the targeted locus in most cells of a population. However, a heterogeneous population is usually formed, and each cell carries a different indel (insertion or deletion of nucleotides). In addition, some CRISPR-induced modifications may lead to incomplete gene depletion, either due to nonsense-associated alternative splicing or exon skipping events, generating an in-frame mRNA that could be translated to a functional protein.[151; 171; 172] Altogether, these findings suggest a need to isolate single-cell clones for future functional analysis. Unfortunately, WM164 melanoma cells failed to grow during single-cell expansion. Thus, initial functional experiments were conducted with the heterogeneous population of cells transduced with Guide 2, aiming to characterize the phenotype of *SIN3B*-depleted melanoma cells.

First, i*n vitro* assays were applied to examine the effects of *SIN3B* depletion on proliferative potential of metastatic melanoma cells, using trypan blue exclusion to assess a growth curve (Section 4.4.2) and long-term clonogenic survival analyses (Section 4.4.3). Results from WM164 *BRAF*-mutant melanoma cell line containing the empty lentiCRISPRv2 plasmid (used as control cells) or *SIN3B* gRNA (Guide 2, cell labeled as *SIN3B* knockout) can be seen in Figure 27. The data demonstrated that in a polyclonal population, *SIN3B* depletion did not significantly affect cell growth and viability *in vitro.* Similar results were found in breast cancer, where knockdown of both human *SIN3* paralogs *SIN3A* and *SIN3B* did not affect the proliferation of MDA-MB-231 and MDA-MB-435 breast cancer cells.[136] Additionally, loss of *SIN3B* in mouse embryonic fibroblasts also did not show effects on proliferation. In fact, it has been recently argued that only on serum deprivation, *SIN3B* null cells entered in quiescence, suggesting a role of *SIN3B* in controlling cell cycle under growth-limiting conditions.[173] Taken together, these results suggest that *SIN3B* deletion does not influence the proliferation of melanoma cells.

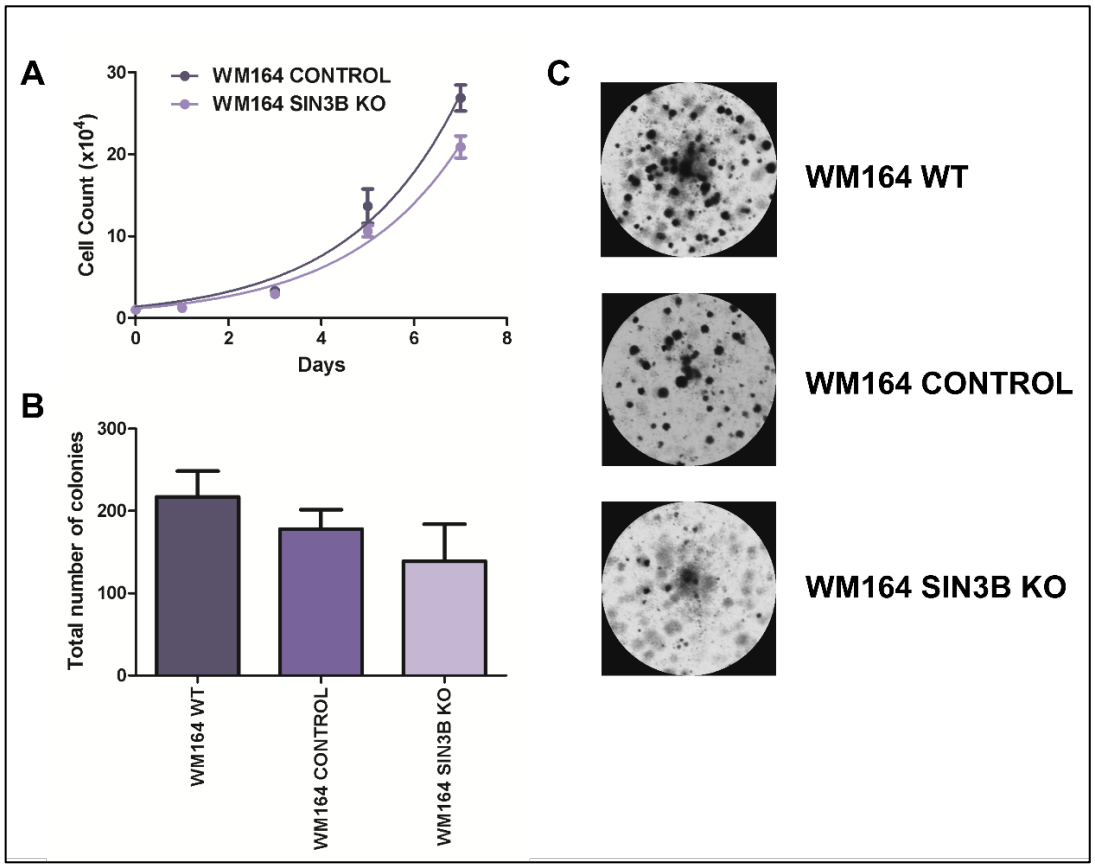

Figure 27. Growth curve and clonogenic assay results of melanoma cells with seemingly *SIN3B* deletion. A) A growth curve of the control WM164 cells (containing lentiCRISPRv2 empty vector) and *SIN3B* knockout cells indicated no significant differences in proliferation. B) A similar number of colonies denoted equal long-term growth rates of control and *SIN3B*-deleted melanoma cells. C) A representative image of the clonogenic assay. Cells were cultivated for 14 days until emerging colonies.

The study of tumor cells' migratory and invasive properties is of paramount importance since about 90% of mortalities occur due to the metastatic capacity of cancer.[174] In the case of melanoma, metastasis derives from aberrant mobility of these cells within the tumor microenvironment. Therefore, to gain further insights into these mechanisms on *SIN3B*–deficient melanoma cells, transwell chambers with or without Matrigel, respectively for migration and invasion assays, were used, as presented in Figure 28.

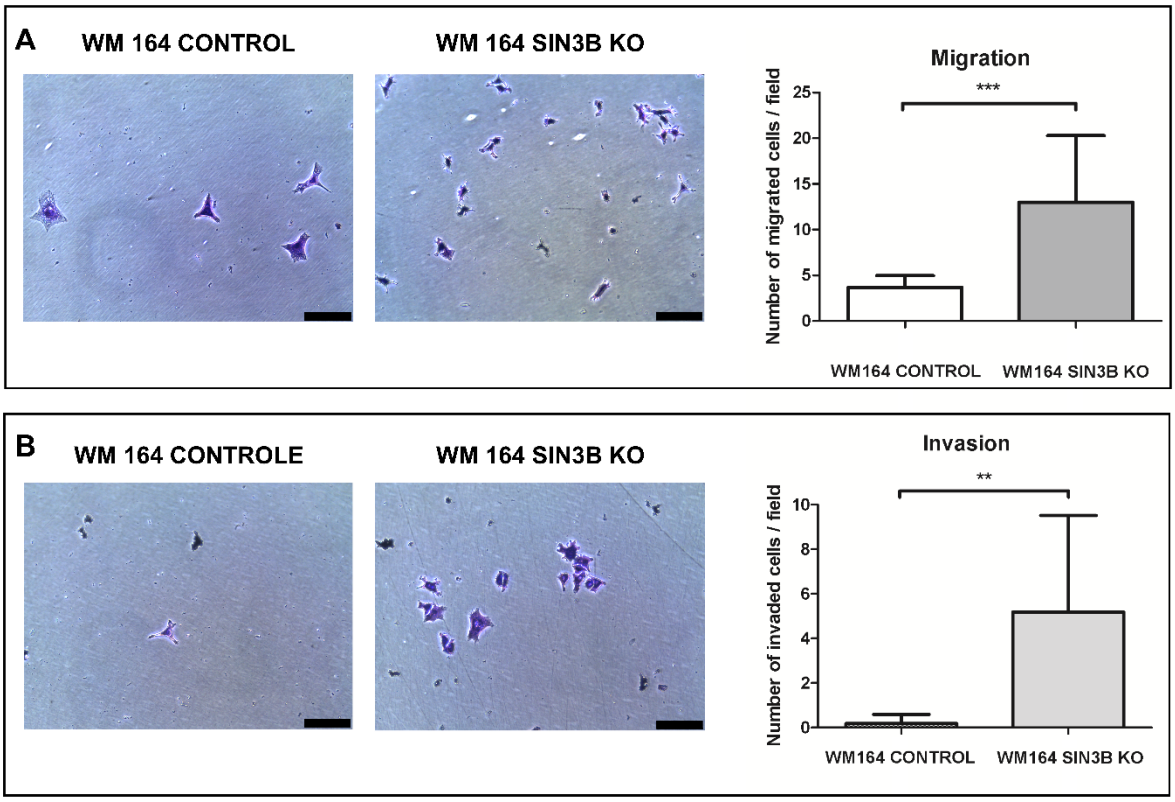

Figure 28. Boyden chamber migration and invasion assays (Transwell). WM164 cells (containing lentiCRISPRv2 empty vector or *SIN3B* gRNA) were cultivated. A) Migration or B) Invasion assays were performed in three independent experiments. A significant yet minimal increase in the number of migrated and invaded cells upon *SIN3B* deletion was observed. An unpaired t-test was used for statistical analysis. ** p-value<0.001, *** p-value<0.001. Scale: 100 µm.

Local tumor cell invasion and migration is crucial for metastasis formation, which worsens prognosis and patient survival.[175] Thus, we examined whether *SIN3B* affects melanoma cell migration and invasion *in vitro*. In Figure 28, a marginal but significant increase in melanoma cells motility and invasion was observed, highlighting a possible pro-invasive phenotype of *SIN3B*-seemingly null melanoma cells.

The transformation of melanocytes to malignant invasive melanoma involves the alteration of several cellular phenotypes.[176] Thus, metastatic melanoma tumors present an

intrinsic phenotypic heterogeneity that stems partly due to these cells' ability to switch from a proliferative and invasive state. This phenotype switch is often represented by epithelial-mesenchymal transition (EMT), restructuring the cytoskeleton, cell membrane, and cell-cell interactions to promote higher migratory and invasive properties of melanoma cells. [177] EMT carries changes in expression of epithelial and mesenchymal markers, such as E-cadherin, N-cadherin, and Vimentin.[178] In addition, EMT is often associated with deregulation of drivers of melanoma progression such as *MITF,* known to suppress tumor invasion and metastasis.[179] Prompted by the premise of high invasion found in *SIN3B*-deleted cells and the critical regulation of EMT-inducing transcription factors, lysate of *SIN3B* knockout melanoma cells (WM164) were probed for EMT markers, as shown in Figure 29.

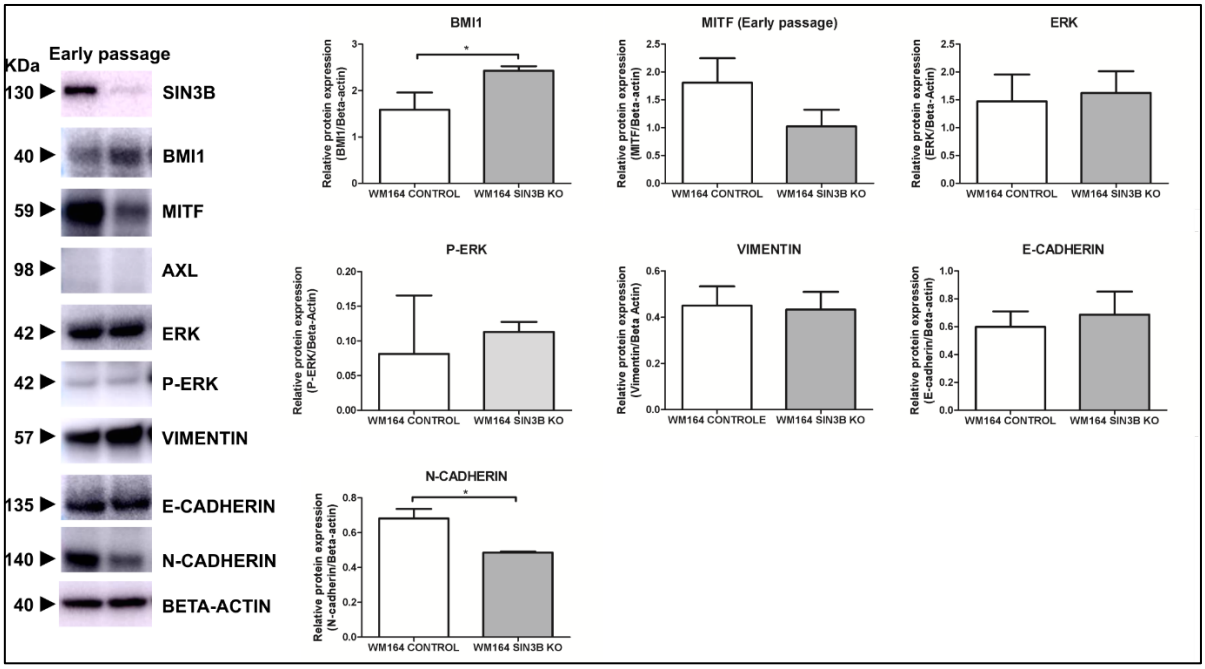

Figure 29. Immunoblot analysis of EMT markers in WM164 pooled cells transduced with lentiCRISPRv2 plasmid (control cells) and *SIN3B* gRNA (knockout cells). Immunoblots of EMT markers and melanoma progression drivers are presented in the left panel. Beta-actin was used as a loading control. On the right are the quantification plots of three independent experiments assessing the differential expression of tested proteins. Noticeably, no significant changes were observed for most proteins, except for BMI1, a known SIN3B repressor, and N-cadherin. Data were normalized to Beta-actin, and a two-tailed unpaired t-test was used to assess statistical significance; * p-value<0.05.

EMT is usually associated with the downregulation of E-cadherin and increased expression of mesenchymal markers such as N-cadherin, vimentin, and fibronectin.[180] Additionally, E-cadherin loss in invasive melanomas is linked to enhanced pERK levels.[181] Nonetheless, as shown in Figure 29, a comparison between controls and *SIN3B* knockout cells failed to demonstrate significant changes in these EMT-induced proteins. In fact, even a

decreased N-cadherin expression was presented in *SIN3B*-depleted cells. Altogether, all data suggest that the pro-invasive phenotype observed previously on Boyden chamber analysis could not be an actual effect of *SIN3B* deletion. Thus, we briefly compare our expression results with some EMT modulations expected in the literature to promote melanoma invasion and discuss the possibilities as to why we observe inconsistent results using a heterogeneous population of *SIN3B*-deleted cells.

Some genes either suppress or contribute to the process of tumor invasion. Among them, *MITF* and *AXL* stand out. *MITF* expression is significantly decreased in resistant melanomas, and *MITF* loss is often associated with increased invasive capacity, characterized by an EMT-like signature, as described by Müller, J. et al. (2014)[182] and Konieczkowski, DJ et al. (2016)[183]. Contrarily, a striking inverse correlation between *MITF* and *AXL* was already reported in the literature, where *AXL* was upregulated in resistant melanomas and induced EMT and metastasis.[182; 184] Recently, a model containing six different phenotypic melanoma states due to *MITF* activity was proposed. These different states refer to differentiated cells with high *MITF* levels, *MITF*-positive proliferative cells, an intermediate state with invasive and proliferative features, starved or therapy-induced cells, and undifferentiated cells with low *MITF* expression.[185] Together, both genes, especially *MITF*, propose a rheostat model, switching expression depending on invasive or proliferative cell properties. Our results with *SIN3B*-depleted cells indicated a trend, unfortunately not significant, of *MITF* downregulation, which could correlate with increased invasion presented in the Boyden chamber analysis. Yet, no *AXL* upregulation was found in these cells. Similarly, *Vimentin* and *BMI1* were also described in the literature to promote tumor invasion and metastasis.[133; 153; 186] However, in our western blot analysis, only *BMI1* was found to be upregulated in *SIN3B* knockout cells, which was partially expected because the epigenetic regulator *BMI1* was already demonstrated as a transcriptional repressor of *SIN3B,* yet not in melanomas.[133]

Collectively, all data presented here using a pooled population of SIN3B-null cells were contradictory in regards to a clean invasive phenotype, excluding increased *BMI1* expression found in these cells, which seems to be consistent with the literature. These findings illustrate how genetic and phenotypic heterogeneity may be present prior to single-cell isolation. As we know, in a heterogeneous cell population post-Cas9-mediated gene knockout, different target modifications are present and, some of them may be in-frame indels that could be tolerated without compromising protein function.[151] Therefore, to ensure a complete loss of gene function, all cells need to harbor a homozygous deletion (deletion in both alleles) to

remove unedited cells since the latter could induce inconsistent functional results. Consequently, generating clonal lines might be a better approach to verify complete knockouts and limit noise in downstream analyses. Since WM164 single-cell isolation was not possible as cells died when grown sparsely, during low cell seeding, we decided to select cell lines that exhibited consistently high clonogenicity (SKMEL28, A2058 and A375 melanoma cells), which will be discussed in the following section.

5.3.2. Functional analysis with isogenic *SIN3B* knockout clones

5.3.2.1. *SIN3B* deletion does not affect melanoma cell growth *in vitro*

As discussed in previous sections, gRNAs were designed targeting an early exonic region of the long *SIN3B* variant (Section 4.3.1). Because only Guide 2 was efficient for the gene deletion (Section 5.3.1), we used this gRNA to generate *SIN3B*-deleted clones. We hereafter used the metastatic melanoma cell lines SKMEL28, A2058, and A375, since they exhibited a high clonogenic capacity for single-cell isolation, presented *SIN3B* upregulation (both at mRNA and protein levels), and were successfully used in a plethora of functional experiments, which included genome-wide CRISPR screening s performed at the Wellcome Trust Sanger Institute, in different tumors. The SKMEL28, A2058, and A375 cell lines were transiently transfected with the empty lentiCRISPRv2 plasmid, as a control, or the vector with Guide 2 (Section 4.3.1). After 24 hours post-transfection, puromycin was introduced to select edited clones (Section 4.3.4). Western blotting and next-generation sequencing (4.3.5) were used to identify single-cell clones containing frameshift indels, as presented in Figure 30.

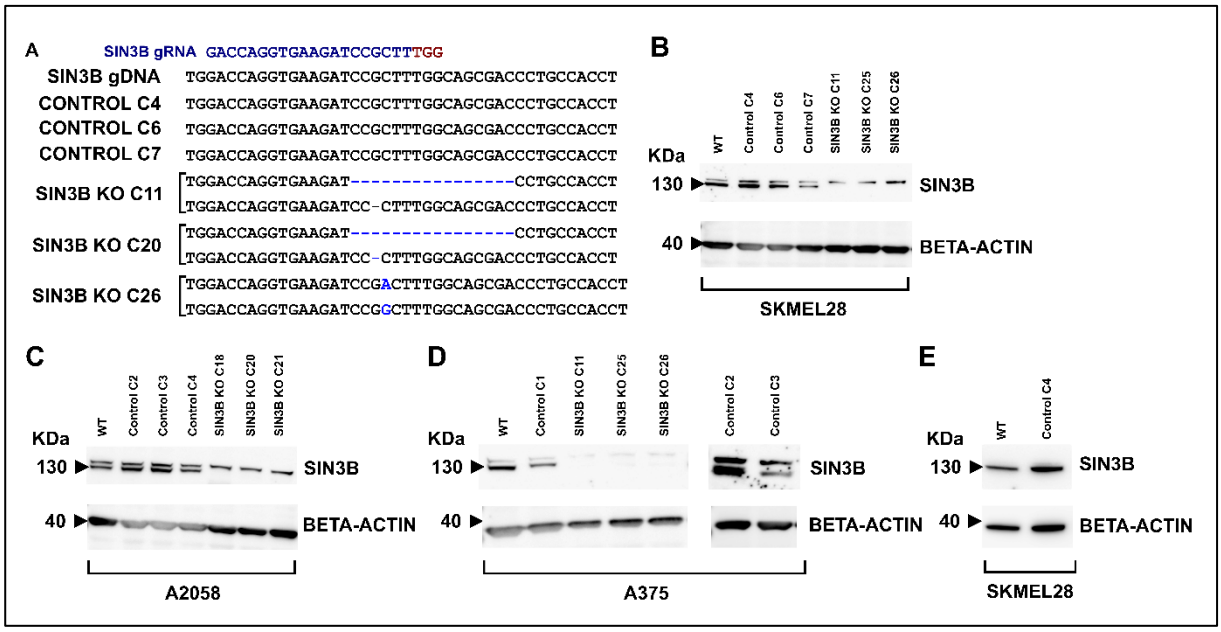

Figure 30. **Evaluation of *SIN3B* deletion through next-generation sequencing (NGS) and western blot.** A) A schematic representation of NGS results for SKMEL28 melanoma cells showed a homozygous deletion for *SIN3B*. Each deleted clone (labeled as SIN3B KO with a C for the clone number) bared either deletion on insertion of nucleotides in both gene alleles, whereas control clones presented the same sequence as the *SIN3B* genomic DNA, used for reference. Similar results were found in the other two cell lines (results not shown). B, C, D) Immunoblots demonstrated clear *SIN3B* knockout, noticed by the lower band of approximately 130KDa. E) Schematic representation of another independent western blot of SKMEL28 melanomas cells (wild type and control clone C4). It is notable, comparing sections B and E, that the upper band is absent, suggesting that in B the upper band is non-specific.

Therefore, we successfully obtained multiple *SIN3B* knockout clones in three different metastatic melanoma cell lines, verified by the frameshift indels in *SIN3B* genomic DNA generated using the CRISPR-Cas9 system. The frameshift mutations presented in all *SIN3B*-null clones are listed in Table 14. The lack of *SIN3B* protein levels was also examined through western blotting analysis, where no residual protein was found. Indeed, through different wester blots experiments performed in independent days, results demonstrated that the upper band is non-specific, since it was not present in all immunoblots. Thus, applying a combination of both methods was crucial to characterize the CRISPR-induced modifications.

Table 14. Frameshift mutations were presented in all SIN3B knockout clones. The sequences of both alleles are presented in this table. Some clones presented the same modification in both alleles, and others one different indel per allele.

		Mutation
SKMEL 28	**SIN3B gDNA**	TGGACCAGGTGAAGATCCGCTTTGGCAGCGACCCTGCCACCTACAACGGCTTCC TGGACCAGGTGAAGATCCGCTTTGGCAGCGACCCTGCCACCTACAACGGCTTCC
	CONTROL C4	TGGACCAGGTGAAGATCCGCTTTGGCAGCGACCCTGCCACCTACAACGGCTTCC TGGACCAGGTGAAGATCCGCTTTGGCAGCGACCCTGCCACCTACAACGGCTTCC
	CONTROL C6	TGGACCAGGTGAAGATCCGCTTTGGCAGCGACCCTGCCACCTACAACGGCTTCC TGGACCAGGTGAAGATCCGCTTTGGCAGCGACCCTGCCACCTACAACGGCTTCC
	CONTROL C7	TGGACCAGGTGAAGATCCGCTTTGGCAGCGACCCTGCCACCTACAACGGCTTCC TGGACCAGGTGAAGATCCGCTTTGGCAGCGACCCTGCCACCTACAACGGCTTCC
	SIN3B KO C11	TGGACCAGGTGAAGAT----------CCTGCCACCTACAACGGCTTCC TGGACCAGGTGAAGATCC-CTTTGGCAGCGACCCTGCCACCTACAACGGCTTCC
	SIN3B KO C20	TGGACCAGGTGAAGAT----------CCTGCCACCTACAACGGCTTCC TGGACCAGGTGAAGATCC-CTTTGGCAGCGACCCTGCCACCTACAACGGCTTCC
	SIN3B KO C26	TGGACCAGGTGAAGATCCGACTTTGGCAGCGACCCTGCCACCTACAACGGCTTCC TGGACCAGGTGAAGATCCGGCTTTGGCAGCGACCCTGCCACCTACAACGGCTTCC
A375	**CONTROL C1**	TGGACCAGGTGAAGATCCGCTTTGGCAGCGACCCTGCCACCTACAACGGCTTCC TGGACCAGGTGAAGATCCGCTTTGGCAGCGACCCTGCCACCTACAACGGCTTCC
	CONTROL C2	TGGACCAGGTGAAGATCCGCTTTGGCAGCGACCCTGCCACCTACAACGGCTTCC TGGACCAGGTGAAGATCCGCTTTGGCAGCGACCCTGCCACCTACAACGGCTTCC
	CONTROL C3	TGGACCAGGTGAAGATCCGCTTTGGCAGCGACCCTGCCACCTACAACGGCTTCC TGGACCAGGTGAAGATCCGCTTTGGCAGCGACCCTGCCACCTACAACGGCTTCC
	CONTROL C4	TGGACCAGGTGAAGATCCGCTTTGGCAGCGACCCTGCCACCTACAACGGCTTCC TGGACCAGGTGAAGATCCGCTTTGGCAGCGACCCTGCCACCTACAACGGCTTCC
	SIN3B KO C11	TGGA----------GCTTCC TGGACCAGGTGAAGATCCGCGCTTTGGCAGCGACCCTGCCACCTACAACGGCTTCC
	SIN3B KO C25	TGGA----------GCTTCC TGGACCAGGTGAAGATCCGCGCTTTGGCAGCGACCCTGCCACCTACAACGGCTTCC
	SIN3B KO C26	TGGA----------GCTTCC TGGACCAGGTGAAGATCCGCGCTTTGGCAGCGACCCTGCCACCTACAACGGCTTCC
A2058	**CONTROL C2**	TGGACCAGGTGAAGATCCGCTTTGGCAGCGACCCTGCCACCTACAACGGCTTCC TGGACCAGGTGAAGATCCGCTTTGGCAGCGACCCTGCCACCTACAACGGCTTCC
	CONTROL C3	TGGACCAGGTGAAGATCCGCTTTGGCAGCGACCCTGCCACCTACAACGGCTTCC TGGACCAGGTGAAGATCCGCTTTGGCAGCGACCCTGCCACCTACAACGGCTTCC
	CONTROL C4	TGGACCAGGTGAAGATCCGCTTTGGCAGCGACCCTGCCACCTACAACGGCTTCC TGGACCAGGTGAAGATCCGCTTTGGCAGCGACCCTGCCACCTACAACGGCTTCC
	SIN3B KO C18	TGGACCAGGTGAAGATCCG—TTGGCAGCGACCCTGCCACCTACAACGGCTTCC TGGACCAGGTGAAGATCCG—TTGGCAGCGACCCTGCCACCTACAACGGCTTCC
	SIN3B KO C20	TGGACCAGGT----------CCCTACAACGGCTTCC TGGACCAGGT----------CCCTACAACGGCTTCC
	SIN3B KO C21	TGGACCAGGTGAAGATCCG—TTGGCAGCGACCCTGCCACCTACAACGGCTTCC TGGACCAGGTGAAGATCCG—TTGGCAGCGACCCTGCCACCTACAACGGCTTCC

Based on the significant *SIN3B* knockout in our selected clones, i.e., presence of homozygous deletion on target genomic region and no protein detected through western blot,

we next assessed the effects of *SIN3B* deletion on the proliferative potential of melanoma cells. Analogously to what was presented in Section 5.3.1, we used trypan blue exclusion assay (Section 4.4.2) to obtain growth curves and colony formation analysis (Section 4.4.3) for long-term cell growth of the knockout derivative clones. Results from both experiments employed with control clones (transfected with the lentiCRISPRv2 empty vector) and *SIN3B*-null clones are demonstrated in Figure 31, Figure 32, and Figure 33.

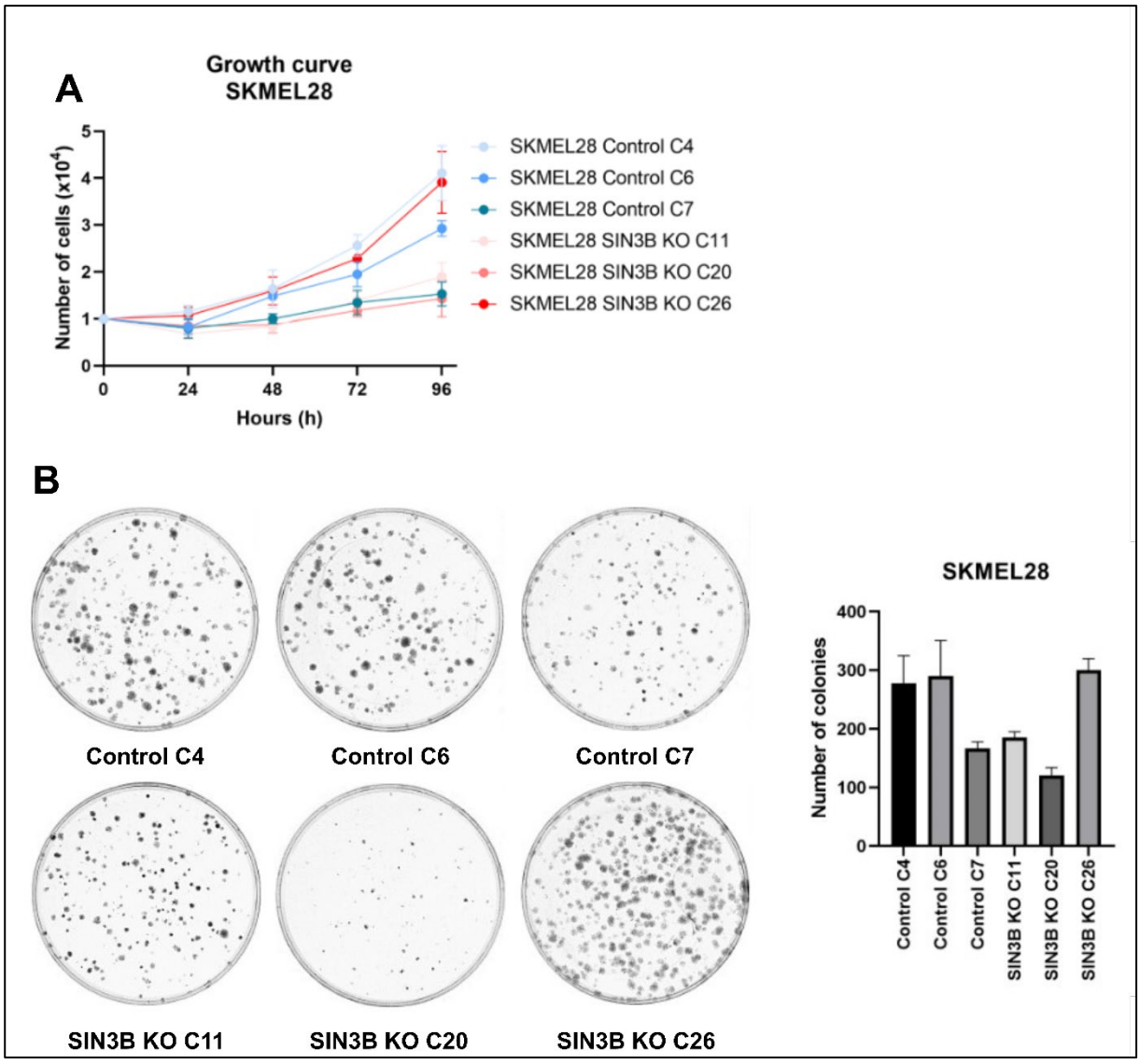

Figure 31. CRISPR-Cas9-mediated *SIN3B* knockout does not globally affect SKMEL28 cell growth. A) Cell growth and viability were determined by trypan blue exclusion assay. Cells were automatically counted each day using Countess II (Thermo Fisher). B) For clonogenic survival, an equal number of viable cells were plated into 35mm dishes at low density and, after 14 days, colonies were stained with crystal violet solution. The images shown are representative of three independent experiments.

Overall, SKMEL28 *SIN3B*-depleted clones did not exhibit significant changes in the proliferative potential of melanoma cells. Interestingly, from both growth curve and colony

formation assays, *SIN3B* knockout clone C20 seemed to decrease proliferation, which is curious since clone C11 and C20 presented the same post-CRISPR indels (16bp deletion and 1bp deletion in the two alleles, as shown in Table 14).

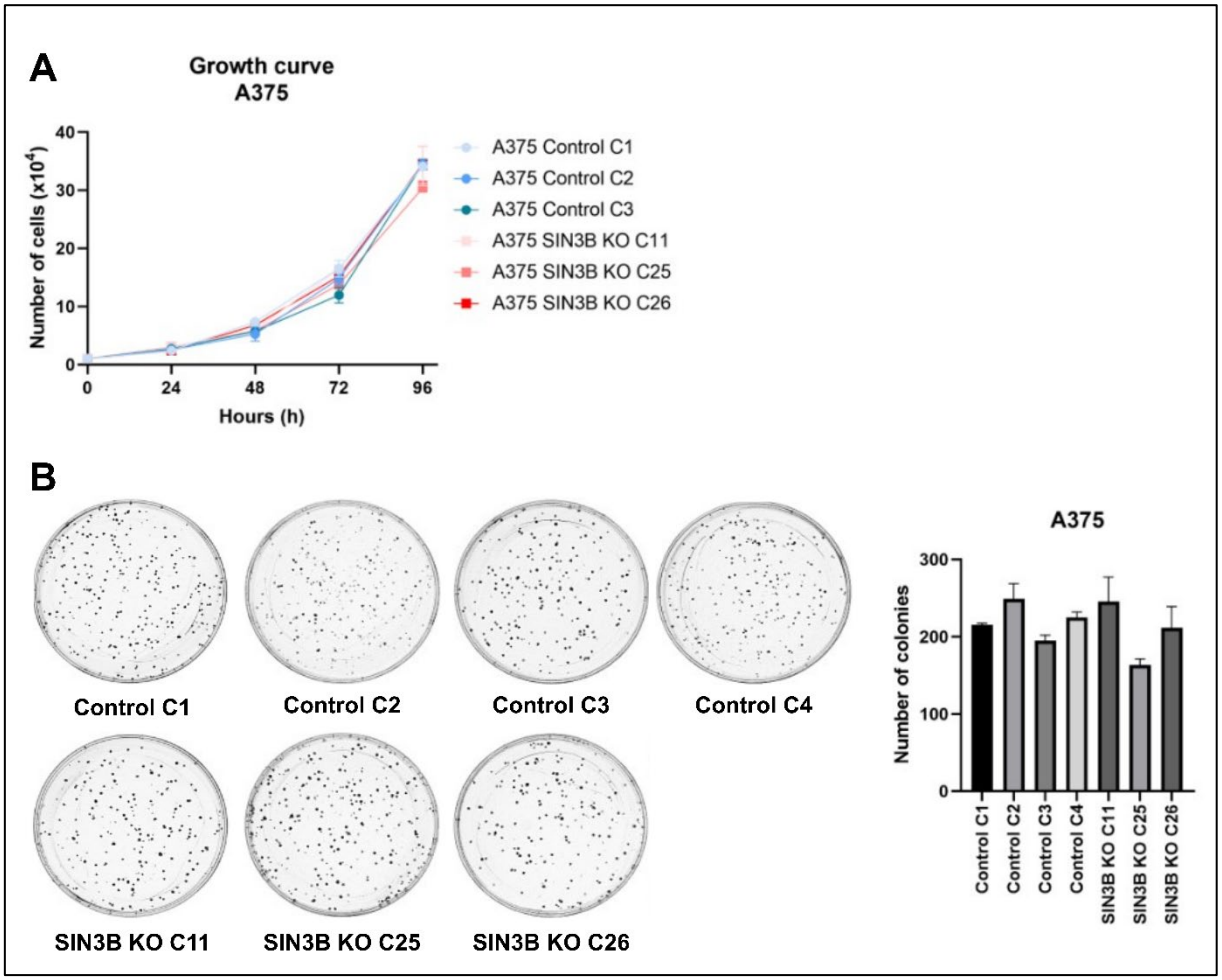

Figure 32. CRISPR-Cas9-mediated *SIN3B* knockout does not affect A375 cell growth. A) Similar cell growth and viability were determined in all A375 *SIN3B* knockout clones by trypan blue exclusion assay. B) For clonogenic survival, an equal number of viable cells were plated into 35mm dishes at low density and, after 10 days, colonies were stained with crystal violet solution. The images shown are representative of three independent experiments.

Similarly, the absence of *SIN3B* did not affect growth of the A375 metastatic melanoma cells (Figure 32). Likewise, all A375 knockout clones remarkably presented the same indels post-CRISPR (a mixture of 44bp nucleotide deletion in one allele and 2bp insertions in the other allele). In addition, A2058 single clones also did not present an overall change in proliferation (Figure 33), from both trypan blue and colony formation assay, except for *SIN3B*-null clone C20, which remarkably had a different indel from the other two deleted clones (as shown in Table 14).

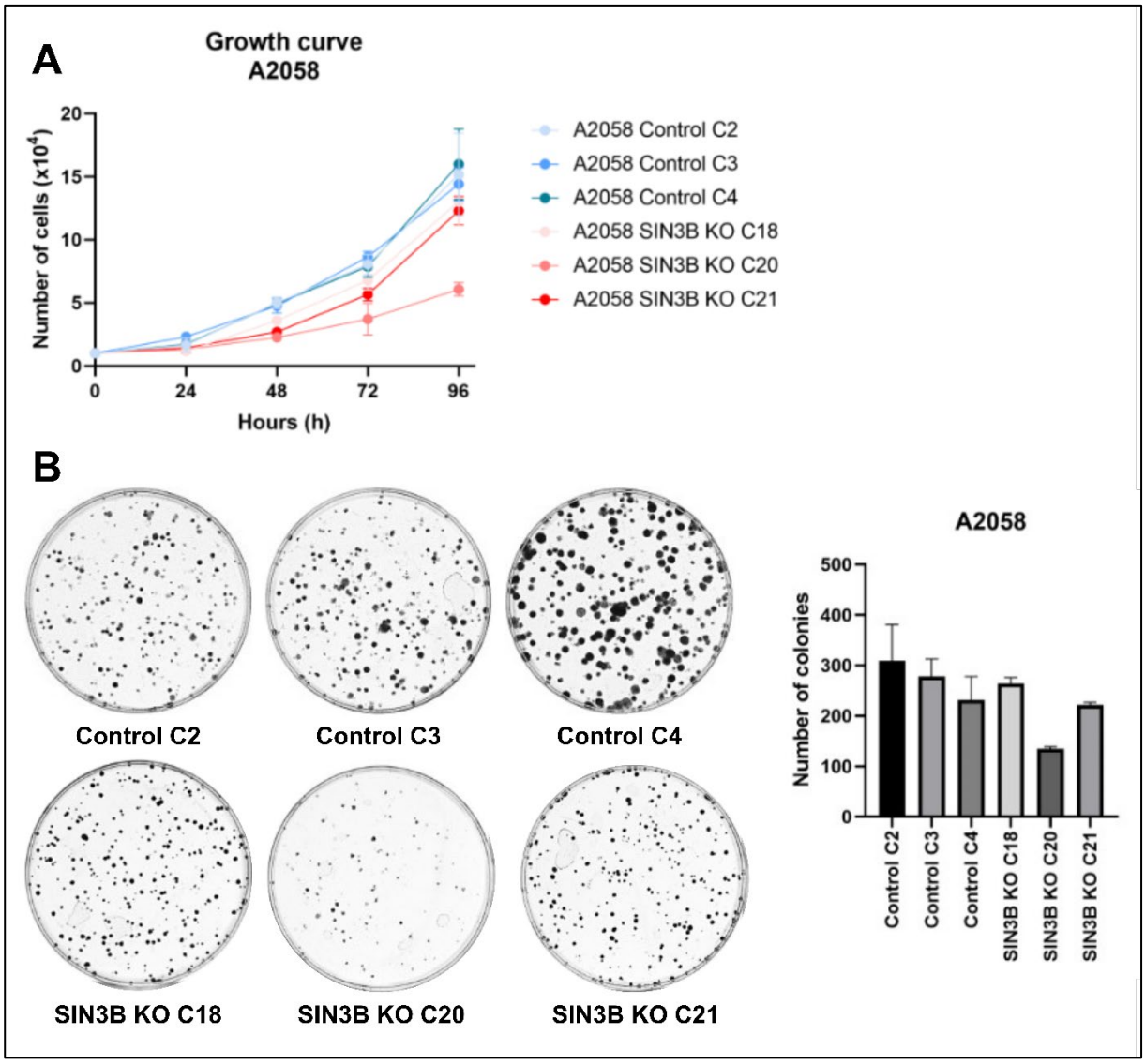

Figure 33. **CRISPR-Cas9-mediated *SIN3B* knockout does not affect A2058 cell growth *in vitro*.** A) Overall, the majority of A2058 *SIN3B* knockout clones had the same proliferative potential, determined by trypan blue exclusion assay. B) A2058 *SIN3B*-null were cultivated for 14 days and stained with crystal violet for colony formation. The images shown are representative of three independent experiments.

Collectively, our data demonstrate that *SIN3B* deletion does not influence melanoma cell growth *in vitro* (in seven out of nine *SIN3B*-null clones). Only a minority exhibited decreased proliferation, specifically SKMEL28 SIN3B clone C20 and A2058 SIN3B clone C20. However, differences of these two clones compared to the others are likely resulted from inter-clonal heterogeneity present in melanoma cells rather than an effect of the gene deletion per se.

The phenotypic plasticity of many tumors has already been reported in the literature. Cancers generally become heterogeneous due to different genetic, transcriptomic, and

epigenetic changes occurring during the course of the disease.[187] Even if we obtain isogenic cancer cells for these tumors and, more specifically, melanoma, they all display a plethora of different phenotypes, which could influence gene expression profile, drug resistance, and proliferation rate.[188; 189] Thus, altogether, single-cell-derived clones may manifest a clonal variability. Whence, we employed CRISPR-Cas9 methodology to obtain *SIN3B*-null cells and generated multiple knockout clones to address this issue. Accordingly, since we tested several clones, all with clear homozygous knockout assessed through next-generation sequencing and western blot, we can attest that the loss of *SIN3B* function does not impair proliferation of melanoma cells.

5.3.2.2. *SIN3B* deletion impacts multiple invasion-related pathways

The effects of *SIN3B* deletion on global gene expression were assessed through RNA sequencing (Section 4.5.2) of *SIN3B* knockout clones and control melanoma cells transfected with the empty lentiCRISPRv2 vector used as experimental controls. All clones from three different metastatic melanoma cell lines (SKMEL28, A2058, and A375) were used, and RNA extraction was conducted in five biological replicates per clone, totalizing 90 samples for sequencing. Principal component analysis (PCA), as shown in Figure 34, grouped the samples into two clusters: control cells and *SIN3B* knockout cells. One sample failed to sequence, and another outlier was removed using DESeq2 package[157] on the R environment. Thus, 88 samples were applied in downstream analysis.

Differentially expressed genes (DEGs) were identified with and adjusted p-value <0.01 and absolute log2 fold-change > 1, generating a list of 116 upregulated and 148 downregulated genes in *SIN3B*-null melanoma cells. To uncover possible biological processes and pathways altered by *SIN3B* deletion, gene ontology (GO) enrichment and KEGG pathway analyses were carried out with the identified DEGs. Of note, most enriched pathways, and processes upon *SIN3B* deletion were found in downregulated genes. Therefore, we present in Figure 35 our transcriptome results focusing on altered mechanisms of downregulated DEGs. Full list of differentially expressed genes is included in Appendix A.1.

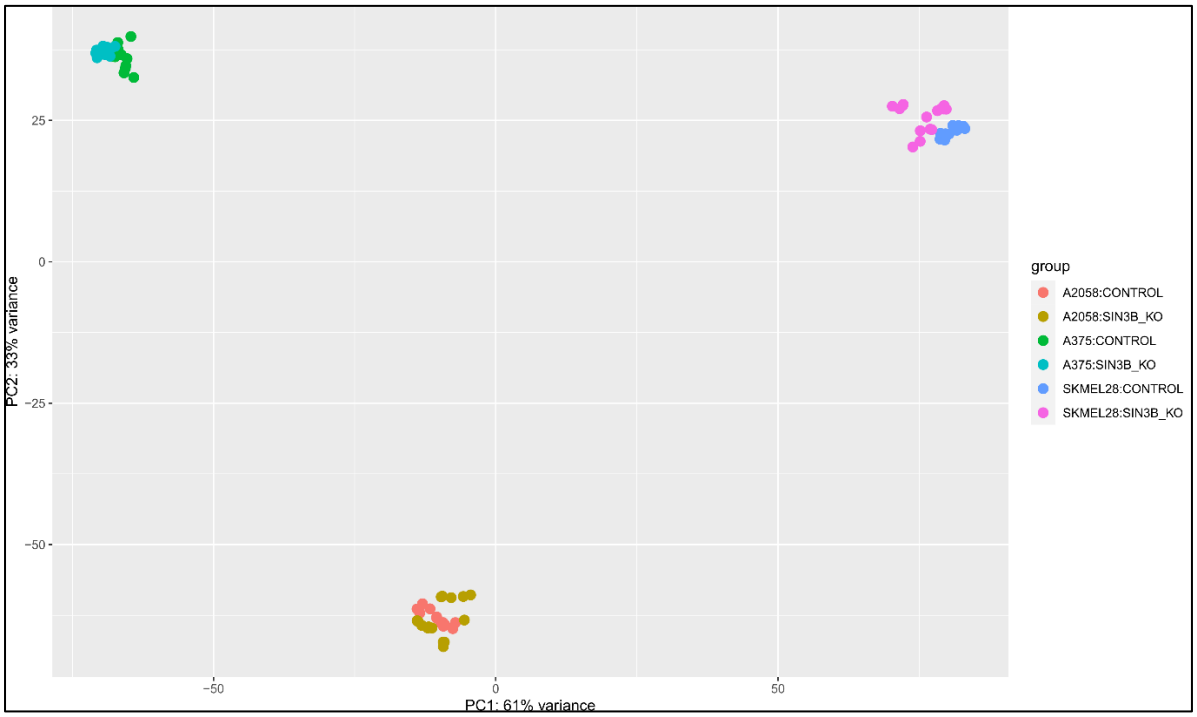

Figure 34. Principal component analysis (PCA) shows clustering of RNA sequencing samples in regard to deletion of the human *SIN3B* gene. Noticeably, each cell line clustered separately, but a clear separation of control and *SIN3B*-depleted cells was observed.

Gene ontology (GO) analysis is widely used to determine whether cellular location, molecular function, and biological processes of differentially expressed genes (DEGs) are over or under-represented.[190] Hence, it is mainly used to effectively characterize the biological features of the DEGs. However, KEGG-based analysis (Kyoto Encyclopedia of Genes and Genomes) provides functional links among the genes, i.e., common enriched pathways found in a gene list. Therefore, to gain further insights into the biological functions of the identified DEGs, we applied both approaches to our transcriptome results, which compared controls and *SIN3B*-deleted cells. As we mentioned previously, the most significantly enriched pathways and GO terms were found for downregulated DEGs, and the results from GO and KEGG analyses are presented in Figure 35.

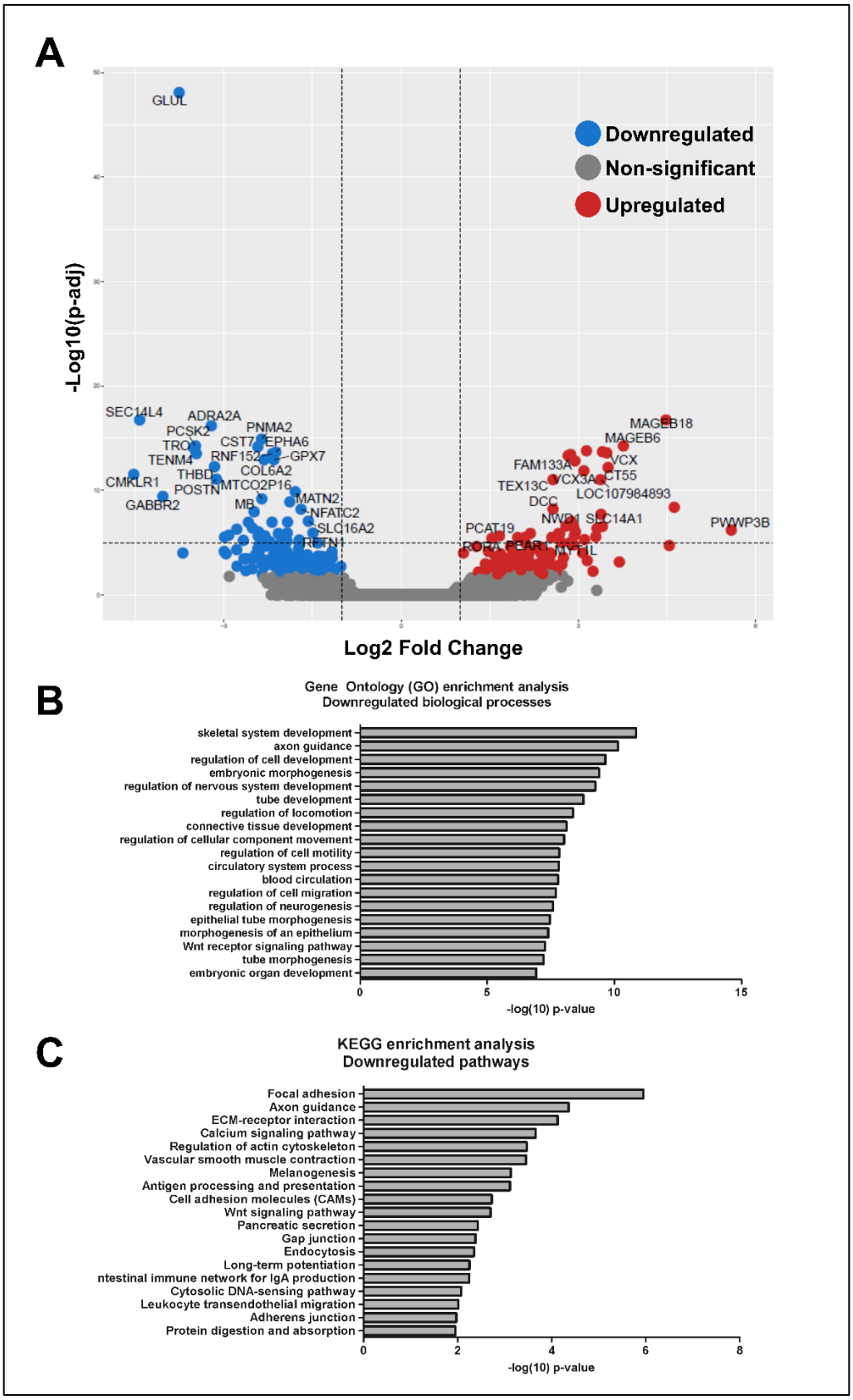

Figure 35. **Effects of *SIN3B* loss on gene expression.** A) Volcano plot shows differentially expressed genes (DEGs) in control versus *SIN3B*-depleted melanoma cells. Red dots represent upregulated DEGs, blue dots downregulated, and gray dots includes genes with no significant alteration. B, C) Respectively Gene ontology (GO) and KEGG analyses showed downregulation of a number of processes, especially those related to cell-cell interactions, cell motility, and tissue structural support.

Significantly enriched biological processes (Figure 35B) and pathways (Figure 35 C) were implicated in the downregulation of extracellular matrix interactions, cell-cell attachment, cell adhesion, and migration.[191] Given these mechanisms play an important role in the process of tumor shedding, adhesion, movement, and hyperplasia, deregulation of these features could contribute to *SIN3B*'s effect on tumor invasion and metastasis in cutaneous melanomas.

Focal adhesion, axon guidance, and receptor interaction with the extracellular matrix were the most downregulated pathways found upon *SIN3B* deletion, and these processes are intrinsically involved with tumor progression and metastasis.[192] Cell adhesion molecules (CAMs) such as cadherin, integrin, selectin and immunoglobulin are indispensable for the maintenance of the tissue, especially the epidermis. They are commonly associated with cell-cell contacts and interactions with the extracellular matrix (ECM). In the context of melanoma, changes in the CAM expression profile allow the tumour to migrate and metastasize. This finding is exemplified by the epithelial-mesenchymal transition (EMT) observed during melanoma progression, where the loss of *CDH1* (E-cadherin) followed by a gain in N-cadherin function mediates a preferential binding of melanoma cells to fibroblasts, promoting tumor invasion into the dermis.[193]

Another highly enriched pathway found in our whole-transcriptome analysis using *SIN3B* knockout cells was the WNT signaling pathway. As discussed in the literature, the WNT/β-catenin pathway has a crucial role in the embryonic development and progression of carcinomas.[194] Hyperactivation of WNT signaling promotes migration, invasion, and proliferation, collectively enhancing an aggressive phenotype of tumors.[195] In fact, the key regulator of the WNT pathway β-*catenin* also functions as a component of the cadherin complex, controlling cell-cell adhesion. Thus, noticeably, most downregulated pathways established through our transcriptome analysis in *SIN3B*-deleted cells converge to the mechanisms of invasion, migration, and cell-cell interactions.

Comparatively, with the results using a heterogeneous population post-CRISPR, we initially noticed a significant yet marginal, high invasion, but with inconsistent results regarding EMT markers. Hence, we argue that our results using either a mixed population or isogenic clones post-CRISPR-mediated editing converged regarding changes in invasion properties. However, when thinking of associating a genetic event with a phenotypic observation, such as changes in expression of specific markers/proteins related to invasion, this association would be better addressed when using clones. This happens because when generating clones and

attesting complete homozygous knockouts, we prove that the actual loss of gene function is generating the observed phenotype. Using a mixed population of edited cells, we could select different modifications, for instance, cells that carry in-frame mutations and keep the gene function or opportunistic cells with no modification, which could outgrow the edited cells and give rise to inconsistent phenotype.

Therefore, we propose in the present thesis a pró-invasive phenotype of *SIN3B* - expressing melanomas, since we observed a high expression of this gene in metastatic melanoma cell lines and the loss of *SIN3B* downregulated the processes related to melanoma migration and invasion, through the consistent RNA sequencing results using isogenic *SIN3B* deleted clones. Further experiments will be conducted to address this relation of invasive properties with *SIN3B* deletion, which includes western blot of EMT markers, boyden chamber analysis, and human melanoma askin reconstructs, which are largely used by our group.

5.3.3. Pooled genome-wide CRISPR screening to identify *SIN3B* synthetic lethal candidates

Melanomas carry a high mutational burden among all types of cancer, often represented by mutations in the primary drivers *BRAF, NRAS* and *NF1*, which collectively cause activation of the MAPK pathway to promote tumor progression and survival.[196] In this context, targeted therapies mainly developed through abrogation of MAPK genes, such as the highly prevalent *BRAF*, have revolutionized systemic therapy for advanced melanoma, improving clinical outcomes.[197] However, acquired resistance was almost inevitable due to a range of mechanisms, such as reactivation of the MAPK-ERK pathway, which we already discussed in Section 1.3. Thus, even with major advances in melanoma treatments, many patients do not respond to current therapies, urging the development of new therapeutic strategies. Hence, identifying synthetic lethal partners in melanoma could provide actionable targets to aid the development of new therapies.

The concept of synthetic lethality describes a scenario in a cell or organism where the loss of one gene still maintains cellular viability, whereas concurrent loss of two genes is lethal to the cell, provoking cell death. In cancers, synthetic lethal interactions frequently stem from the loss of a tumor suppressor gene which causes a second gene to become essential for cell survival. Thus, pharmacological inhibition of this second gene could be specifically lethal for tumor cells and not non-malignant cells.[198; 199] Therefore, this mechanism provides details about

the functional relationship between two genes and confers a new approach for cancer therapy. In human cancer cell lines, a screening in an isogenic cell pair is often used. To generate an isogenic pair, wild type cells can be engineered to carry a loss of function mutation with techiniques such as CRISPR-Cas9. Then, screening both parental and the derivative depleted cells may be compared to identify vulnerabilities found only when the gene of interest is lost.

Therefore, we aimed to employ genome-wide CRISPR-Cas9 screens to identify *SIN3B* synthetic lethal partners using isogenic *SIN3B*-deleted melanoma cells. The process to obtain these candidates will be described in the following topics.

5.3.3.1. Assessing Cas9 activity on *SIN3B* knockout clones

As previously discussed in Section 5.3.2, we successfully obtained *SIN3B* knockout clones in three different melanoma cell lines (SKMEL28, A2058, and A375). Thus, to decide which cells we would introduce in our CRISPR screens, we ended up selecting the A375 *SIN3B*-derivative clones because the parental A375 melanoma cells are easily transducible, fast-growing, and were already extensively used in screens at the Wellcome Trust Sanger Institute.

Since the genome-wide library encoded the gRNAs but not Cas9, the next step in preparation for the pooled genome-wide CRISPR screen would be generating a cell line expressing Cas9 to transduce the pooled library. However, since our clones (both control and *SIN3B* knockout) already carried Cas9 expression due to the previous transfection with the lentiCRISPRv2 plasmid, we sought to test Cas9 efficiency in these cells. All clones were transduced with a control plasmid expressing BFP and GFP (Addgene #67979) or a reporter expressing BFP, GFP and a gRNA targeting GFP (Addgene #67980). In the presence of active Cas9, the gRNA targeted GFP switching off its expression, hence, only a BFP positive population could be found. Cas9 activity was calculated as the percentage of cells harboring only BFP fluorescence, measured by flow cytometry. A representative image of the results from two clones (one control and another *SIN3B* KO) is presented in Figure 36. Almost 90% of Cas9 activity was found for all knockout clones (C11, C25, and C26) and for two control clones (C1 and C4). Thus, these five clones were employed in the CRISPR screen analysis.

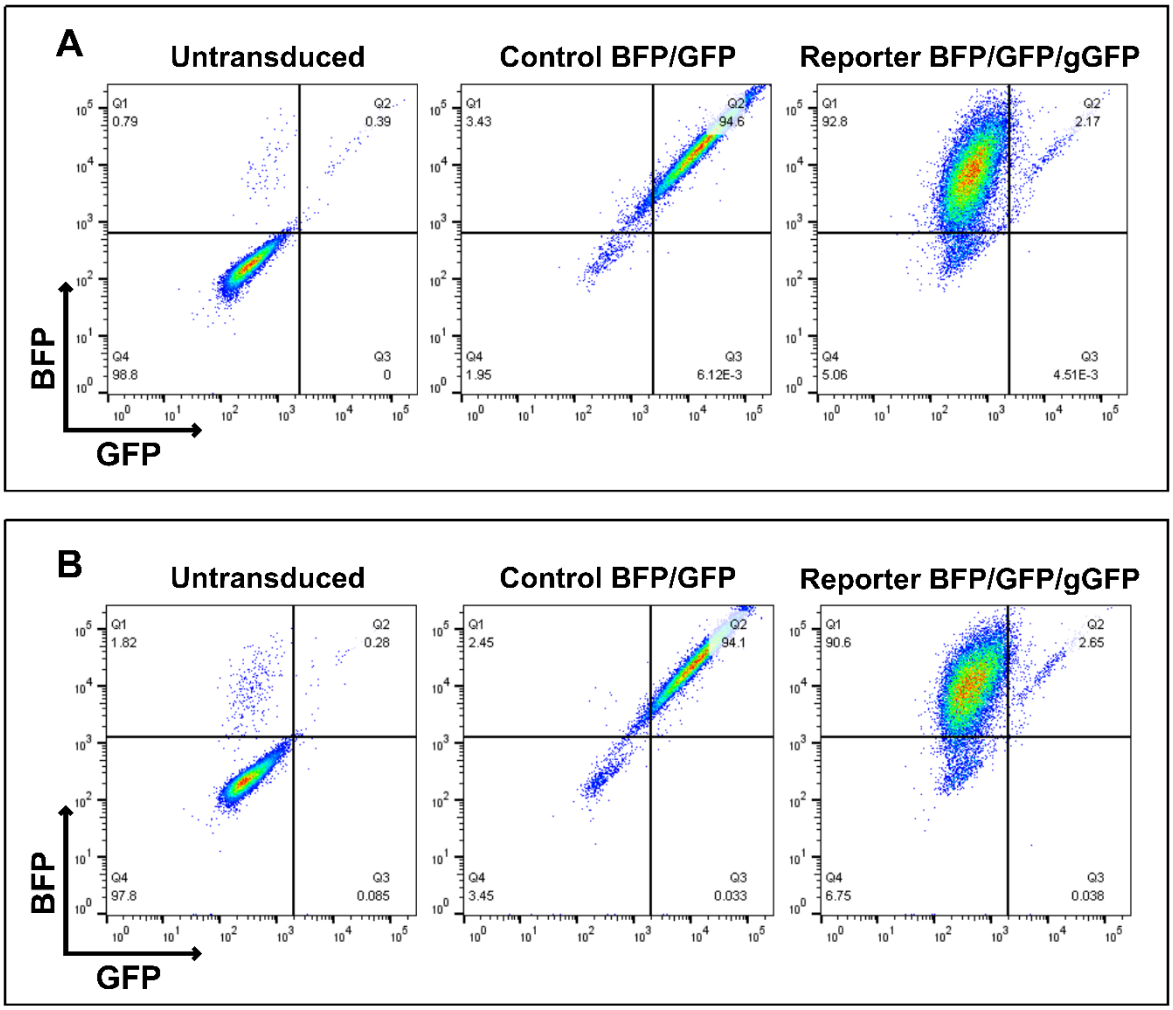

Figure 36. **Cas9 activity in A375 control and *SIN3B* knockout clones.** A) A375 control clone C1 was transduced with a control BFP/BFP vector (middle), a reporter BFP/GFP/gGFP (right) or untransduced (left). B) A375 *SIN3B* knockout clones C25 transduced with the same vectors. In both cases, untransduced cells were used as control for gating flow cytometry results. Almost 90% Cas9 activity was measured.

5.3.3.2. NeoR-IRES library lentivirus titration

As described in Section 4.6.1, the NeoR-IRES genome-wide library was packaged into a lentivirus. All five Cas9 expressing clones from A375 metastatic melanoma cells (control C1, control C4, *SIN3B* knockout C11, *SIN3B* knockout C25, and *SIN3B* knockout C26) were transduced with the library at an MOI (multiplicity of infection) of 0,3 to secure each cell carrying a single gRNA. Subsequently, the library lentivirus was titrated in each clone (volumes of lentivirus presented in Figure 14), using BFP as a marker. BFP expression was measured by flow cytometry (Figure 37), and the amount of lentivirus required for the screening was calculated as the volume equivalent of 30% BFP positive cells.

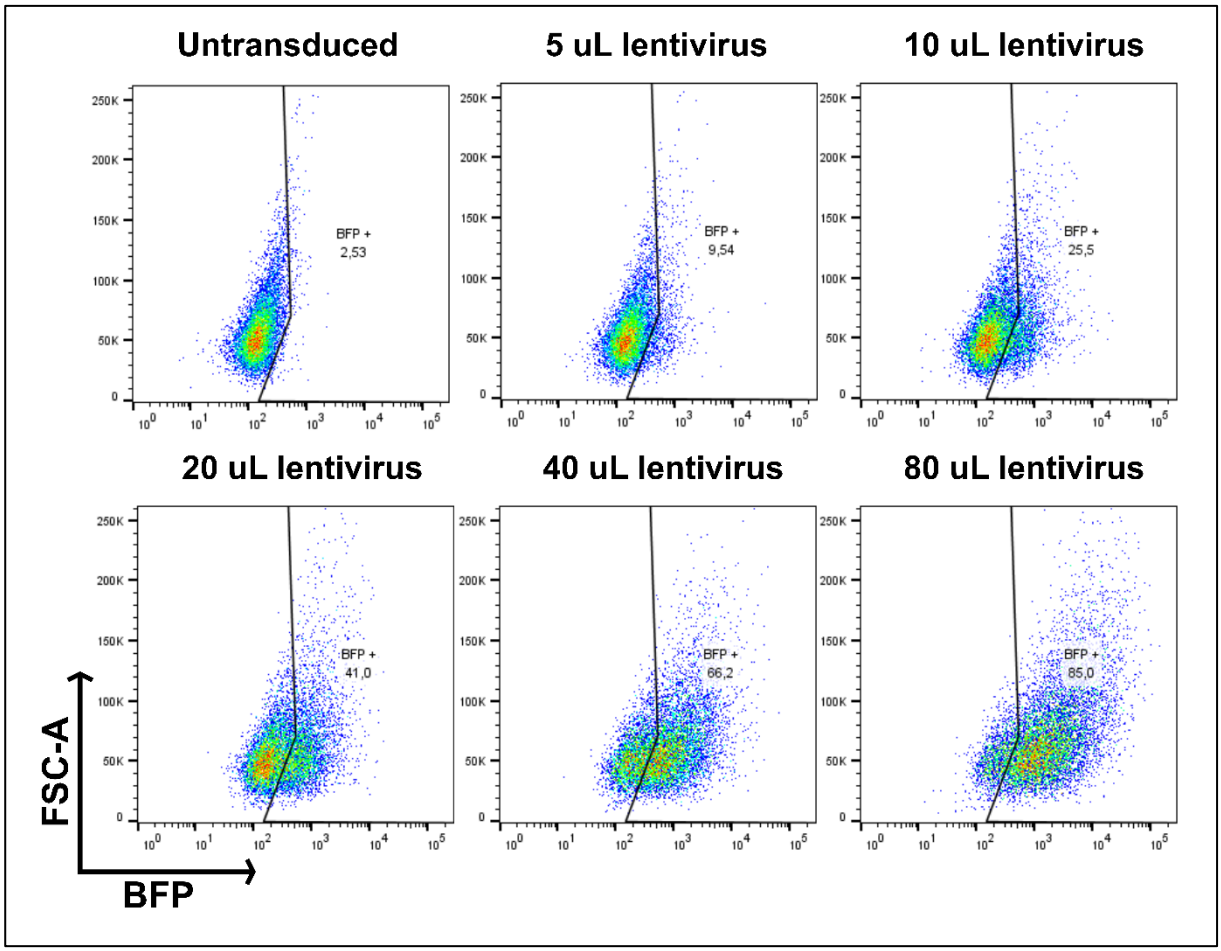

Figure 37. **Representative image of library titration results in A375 control clone C1**. Flow cytometry plots present increasing BFP expression with various volumes of the NeoR-IRES library lentivirus. Untransduced cells were used as control to gate the plots.

The representative image of library titration results from A375 control clone C1 was presented in Figure 37. A dose-dependent effect was noted during titration, where increasing volumes of lentivirus led to higher BFP expression. Similar results were obtained for all five clones used in the screening. Thus, we estimated the amount of virus required for the pooled library transduction in our melanoma clones (MOI=0.3) by plotting the percentage of BFP positive cells versus the different volumes of the virus used in the titration. A linear regression of the dose-dependent curve allowed us to identify how much virus was equivalent to 30% BFP expression. Since we performed the titration in 6-well plates, we scaled up virus volumes for T150 prior to the screen.

5.3.3.3. *USP7* and *STK11* as *SIN3B* synthetic lethal candidates

After establishing optimal conditions for the screen, which included high Cas9 activity in our cells and proper volume of virus requered for transduction, we performed the pooled genome-wide CRISPR screen to identify *SIN3B* synthetic lethal candidates. The protocol is presented in Section 4.6.4. Briefly, all five A375 clones were infected in triplicates at a MOI close to 0,3 and with a library coverage of 100x. Then, successfully transduced cells were selected with neomycin (G418, geneticin, Thermo Fisher, #10131027) for five days and expanded. After expansion for more two weeks, DNA was extracted from cell pellets, PCR amplified and subjected to sequencing. Finally, sequencing, reads were aligned to the gRNAs present in the library and data analysis was conducted by Victoria Offord, from David Adam´s group at the Wellcome Trust Sanger Institute. Of note, each screen was carried out in techinical triplicate to ensure data reproducibility.

In sum, after the sequencing, a few steps of quality control check of the data were employed prior to analysis. First, the CASM IT pipelines at Sanger correlated the sequencing reads with the gRNA sequences, generating a count file per sample. Read counts were quantified using the crisprReadCounts2 package (version 2.1.0) and filtered, removing all 1004 non-targeting controls gRNAs presented in the library since they were enriched and skewed results. gRNAs with low reads (<30 reads) were also removed to eliminate noise. After that, the CRISPRcleanR package was used to normalize all samples and correct reads for copy numbers to account for false-positive rates. Additionally, Pearson Spearman's rank correlation was performed to infer similarities among the samples' replicates, comparing the counts of each screened control clones with the plasmid library.

Finally, after all data filtering, MAGeCK analysis was employed to remove zero gRNA counts (missing gRNAs) and identify enriched and depleted gRNAs in the isogenic *SIN3B* depleted clones. The MAGeCK (Model-based Analysis of Genome-wide CRISPR/Cas9 Knockout) algorithm identifies significant differences in gRNA abundance between control and treatment (in this project, control and *SIN3B* deleted cells).[98] Thus, Pearson's correlation plots between the control clones and MAGeCK results comparing best performance control clone C4 with the other three deleted for *SIN3B* clones are presented in Figure 38.

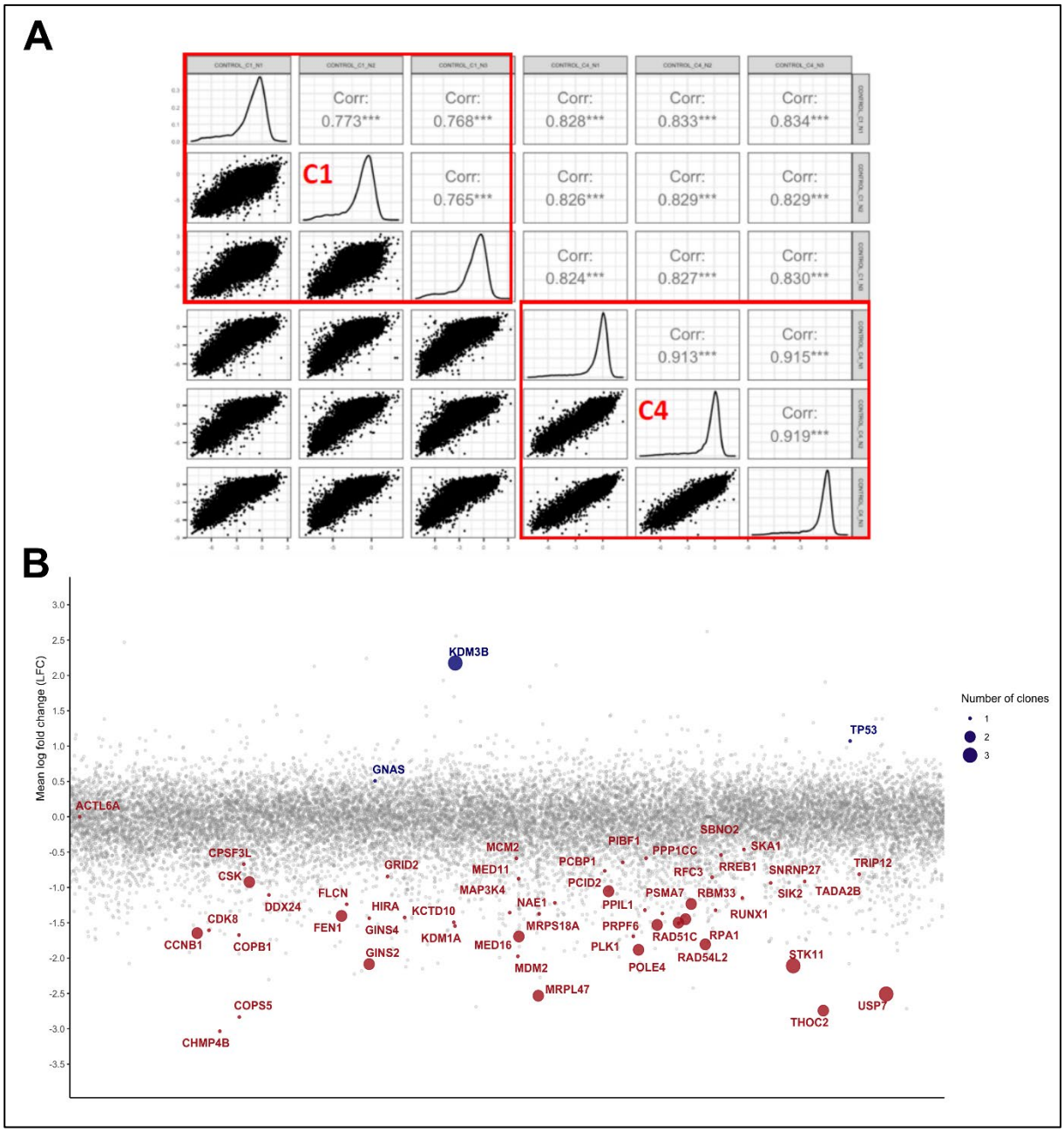

Figure 38. **Quality control metrics from the screen and candidate synthetic lethal partners of SIN3B.** A) Correlation scatterplots of gRNA counts (log2-normalized) between control replicates. Pearson's R values are presented for each comparison. Values close to one indicates that the replicates of one sample are similar. In this case, control clone C4 presented a higher correlation, hence, less variability among replicates. B) Genome-wide CRISPR screen identified genes essential for viability of SIN3B-deleted cells. Dots in red represent depleted genes found on the screen. Conversely, dots in blue are enriched genes. Size dots indicate how many clones a specific gene was found as significant Data was presented by mean log fold change and considered significant with a p-value<0.05.

The Pearson's pairwise plots from the control clone C4 showed a higher correlation value, over 0.9, compared to control clone C1 suggesting less variability within replicates, so we decided to use the clone C4 for MAGeCK analysis. MAGeCK then was used to pinpoint either a gene whose knockout impairs cell fitness, coming up as depleted, or a gene whose

knockout induces cell proliferation, having significant enrichment of gRNAs.[98] The list of all enriched and depleted genes are presented in Appendix A.2.

We found in our data two genes significantly depleted in all three *SIN3B*-null clones, i.e., *SIN3B* synthetic lethal partners: USP7 and STK11. Interestingly, we also found *KDM3B* enriched in all *SIN3B* deleted clones. Both results have never been reported in the literature. In addition, we further looked at the STRING (Search Tool for Retrieval of Interacting Genes/Proteins, https://string-db.org/) online database to determine the functional association between the synthetic lethal hits *USP7, STK11* and *SIN3B* (Figure 39).[1]

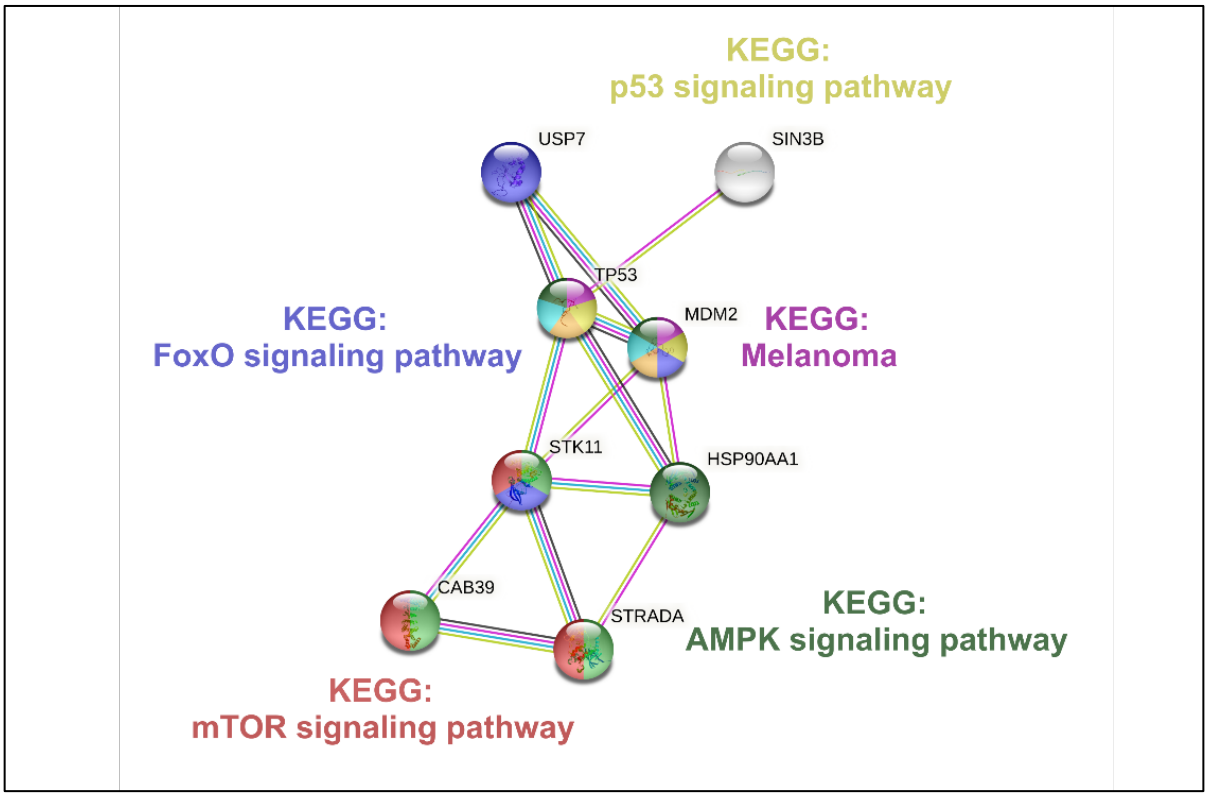

Figure 39. **Output from STRING analysis of pooled validation screen hits**. The proteins encoded by the screen hits were analyzed using STRING[1] to pinpoint their interactions. Lines between the nodes indicate predicted interactions. Common pathways of the interactor proteins are highlighted in different colors.

Altogether, these findings describe novel mechanisms which could aid in the understanding of *SIN3B* gene function, highlighting that *SIN3B* inhibition could have a synergistic effect on melanoma cell lines with *USP7* and *STK11* deficiency. *SIN3B* has never been studied in melanomas, but U*SP7* and *STK11* have been addressed.

USP7 (also known as Herpesvirus-associated ubiquitin-specific protease, HAUSP) is a deubiquitinating enzyme that has been extensively characterized, participating in regulating

many cellular processes, including DNA damage epigenetic regulation and tumor progression.[200] USP7 associates with the ubiquitin ligase MDM2 to target the tumor suppressor P53 for degradation and affects oncogenesis through several modulators, including PTEN and FOXO.[201] In melanomas, it is upregulated, and its function loss significantly inhibits melanoma cell proliferation and induces apoptosis.[200] Additionally, pharmacological inhibition of USP7 has been reported, suppressing growth and invasion of melanomas *in* vitro, and tumor growth *in vivo*.[202] Contrarily, *STK11* (also know as *LKB1*) encodes a highly conserved serine/threonine kinase and is often mutated in melanomas (~10%)[203], resulting in its somatic inactivation which facilitates melanoma invasion and metastasis.[204] Several works support the evidence of *STK11* acting as a tumor suppressor, where the loss of the gene promotes metastatic behaviors through diverse mechanisms such as the AMPK signaling pathway and activation of epithelial-mesenchymal transition (EMT), and activation of focal adhesion.[205; 206; 207] Collectively, it is noteworthy how both *USP7* and *STK11* genes are associated to invasive processes in melanomas, findings that might correlate with our *SIN3B* results. As previously discussed with our transcriptome analysis, we found that *SIN3B* deletion downregulated several pathways related to cell migration, invasion, cell-cell interactions, and cell motility. Therefore, in regards to the synthetic lethality we found of *SIN3B* with *USP7* and *STK11,* we reasoned that a combinatory approach of simultaneous inhibition of *SIN3B* and *USP7,* given both are highly expressed in melanomas, or inhibition of *SIN3B* of *STK11* mutated melanomas (since they harbor loss of the *STK11* tumor suppressor) could aid to a more effective therapy for advanced melanomas.

MAGeCK can also be applied to identify significantly enriched genes. The demethylase KDM3B was enriched in our *SIN3B-depleted* clones. This alludes to the epigenetic role of the *SIN3B* gene. The corepressor *SIN3,* which includes the paralog *SIN3B*, is a histone-modifying complex that regulates several biological processes frequently through the repression of genes. Its activity is often attributed to its association with the deacetylase enzymes HDAC1 and HDAC2. However, besides deacetylases, a demethylase KDM5A/B was found to be part of this complex to regulate transcription .[208] [209] KDM3B catalyzes the demethylation of the lysine 9 of histone H3, thereby mediating transcriptional activation. However, KDM3B is reported in the literature to have cancer-type-dependent features, either promoting oncogenesis or acting as a tumor suppressor.[210] Altogether, we suggest that *SIN3B* deletion might promote *KDM3B* activation and abrogate invasive processes in melanomas.

6. CONCLUSION

Melanoma is frequently curable when diagnosed at early stages. However, advanced cases are usually refractory to current therapies. Therefore, we aimed with this project to explore the effects of the *SIN3B* gene on the biology of human melanomas. First, we have presented a comprehensive evaluation of how *SIN3B* is overexpressed in melanomas, using both bioinformatic analyses with patient samples and a panel of human melanoma cell lines, suggesting a role of the gene on melanoma progression. Subsequently, we engineered isogenic derivatives of melanoma cell lines carrying a loss of function of *SIN3B* through CRISPR-Cas9 methodology. Knockout of *SIN3B* was confirmed at the DNA and protein level, respectively, with next-generation sequencing and western blot. We then addressed the advantages of employing isogenic single clones to assess a gene function. Additionally, we focused on evaluating the phenotypical changes associated with *SIN3B* deletion, where we noticed no changes in proliferation but downregulation of pathways associated with tumor invasion, migration, and cell-cell interactions, through whole transcriptome analysis. Finally, we employed a pooled genome-wide CRISPR screening to determine *SIN3B* synthetic lethal targets. Our screen data showed *USP7* and *STK11*, both genes extensively studied in melanomas, as *SIN3B* synthetic lethal partners, contributing to the pro-invasive effects of *SIN3B*-expressing melanomas. Collectively, we stressed how CRISPR-Cas9 and high high-throughput analyses, such as RNA sequencing and genome-wide CRISPR screening, might be helpful to interrogate gene function. Primarily, we suggest a role of the *SIN3B* gene as a possible biomarker on cutaneous melanoma since a lack of this gene could contribute to a less invasive melanoma phenotype.

CHAPTER II: INTERFERON REGULATORY FACTOR 4 (IRF4) IN CUTANEOUS MELANOMAS

7. INTRODUCTION

IRF4 is a member of the Interferon Regulatory Factor (IRF) family of transcription factors expressed in the immune system cells, first reported as downstream mediators of the interferon signaling. They are widely expressed and have a central role in the regulation of immune responses, cell growth, induction of apoptosis, and transformation by oncogenes.[211; 212] However, differing from its family members, *IRF4* is not interferon responsive but instead seems to be activated by stimuli known to induce lymphocyte activation and differentiation, such as antigen receptor engagement, lipopolysaccharides, CD-40 signaling, and through association with the cytokine IL-4.[213; 214]

Remarkably, *IRF4* is restricted to cells of the immune system and melanocytic lineages. It is currently a diagnostic and prognostic marker for several hematological malignancies, including myeloma and T cell lymphoma/leukemia. In both diseases, *IRF4* is upregulated, inducing tumor growth.[215; 216] Thus, *IRF4* has oncogenic activity *in vitro*, assessed through an RNA interference genetic screen. Noticeably, knockdown of *IRF4* induced rapid and profound cell death in myelomas, attesting a gene addiction in this disease.[217] Therefore, these and related studies suggested *IRF4* as a therapy target in cancer.

In 2001, a tissue microarray and immunohistochemistry analysis showed that *IRF4* is widely expressed in melanomas.[218] Yet, this expression decreases according to tumor progression, suggesting that this transcription factor is detected in primary melanocytic lesions. In reality, another work using tissue microarray with 165 malignant melanoma samples of distinct progression phases demonstrated that 50% of benign nevi presented *IRF4,* whereas only 7% of metastatic cases had *IRF4* expression.[167] Nonetheless, despite the observed genetic link of *IRF4* expression, the role of this gene in melanoma is still poorly understood.

Large-scale sequencing of cutaneous melanoma has been extensively conducted and defined the key known driver mutations that promote melanoma development, such as *BRAF*, *NRAS* and *NF1*.[75] Nevertheless, most of them relied on advanced melanomas. So, in an attempt to fully explore early-stage tumors, a previous Ph.D. student from David Adam´s group at the Wellcome Trust Sanger Institute sequenced 524 primary melanomas and described

the mutational landscape of these tumors. Among novel driver genes, hotspot mutations, and promoter variants, Dr. Sofia Chen identified *IRF4*, located in chromosome 6p, as being highly amplified. Subsequently, Dr. Chen, together with Dr. Rashid Mamunur, intersected this dataset of primary melanomas with the DepMap CRISPR-Cas9 dropout screen dataset and discovered *IRF4* as one of the genes significantly associated with lethality in skin cancer cell lines, compared to those of other tissue origins.[219; 220; 221] Additionally, Dr. Chen looked at the expression of *IRF4* in TCGA data and pinpointed an increased expression of this gene in melanomas compared to normal tissues. Collectively, she built the hypothesis that *IRF4* could be essential to melanomas, i.e., that absence of this gene could be lethal to cutaneous melanomas. Her results are presented in Figure 40.

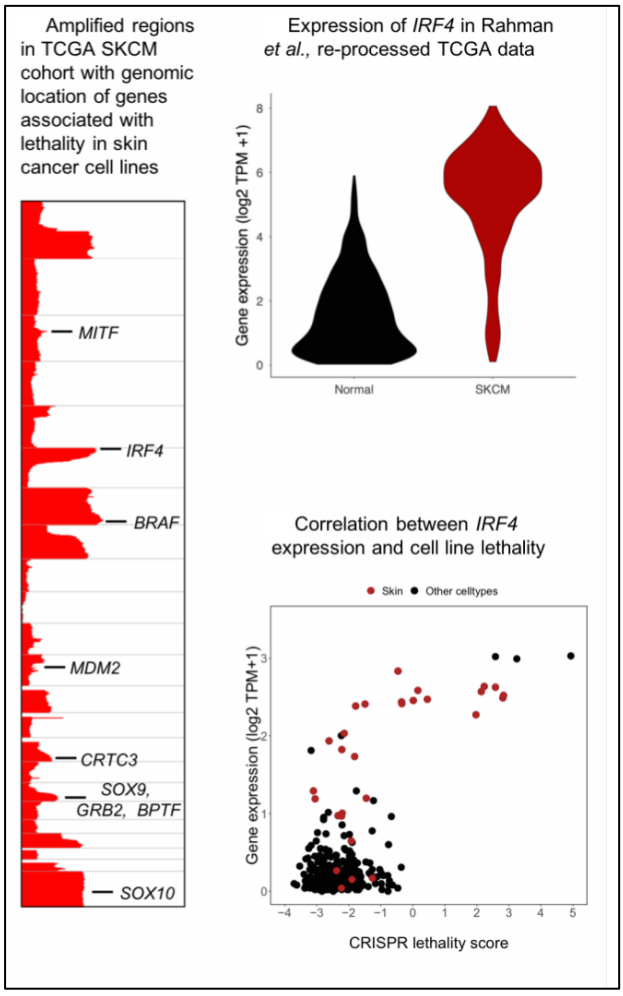

Figure 40. **Overview of highly amplified regions of melanomas and IRF4-associated lethality.** In the left panel are the regions commonly amplified in skin cancers through TCGA data and the genomic location of the genes found associated with lethality. The upper graph shows the expression of *IRF4* in reprocessed TCGA data, including normal tissue samples.[222] Data showed a higher expression of *IRF4* in skin cancers. The bottom graph is the result from the CRISPR-Cas9 dropout screen with melanoma cell lines and several other tumor cells. Melanoma cells are highlighted in red dots. These results show that increased *IRF4* expression correlates with a higher lethality score, i.e., high *IRF4*-expressing melanomas die upon the gene deletion.

8. CHAPTER AIMS

This small *IRF4* project aims to determine if *IRF4* loss is lethal to melanoma cell lines by:

- Silencing the *IRF4* gene in primary melanoma cell lines;
- Confirming *IRF4* knockdown through western blot;
- Assessing viability of primary melanomas post siRNA-mediated knockdown through flow cytometry.

9. MATERIALS AND METHODS

9.1. Cell culture

Primary melanoma cell lines were used. RVH421 and WM1799 were cultured in RPMI supplemented with 10% fetal bovine serum (FBS, Gibco) and 2 mM L-glutamine. WM983B and HT-144 cells were cultivated in Dulbecco's modified Eagle's medium (DMEM) supplemented with 10%FBS. All cultures were regularly tested and confirmed negative for *Mycoplasma spp.* infection. PCR (polymerase chain reaction) with specific primers for *Mycoplasma* detection was used. In addition, all cells were authenticated by STR profiling (short-tandem repeat profiling) and confirmed as equivalent to those published in the literature

9.2. siRNA-mediated knockdown

All primary melanoma cells were cultivated as previously described in Section 8.1. Cells were seeded at 2.10^5 cells/well in 6-well plates and incubated at 37°C, 5%CO_2 overnight. The next day, cells were transfected using a pool of siRNAs against *IRF4*, *ERH* (used as a positive control since this gene is lethal, data not shown), and nontargeting pool (introduced as a negative control because they do not target any coding region), according to the manufacturer's protocol (Dharmacon, ON-TARGETplus - SMARTpool). The siRNA sequences are illustrated in Table 15. Cells were re-transfected after 6 days and harvested for

flow cytometry analysis at day 10 post-transfection. All analyses were conducted in three independent experiments (biological triplicates).

Table 15. Sequences for siRNA-mediated knockdown

Gene	siRNA sequences
IRF4	CAUCACAGCUCACGUAGAA
	CCACAGAUCUAUCCGCCAU
	UGUCAGAGCUGCAAGCGUU
	GAAAAUGGUUGCCAGGUGA
ERH	AGACAUACCAGCCUUAUAA
	GGGAAAUAAUUGUGUUGGA
	AAGAGAAGAUCUACGUGCU
	UAGCCAAGAUUGACUGUAU
Non-targeting	UGGUUUACAUGUCGACUAA
	UGGUUUACAUGUUGUGUGA
	UGGUUUACAUGUUUUCUGA
	UGGUUUACAUGUUUUCCUA

9.3. Flow cytometry viability analysis

The primary melanoma cell lines were collected after 10 of transfection and harvested. Subsequently, all cells were washed with PBS and Annexin V binding buffer (BD Phamingen, #556454). Samples were subjected to Annexin V-PE staining (BioLegend, #640908) at a concentration of 5 µL/samples for 15 minutes at room temperature, followed by the addition of DAPI (Sigma, 1:5000 dilution). Samples were centrifuged, resuspended in Annexin V binding buffer, run in a flow cytometer (BD Fortessa II), and results were analyzed using FlowJo v.10.

9.4. Western blot to confirm successful knockdown

After 10 days of transfection with siRNAs against *IRF4*, *ERH* (positive control), and non-targeting pool, culture plates were placed on ice, and the cells were washed twice with ice-cold PBS. RIPA lysis buffer supplemented with protease inhibitor (as described in Section 4.2.5). Cells were incubated on ice for 5-10 minutes, then scraped and transferred to Eppendorfs. Samples were centrifuged at 14,000g for 30 minutes at 4°C. The supernatant was transferred to fresh Eppendorfs and stored at -80°C. Protein lysates were quantified using the PierceTM BCA Protein Assay Kit (#23227, Thermo Fisher Scientific), as instructed by the manufacturer's protocol. All protein samples were run under reducing conditions (as discussed in Section 4.2.5) and PVDF membranes stained with primary rabbit antibodies against GAPDH (Cell Signaling, clone 14C10), IRF4 (Cell Signaling, #4964), or c-Myc (Abcam, clone Y69) followed by a Horseradish Peroxidase-conjugated goat anti-rabbit secondary antibody (Abcam, #ab6721). Protein chemiluminescence detection was performed using ImageQuant (GE LifeSciences).

10. RESULTS AND DISCUSSION

10.1. *IRF4* is essential for primary melanomas

IRF4 is widely expressed in melanomas, and its expression decreases during tumor progression. Therefore, *IRF4* is commonly detected in primary melanocytic lesions.[218; 223] A previous study led by Dr. Sofia Chen at the Wellcome Trust Sanger Institute profiled 524 primary melanomas and found that *IRF4* was highly amplified and expressed. Also, correlating this data with the DepMap dataset[221], where CRISPR-Cas9 screening was employed to identify essential genes in 342 cancer cell lines, *IRF4* was found to be essential in high *IRF4*-expressed melanomas. Therefore, we sought to validate whether loss of *IRF4* expression was lethal to melanoma cell lines.

To test this hypothesis, we knocked down *IRF4* in four different melanoma cell lines, two low *IRF4*-expressed cells used as controls, and two high *IRF4*-expressed cells. Additionally, we used cells transfected with non-targeting siRNAs as negative controls and cells transfected with siRNA targeting *ERH* gene because it was confirmed through the DepMap analysis as an essential gene (data not shown), so it should be lethal to the melanoma cells. All experiments were conducted in three independent experiments, each in technical triplicate. Thus, we confirmed a knockdown by measuring *IRF4* protein levels with western blot, as shown in Figure 41.

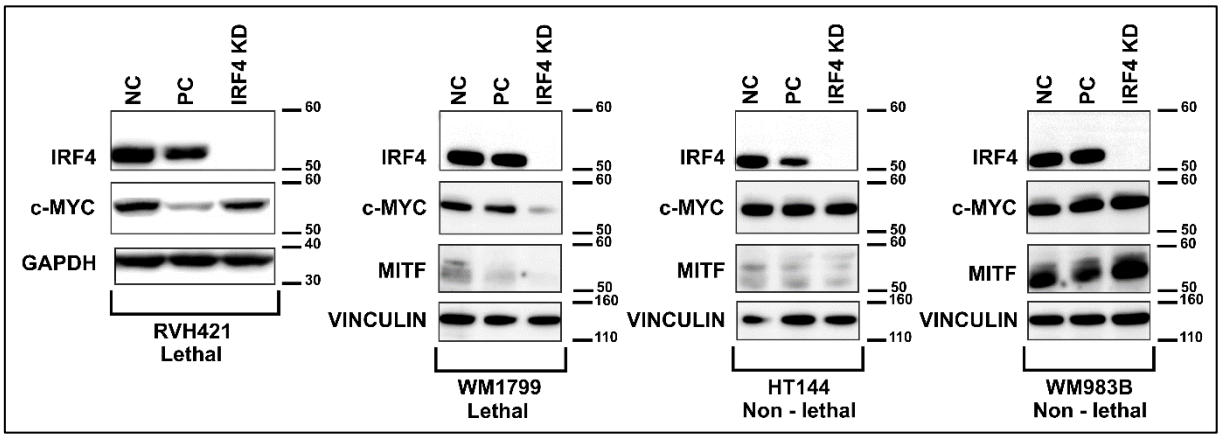

Figure 41. Immunoblots of melanoma cells post-transfection with *IRF4* siRNAs. Control low-*IRF4* expressing cells (HT-144 and WM983B) and high *IRF4*-expressing cells (RVH421 and WM1799) were transfected with non-targeting siRNAs (NT, negative control), *ERH* siRNAs (PC, positive control), and siRNAs for *IRF4.* In addition, known *IRF4* targets *MITF* and *MYC* were also assessed. All data is representative of three independent experiments.

Successful *IRF4* knockdown was achieved for all cells. Interestingly, common *IRF4* downstream targets *MITF* and *MYC* were not generally affected by *IRF4* loss, except for the WM1799 cell lines. Both the proto-oncogene *MYC* and the transcription factor *MITF* have a positive regulation with *IRF4*. *MYC* is highly expressed in metastatic melanomas, and it is a primary target of *IRF4* since *MYC* overexpression upregulates *IRF4*.[224] Similarly, *MITF* activates the expression of *IRF4* in human melanocytes. Hence both genes are associated with human pigmentation.[225] Altogether, we reasoned that *IRF4* silencing should have an effect in *MYC* and *MITF*. However, through our western blots, no changes were noted. For the analysis of dying cells, fluorescently labeled Annexin V and DAPI were checked through flow cytometry. Briefly, Annexin V detects apoptotic cells since this protein binds to phosphatidylserine commonly externalized during apoptosis, while DAPI measures necrotic cells since it labels nucleic acids, which are reached when plasma membrane integrity is lost. The effects of *IRF4* knockdown in human melanoma cell lines are presented in Figure 42.

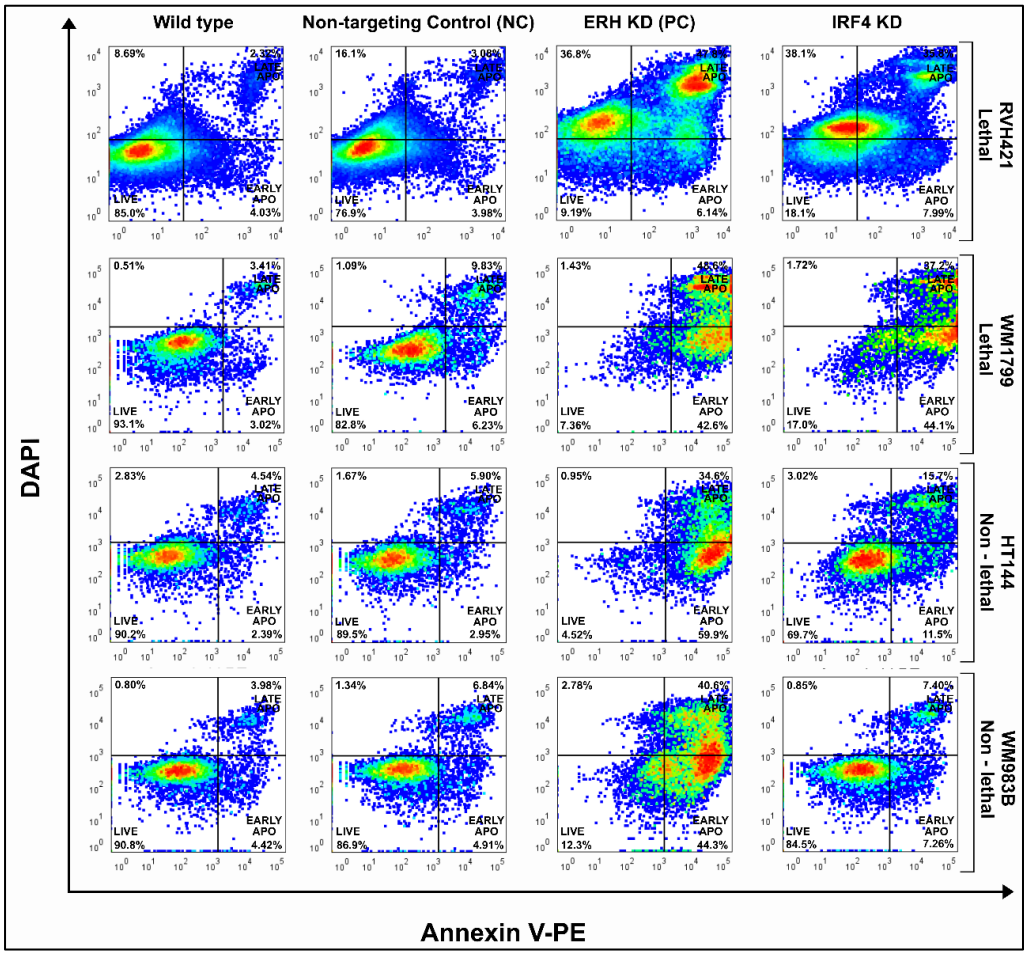

Figure 42. **Flow cytometry analysis of melanomas cells silenced for *IRF4*.** Low *IRF4*-expressing control cells (HT-144 and WM983B) did not die upon *IRF4* knockdown when compared with the positive control cells (transfected with *ERH* siRNAs). However, in the high *IRF4*-expressing cells (RVH421 and WM1799), *IRF4* loss resulted in cell death, highlighted by positive staining for DAPI and Annexin V-PE.

Low *IRF4*-expressing melanoma cells, used as controls, did not die upon the gene silencing. However, high expressing cells, which have similar conditions often presented in melanomas (since *IRF4* is amplified and overexpressed), died, comparably to what was found with the positive control cells, transfected with *ERH*. Remarkably, upon *IRF4* deletion, cells died through apoptosis, due to either double-positive staining for DAPI and Annexin V-PE or positive staining only for Annexin V-PE. Figure 43 presents the quantification plots from three independent experiments, indicating the percentage of living, necrotic, early apoptotic, or late apoptotic cells. Altogether, *IRF4* knockdown sustained *MYC* and *MITF* expression, and loss of *IRF4* resulted in melanoma cell death. Thus, we suggest that *IRF4* amplification could be an oncogenic event in melanoma, favoring its maintenance, and a lack of this gene may cause a tumor cell vulnerability, independent of *MYC* and MITF, which could be further exploited therapeutically.

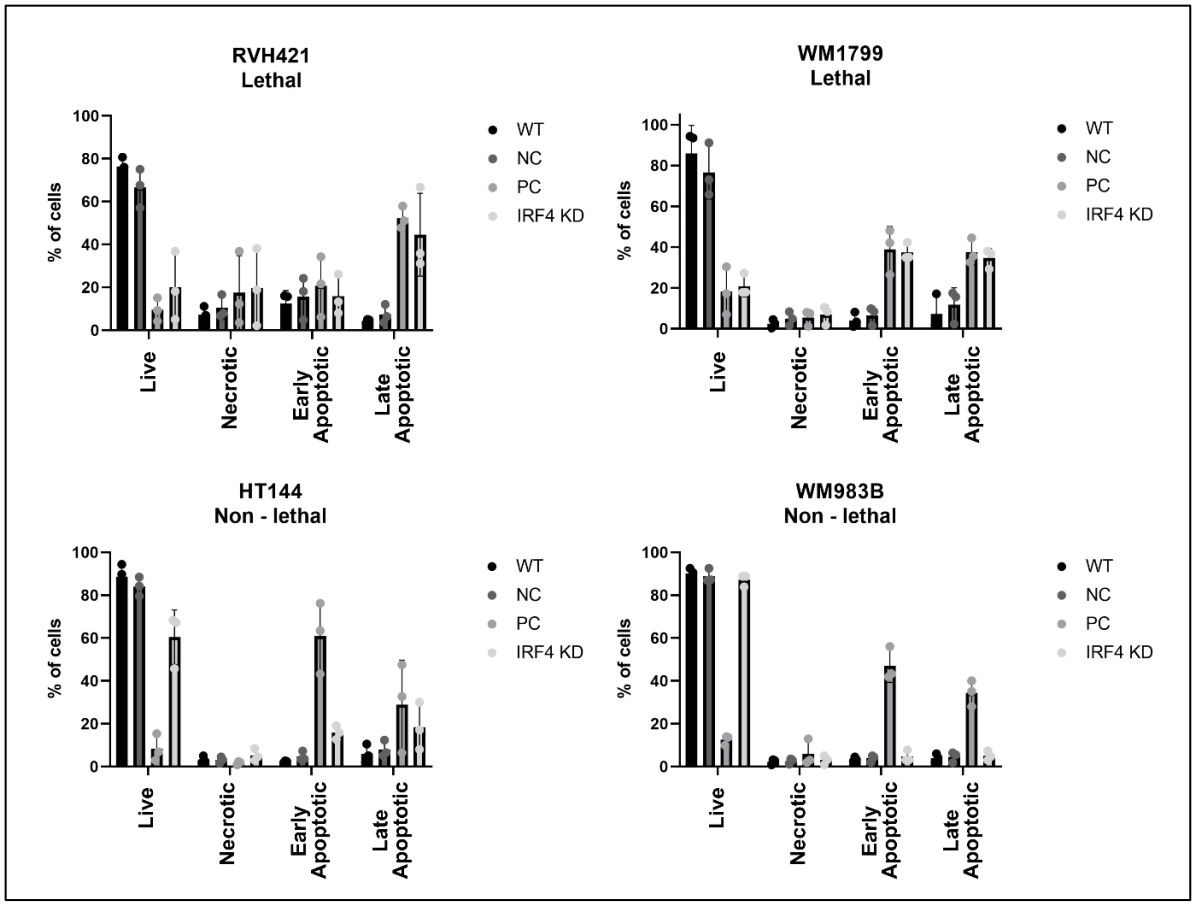

Figure 43. ***IRF4* silencing induces apoptosis on melanoma cells.** Quantitation of the percentage of living, necrotic, early apoptotic, and late apoptotic cells. These populations were labeled due to positive or negative staining for DAPI and Annexin V-PE staining. Quantitative plots are representative of three independent experiments. Noticeably, control cells (low *IRF4*-expressing cells HT144 and WM983B) do not die upon *IRF4* deletion when comparing the results with negative control (NC, cells transfected with non-targeting siRNAs). Conversely, high *IRF4*-expressing melanoma cells (RVH421 and WM1799) die through apoptosis, compared with the positive control (PC, cells transfected with *ERH* siRNAs).

11. CONCLUSION

IRF4 is highly amplified in primary melanomas, and depletion of this gene was associated with lethality in several melanoma cell lines through DepMap CRISPR-Cas9 screen data. Thus, *IRF4* was hypothesized to be an oncogenic event in melanoma since a subset of melanomas presented an *IRF4*-dependency. Our results found that loss of *IRF4* expression in primary melanoma cell lines caused cell death, mainly through apoptosis. Hence, we suggest that *IRF4* inhibition could be exploited as an alternative therapy for melanoma patients. These results are part of a project conducted by Dr. Sofia Chen during her Ph.D. that aimed to present a comprehensive evaluation into the somatic alteration landscape of primary melanomas. The experiments discussed in this thesis were performed during my sandwich Ph.D. at the Wellcome Trust Sanger Institute (Cambridge, United Kingdom), as a collaboration with the group of Dr. David Adams. These data will be included in a manuscript currently being prepared for submission, with a provisional name of "Mutually exclusive genetic interactions and gene essentiality shape the genomic landscape of primary melanoma".

REFERENCES

[1] SZKLARCZYK, D. et al. STRING v11: protein-protein association networks with increased coverage, supporting functional discovery in genome-wide experimental datasets. **Nucleic Acids Research,** v. 47, n. D1, p. D607-D613, 01 08 2019. ISSN 1362-4962. Disponível em: < https://www.ncbi.nlm.nih.gov/pubmed/30476243 >.

[2] SATYAMOORTHY, K.; HERLYN, M. Cellular and molecular biology of human melanoma. **Cancer Biology and Therapy,** v. 1, n. 1, p. 14-17, 2002 Jan-Feb 2002. ISSN 1538-4047. Disponível em: < https://www.ncbi.nlm.nih.gov/pubmed/12170758 >.

[3] MILLER, A. J.; MIHM, M. C. Melanoma. **N Engl J Med,** v. 355, n. 1, p. 51-65, Jul 06 2006. ISSN 1533-4406. Disponível em: < https://www.ncbi.nlm.nih.gov/pubmed/16822996 >.

[4] Câncer de pele melanoma. Disponível em: < https://www.inca.gov.br/tipos-de-cancer/cancer-de-pele-melanoma >. Acesso em: 18/09/2021.

[5] SUNG, H. et al. Global Cancer Statistics 2020: GLOBOCAN Estimates of Incidence and Mortality Worldwide for 36 Cancers in 185 Countries. **CA: A Cancer Journal for Clinicians,** v. 71, n. 3, p. 209-249, 05 2021. ISSN 1542-4863. Disponível em: < https://www.ncbi.nlm.nih.gov/pubmed/33538338 >.

[6] Global Cancer Observatory. Disponível em: < https://gco.iarc.fr/ >. Acesso em: 20/09/2021.

[7] EDDY, K.; SHAH, R.; CHEN, S. Decoding Melanoma Development and Progression: Identification of Therapeutic Vulnerabilities. **Front Oncol,** v. 10, p. 626129, 2020. ISSN 2234-943X. Disponível em: < https://www.ncbi.nlm.nih.gov/pubmed/33614507 >.

[8] GARBE, C. et al. European consensus-based interdisciplinary guideline for melanoma. Part 1: Diagnostics - Update 2019. **European Journal of Cancer,** v. 126, p. 141-158, 02 2020. ISSN 1879-0852. Disponível em: < https://www.ncbi.nlm.nih.gov/pubmed/31928887 >.

[9] SIEGEL, R. L. et al. Cancer Statistics, 2021. **CA: A Cancer Journal for Clinicians,** v. 71, n. 1, p. 7-33, 01 2021. ISSN 1542-4863. Disponível em: < https://www.ncbi.nlm.nih.gov/pubmed/33433946 >.

[10] ORGAZ, J. L.; SANZ-MORENO, V. Emerging molecular targets in melanoma invasion and metastasis. **Pigment Cell Melanoma Research,** v. 26, n. 1, p. 39-57, Jan 2013. ISSN 1755-148X. Disponível em: < https://www.ncbi.nlm.nih.gov/pubmed/23095214 >.

[11] SHAIN, A. H.; BASTIAN, B. C. From melanocytes to melanomas. **Nature Reviews Cancer,** v. 16, n. 6, p. 345-358, Jun 2016. ISSN 1474-1768. Disponível em: < https://www.ncbi.nlm.nih.gov/pubmed/27125352 >.

[12] MILLER, A. J.; MIHM, M. C. Melanoma. **The New England Journal of Medicine,** v. 355, n. 1, p. 51-65, Jul 06 2006. ISSN 1533-4406. Disponível em: < https://www.ncbi.nlm.nih.gov/pubmed/16822996 >.

[13] TAKATA, M.; MURATA, H.; SAIDA, T. Molecular pathogenesis of malignant melanoma: a different perspective from the studies of melanocytic nevus and acral melanoma. **Pigment Cell**

Melanoma Res, v. 23, n. 1, p. 64-71, Feb 2010. ISSN 1755-148X. Disponível em: < https://www.ncbi.nlm.nih.gov/pubmed/19788535 >.

14 DAMSKY, W. E.; BOSENBERG, M. Melanocytic nevi and melanoma: unraveling a complex relationship. **Oncogene,** v. 36, n. 42, p. 5771-5792, 10 19 2017. ISSN 1476-5594. Disponível em: < https://www.ncbi.nlm.nih.gov/pubmed/28604751 >.

15 VOGELSTEIN, B. et al. Cancer genome landscapes. **Science,** v. 339, n. 6127, p. 1546-58, Mar 29 2013. ISSN 1095-9203. Disponível em: < https://www.ncbi.nlm.nih.gov/pubmed/23539594 >.

16 ALEXANDROV, L. B. et al. Signatures of mutational processes in human cancer. **Nature,** v. 500, n. 7463, p. 415-21, Aug 22 2013. ISSN 1476-4687. Disponível em: < https://www.ncbi.nlm.nih.gov/pubmed/23945592 >.

17 LEONARDI, G. C. et al. Cutaneous melanoma: From pathogenesis to therapy (Review). **International Journal of Oncology,** v. 52, n. 4, p. 1071-1080, Apr 2018. ISSN 1791-2423. Disponível em: < https://www.ncbi.nlm.nih.gov/pubmed/29532857 >.

18 HAYWARD, N. K. et al. Whole-genome landscapes of major melanoma subtypes. **Nature,** v. 545, n. 7653, p. 175-180, 05 11 2017. ISSN 1476-4687. Disponível em: < https://www.ncbi.nlm.nih.gov/pubmed/28467829 >.

19 NETWORK, C. G. A. Genomic Classification of Cutaneous Melanoma. **Cell,** v. 161, n. 7, p. 1681-96, Jun 18 2015. ISSN 1097-4172. Disponível em: < https://www.ncbi.nlm.nih.gov/pubmed/26091043 >.

20 COLOMBINO, M. et al. BRAF/NRAS mutation frequencies among primary tumors and metastases in patients with melanoma. **Journal of Clinical Oncology,** v. 30, n. 20, p. 2522-9, Jul 10 2012. ISSN 1527-7755. Disponível em: < https://www.ncbi.nlm.nih.gov/pubmed/22614978 >.

21 DAVIES, H. et al. Mutations of the BRAF gene in human cancer. **Nature,** v. 417, n. 6892, p. 949-54, Jun 27 2002. ISSN 0028-0836. Disponível em: < https://www.ncbi.nlm.nih.gov/pubmed/12068308 >.

22 ASCIERTO, P. A. et al. The role of BRAF V600 mutation in melanoma. **Journal of Translational Medicine,** v. 10, p. 85, 2012. ISSN 1479-5876. Disponível em: < https://www.ncbi.nlm.nih.gov/pubmed/22554099 >.

23 MAURER, G.; TARKOWSKI, B.; BACCARINI, M. Raf kinases in cancer-roles and therapeutic opportunities. **Oncogene,** v. 30, n. 32, p. 3477-3488, Aug 2011. ISSN 1476-5594. Disponível em: < https://www.ncbi.nlm.nih.gov/pubmed/21577205 >.

24 PLATZ, A. et al. Human cutaneous melanoma; a review of NRAS and BRAF mutation frequencies in relation to histogenetic subclass and body site. **Molecular Oncology,** v. 1, n. 4, p. 395-405, 4// 2008. ISSN 1574-7891. Disponível em: < http://www.sciencedirect.com/science/article/pii/S1574789107001044 >.

25 HERTZMAN, J. C.; EGYHAZI, S. B. BRAF inhibitors in cancer therapy. **Pharmacology & Therapeutics,** v. 142, n. 2, p. 176-182, 5// 2014. ISSN 0163-7258. Disponível em: < http://www.sciencedirect.com/science/article/pii/S0163725813002416 >.

[26] YAJIMA, I. et al. RAS/RAF/MEK/ERK and PI3K/PTEN/AKT Signaling in Malignant Melanoma Progression and Therapy. **Dermatology Research and Practice,** v. 2012, p. 354191, 2012. ISSN 1687-6113. Disponível em: < https://www.ncbi.nlm.nih.gov/pubmed/22013435 >.

[27] VANNI, I. et al. Non-BRAF Mutant Melanoma: Molecular Features and Therapeutical Implications. **Front Mol Biosci,** v. 7, p. 172, 2020. ISSN 2296-889X. Disponível em: < https://www.ncbi.nlm.nih.gov/pubmed/32850962 >.

[28] KELLEHER, F. C.; MCARTHUR, G. A. Targeting NRAS in melanoma. **Cancer J,** v. 18, n. 2, p. 132-6, 2012 Mar-Apr 2012. ISSN 1540-336X. Disponível em: < https://www.ncbi.nlm.nih.gov/pubmed/22453013 >.

[29] PALMIERI, G. et al. Multiple Molecular Pathways in Melanomagenesis: Characterization of Therapeutic Targets. **Frontiers in Oncology,** v. 5, p. 183, 2015. ISSN 2234-943X. Disponível em: < https://www.ncbi.nlm.nih.gov/pubmed/26322273 >.

[30] MAERTENS, O. et al. Elucidating distinct roles for NF1 in melanomagenesis. **Cancer Discovery,** v. 3, n. 3, p. 338-49, Mar 2013. ISSN 2159-8290. Disponível em: < https://www.ncbi.nlm.nih.gov/pubmed/23171796 >.

[31] KIURU, M.; BUSAM, K. J. The NF1 gene in tumor syndromes and melanoma. **Laboratory Investigation,** v. 97, n. 2, p. 146-157, 02 2017. ISSN 1530-0307. Disponível em: < https://www.ncbi.nlm.nih.gov/pubmed/28067895 >.

[32] BEADLING, C. et al. KIT gene mutations and copy number in melanoma subtypes. **Clinical Cancer Research,** v. 14, n. 21, p. 6821-8, Nov 01 2008. ISSN 1078-0432. Disponível em: < https://www.ncbi.nlm.nih.gov/pubmed/18980976 >.

[33] FECHER, L. A. et al. Toward a molecular classification of melanoma. **Journal of Clinical Oncology,** v. 25, n. 12, p. 1606-20, Apr 20 2007. ISSN 1527-7755. Disponível em: < https://www.ncbi.nlm.nih.gov/pubmed/17443002 >.

[34] LIM, S. Y.; MENZIES, A. M.; RIZOS, H. Mechanisms and strategies to overcome resistance to molecularly targeted therapy for melanoma. **Cancer,** v. 123, n. S11, p. 2118-2129, 06 01 2017. ISSN 1097-0142. Disponível em: < https://www.ncbi.nlm.nih.gov/pubmed/28543695 >.

[35] DOMINGUES, B. et al. Melanoma treatment in review. **Immunotargets and Therapy,** v. 7, p. 35-49, 2018. ISSN 2253-1556. Disponível em: < https://www.ncbi.nlm.nih.gov/pubmed/29922629 >.

[36] ROSS, M. I.; GERSHENWALD, J. E. Evidence-based treatment of early-stage melanoma. **Journal of Surgical Oncology,** v. 104, n. 4, p. 341-53, Sep 2011. ISSN 1096-9098. Disponível em: < https://www.ncbi.nlm.nih.gov/pubmed/21858828 >.

[37] WILSON, M. A.; SCHUCHTER, L. M. Chemotherapy for Melanoma. **Cancer Treatment and Research,** v. 167, p. 209-29, 2016. ISSN 0927-3042. Disponível em: < https://www.ncbi.nlm.nih.gov/pubmed/26601864 >.

[38] MIDDLETON, M. R. et al. Randomized phase III study of temozolomide versus dacarbazine in the treatment of patients with advanced metastatic malignant melanoma. **Journal of Clinical Oncology,** v. 18, n. 1, p. 158-66, Jan 2000. ISSN 0732-183X. Disponível em: < https://www.ncbi.nlm.nih.gov/pubmed/10623706 >.

[39] DAVIS, L. E.; SHALIN, S. C.; TACKETT, A. J. Current state of melanoma diagnosis and treatment. **Cancer Biology and Therapy,** v. 20, n. 11, p. 1366-1379, 2019. ISSN 1555-8576. Disponível em: < https://www.ncbi.nlm.nih.gov/pubmed/31366280 >.

[40] LUKE, J. J. et al. Targeted agents and immunotherapies: optimizing outcomes in melanoma. **Nature Reviews Clinical Oncology,** v. 14, n. 8, p. 463-482, Aug 2017. ISSN 1759-4782. Disponível em: < https://www.ncbi.nlm.nih.gov/pubmed/28374786 >.

[41] BOLLAG, G. et al. Clinical efficacy of a RAF inhibitor needs broad target blockade in BRAF-mutant melanoma. **Nature,** v. 467, n. 7315, p. 596-9, Sep 30 2010. ISSN 1476-4687. Disponível em: < https://www.ncbi.nlm.nih.gov/pubmed/20823850 >.

[42] CHAPMAN, P. B. et al. Improved survival with vemurafenib in melanoma with BRAF V600E mutation. **The New England Journal of Medicine,** v. 364, n. 26, p. 2507-16, Jun 30 2011. ISSN 1533-4406. Disponível em: < https://www.ncbi.nlm.nih.gov/pubmed/21639808 >.

[43] FLAHERTY, K. T. et al. Inhibition of mutated, activated BRAF in metastatic melanoma. **The New England Journal of Medicine,** v. 363, n. 9, p. 809-19, Aug 26 2010. ISSN 1533-4406. Disponível em: < https://www.ncbi.nlm.nih.gov/pubmed/20818844 >.

[44] NGUYEN, K.; HIGNETT, E.; KHACHEMOUNE, A. Current and emerging treatment options for metastatic melanoma: a focused review. **Dermatology Online Journal,** v. 26, n. 7, Jul 15 2020. ISSN 1087-2108. Disponível em: < https://www.ncbi.nlm.nih.gov/pubmed/32898395 >.

[45] FALCHOOK, G. S. et al. Dabrafenib in patients with melanoma, untreated brain metastases, and other solid tumours: a phase 1 dose-escalation trial. **Lancet,** v. 379, n. 9829, p. 1893-901, May 19 2012. ISSN 1474-547X. Disponível em: < https://www.ncbi.nlm.nih.gov/pubmed/22608338 >.

[46] AZIJLI, K. et al. New developments in the treatment of metastatic melanoma: immune checkpoint inhibitors and targeted therapies. **Anticancer Research,** v. 34, n. 4, p. 1493-505, Apr 2014. ISSN 1791-7530. Disponível em: < https://www.ncbi.nlm.nih.gov/pubmed/24692676 >.

[47] BALLANTYNE, A. D.; GARNOCK-JONES, K. P. Dabrafenib: first global approval. **Drugs,** v. 73, n. 12, p. 1367-76, Aug 2013. ISSN 1179-1950. Disponível em: < https://www.ncbi.nlm.nih.gov/pubmed/23881668 >.

[48] APLIN, A. E.; KAPLAN, F. M.; SHAO, Y. Mechanisms of resistance to RAF inhibitors in melanoma. **Journal of Investigative Dermatology,** v. 131, n. 9, p. 1817-1820, Sep 2011. ISSN 1523-1747. Disponível em: < https://www.ncbi.nlm.nih.gov/pubmed/21593776 >.

[49] SANDRI, S. et al. Vemurafenib resistance increases melanoma invasiveness and modulates the tumor microenvironment by MMP-2 upregulation. **Pharmacological Research,** v. 111, p. 523-533, Jul 2016. ISSN 1096-1186. Disponível em: < https://www.ncbi.nlm.nih.gov/pubmed/27436149 >.

[50] WAGLE, N. et al. Dissecting therapeutic resistance to RAF inhibition in melanoma by tumor genomic profiling. **Journal of Clinical Oncology,** v. 29, n. 22, p. 3085-96, Aug 2011. ISSN 1527-7755. Disponível em: < https://www.ncbi.nlm.nih.gov/pubmed/21383288 >.

[51] GOETZ, E. M. et al. ERK mutations confer resistance to mitogen-activated protein kinase pathway inhibitors. **Cancer Research,** v. 74, n. 23, p. 7079-89, Dec 01 2014. ISSN 1538-7445. Disponível em: < https://www.ncbi.nlm.nih.gov/pubmed/25320010 >.

[52] GRIMALDI, A. M.; SIMEONE, E.; ASCIERTO, P. A. The role of MEK inhibitors in the treatment of metastatic melanoma. **Current Opinion in Oncology,** v. 26, n. 2, p. 196-203, Mar 2014. ISSN 1531-703X. Disponível em: < https://www.ncbi.nlm.nih.gov/pubmed/24419498 >.

[53] AKINLEYE, A. et al. MEK and the inhibitors: from bench to bedside. **Journal of Hematology and Oncology,** v. 6, p. 27, Apr 12 2013. ISSN 1756-8722. Disponível em: < https://www.ncbi.nlm.nih.gov/pubmed/23587417 >.

[54] INFANTE, J. R. et al. Safety, pharmacokinetic, pharmacodynamic, and efficacy data for the oral MEK inhibitor trametinib: a phase 1 dose-escalation trial. **The Lancet Oncology,** v. 13, n. 8, p. 773-81, Aug 2012. ISSN 1474-5488. Disponível em: < https://www.ncbi.nlm.nih.gov/pubmed/22805291 >.

[55] YU, C. et al. Combination of Immunotherapy With Targeted Therapy: Theory and Practice in Metastatic Melanoma. **Frontiers in Immunology,** v. 10, p. 990, 2019. ISSN 1664-3224. Disponível em: < https://www.ncbi.nlm.nih.gov/pubmed/31134073 >.

[56] PELSTER, M. S.; AMARIA, R. N. Combined targeted therapy and immunotherapy in melanoma: a review of the impact on the tumor microenvironment and outcomes of early clinical trials. **Therapeutic Advances in Medical Oncology,** v. 11, p. 1758835919830826, 2019. ISSN 1758-8340. Disponível em: < https://www.ncbi.nlm.nih.gov/pubmed/30815041 >.

[57] SRIVASTAVA, N.; MCDERMOTT, D. Update on benefit of immunotherapy and targeted therapy in melanoma: the changing landscape. **Cancer Management and Research,** v. 6, p. 279-89, 2014. ISSN 1179-1322. Disponível em: < https://www.ncbi.nlm.nih.gov/pubmed/25018651 >.

[58] SILVA, I. P.; LONG, G. V. Systemic therapy in advanced melanoma: integrating targeted therapy and immunotherapy into clinical practice. **Current Opinion in Oncology,** v. 29, n. 6, p. 484-492, Nov 2017. ISSN 1531-703X. Disponível em: < https://www.ncbi.nlm.nih.gov/pubmed/28914644 >.

[59] PARK, Y. J.; KUEN, D. S.; CHUNG, Y. Future prospects of immune checkpoint blockade in cancer: from response prediction to overcoming resistance. **Experimental and Molecular Medicine,** v. 50, n. 8, p. 1-13, 08 22 2018. ISSN 2092-6413. Disponível em: < https://www.ncbi.nlm.nih.gov/pubmed/30135516 >.

[60] REDMAN, J. M.; GIBNEY, G. T.; ATKINS, M. B. Advances in immunotherapy for melanoma. **BMC Medicine,** v. 14, p. 20, Feb 06 2016. ISSN 1741-7015. Disponível em: < https://www.ncbi.nlm.nih.gov/pubmed/26850630 >.

[61] LA-BECK, N. M. et al. Immune Checkpoint Inhibitors: New Insights and Current Place in Cancer Therapy. **Pharmacotherapy,** v. 35, n. 10, p. 963-76, Oct 2015. ISSN 1875-9114. Disponível em: < https://www.ncbi.nlm.nih.gov/pubmed/26497482 >.

[62] WEBER, J. S.; KÄHLER, K. C.; HAUSCHILD, A. Management of immune-related adverse events and kinetics of response with ipilimumab. **Journal of Clinical Oncology,** v. 30, n. 21, p. 2691-7, Jul 20 2012. ISSN 1527-7755. Disponível em: < https://www.ncbi.nlm.nih.gov/pubmed/22614989 >.

63 TOPALIAN, S. L. et al. Survival, durable tumor remission, and long-term safety in patients with advanced melanoma receiving nivolumab. **Journal of Clinical Oncology,** v. 32, n. 10, p. 1020-30, Apr 01 2014. ISSN 1527-7755. Disponível em: < https://www.ncbi.nlm.nih.gov/pubmed/24590637 >.

64 HIRANO, F. et al. Blockade of B7-H1 and PD-1 by monoclonal antibodies potentiates cancer therapeutic immunity. **Cancer Research,** v. 65, n. 3, p. 1089-96, Feb 01 2005. ISSN 0008-5472. Disponível em: < https://www.ncbi.nlm.nih.gov/pubmed/15705911 >.

65 BEATTY, G. L.; GLADNEY, W. L. Immune escape mechanisms as a guide for cancer immunotherapy. **Clinical Cancer Research,** v. 21, n. 4, p. 687-92, Feb 15 2015. ISSN 1557-3265. Disponível em: < https://www.ncbi.nlm.nih.gov/pubmed/25501578 >.

66 SANGER, F.; NICKLEN, S.; COULSON, A. R. DNA sequencing with chain-terminating inhibitors. **Proceedings of the National Academy of Sciences of the United States of America,** v. 74, n. 12, p. 5463-7, Dec 1977. ISSN 0027-8424. Disponível em: < https://www.ncbi.nlm.nih.gov/pubmed/271968 >.

67 HEATHER, J. M.; CHAIN, B. The sequence of sequencers: The history of sequencing DNA. **Genomics,** v. 107, n. 1, p. 1-8, Jan 2016. ISSN 1089-8646. Disponível em: < https://www.ncbi.nlm.nih.gov/pubmed/26554401 >.

68 CONSORTIUM, I. H. G. S. Finishing the euchromatic sequence of the human genome. **Nature,** v. 431, n. 7011, p. 931-45, Oct 21 2004. ISSN 1476-4687. Disponível em: < https://www.ncbi.nlm.nih.gov/pubmed/15496913 >.

69 SHYR, D.; LIU, Q. Next generation sequencing in cancer research and clinical application. **Biological Procedures Online,** v. 15, n. 1, p. 4, Feb 13 2013. ISSN 1480-9222. Disponível em: < https://www.ncbi.nlm.nih.gov/pubmed/23406336 >.

70 SHENDURE, J. et al. DNA sequencing at 40: past, present and future. **Nature,** v. 550, n. 7676, p. 345-353, 10 19 2017. ISSN 1476-4687. Disponível em: < https://www.ncbi.nlm.nih.gov/pubmed/29019985 >.

71 SLATKO, B. E.; GARDNER, A. F.; AUSUBEL, F. M. Overview of Next-Generation Sequencing Technologies. **Current Protocols in Molecular Biology,** v. 122, n. 1, p. e59, 04 2018. ISSN 1934-3647. Disponível em: < https://www.ncbi.nlm.nih.gov/pubmed/29851291 >.

72 TEER, J. K. An improved understanding of cancer genomics through massively parallel sequencing. **Translational Cancer Research,** v. 3, n. 3, p. 243-259, Jun 2014. ISSN 2218-676X. Disponível em: < https://www.ncbi.nlm.nih.gov/pubmed/26146607 >.

73 GOODWIN, S.; MCPHERSON, J. D.; MCCOMBIE, W. R. Coming of age: ten years of next-generation sequencing technologies. **Nature Reviews Genetics,** v. 17, n. 6, p. 333-51, 05 17 2016. ISSN 1471-0064. Disponível em: < https://www.ncbi.nlm.nih.gov/pubmed/27184599 >.

74 WEINSTEIN, J. N. et al. The Cancer Genome Atlas Pan-Cancer analysis project. **Nature Genetics,** v. 45, n. 10, p. 1113-20, Oct 2013. ISSN 1546-1718. Disponível em: < https://www.ncbi.nlm.nih.gov/pubmed/24071849 >.

[75] CONSORTIUM, I. T. P.-C. A. O. W. G. Pan-cancer analysis of whole genomes. **Nature,** v. 578, n. 7793, p. 82-93, 02 2020. ISSN 1476-4687. Disponível em: < https://www.ncbi.nlm.nih.gov/pubmed/32025007 >.

[76] LOFTUS, S. K. The next generation of melanocyte data: Genetic, epigenetic, and transcriptional resource datasets and analysis tools. **Pigment Cell Melanoma Research,** v. 31, n. 3, p. 442-447, 05 2018. ISSN 1755-148X. Disponível em: < https://www.ncbi.nlm.nih.gov/pubmed/29337423 >.

[77] GUAN, J.; GUPTA, R.; FILIPP, F. V. Cancer systems biology of TCGA SKCM: efficient detection of genomic drivers in melanoma. **Scientific Reports,** v. 5, p. 7857, Jan 20 2015. ISSN 2045-2322. Disponível em: < https://www.ncbi.nlm.nih.gov/pubmed/25600636 >.

[78] BARRANGOU, R. et al. CRISPR provides acquired resistance against viruses in prokaryotes. **Science,** v. 315, n. 5819, p. 1709-12, Mar 23 2007. ISSN 1095-9203. Disponível em: < https://www.ncbi.nlm.nih.gov/pubmed/17379808 >.

[79] RAN, F. A. et al. Genome engineering using the CRISPR-Cas9 system. **Nature Protocols,** v. 8, n. 11, p. 2281-2308, Nov 2013. ISSN 1750-2799. Disponível em: < https://www.ncbi.nlm.nih.gov/pubmed/24157548 >.

[80] WANG, H.; LA RUSSA, M.; QI, L. S. CRISPR/Cas9 in Genome Editing and Beyond. **Annual Review of Biochemistry,** v. 85, p. 227-64, Jun 02 2016. ISSN 1545-4509. Disponível em: < https://www.ncbi.nlm.nih.gov/pubmed/27145843 >.

[81] MAKAROVA, K. S. et al. An updated evolutionary classification of CRISPR-Cas systems. **Nature Reviews Microbiology,** v. 13, n. 11, p. 722-36, 11 2015. ISSN 1740-1534. Disponível em: < https://www.ncbi.nlm.nih.gov/pubmed/26411297 >.

[82] GARNEAU, J. E. et al. The CRISPR/Cas bacterial immune system cleaves bacteriophage and plasmid DNA. **Nature,** v. 468, n. 7320, p. 67-71, Nov 04 2010. ISSN 1476-4687. Disponível em: < https://www.ncbi.nlm.nih.gov/pubmed/21048762 >.

[83] JIANG, F.; DOUDNA, J. A. CRISPR-Cas9 Structures and Mechanisms. **Annual Review of Biophysics,** v. 46, p. 505-529, 05 22 2017. ISSN 1936-1238. Disponível em: < https://www.ncbi.nlm.nih.gov/pubmed/28375731 >.

[84] LIEBER, M. R. The mechanism of double-strand DNA break repair by the nonhomologous DNA end-joining pathway. **Annual Review of Biochemistry,** v. 79, p. 181-211, 2010. ISSN 1545-4509. Disponível em: < https://www.ncbi.nlm.nih.gov/pubmed/20192759 >.

[85] SAN FILIPPO, J.; SUNG, P.; KLEIN, H. Mechanism of eukaryotic homologous recombination. **Annual Review of Biochemistry,** v. 77, p. 229-57, 2008. ISSN 0066-4154. Disponível em: < https://www.ncbi.nlm.nih.gov/pubmed/18275380 >.

[86] RAN, F. A. et al. Double nicking by RNA-guided CRISPR Cas9 for enhanced genome editing specificity. **Cell,** v. 154, n. 6, p. 1380-9, Sep 12 2013. ISSN 1097-4172. Disponível em: < https://www.ncbi.nlm.nih.gov/pubmed/23992846 >.

[87] TYCKO, J.; MYER, V. E.; HSU, P. D. Methods for Optimizing CRISPR-Cas9 Genome Editing Specificity. **Molecular Cell,** v. 63, n. 3, p. 355-70, 08 04 2016. ISSN 1097-4164. Disponível em: < https://www.ncbi.nlm.nih.gov/pubmed/27494557 >.

88 SLAYMAKER, I. M. et al. Rationally engineered Cas9 nucleases with improved specificity. **Science,** v. 351, n. 6268, p. 84-8, Jan 01 2016. ISSN 1095-9203. Disponível em: < https://www.ncbi.nlm.nih.gov/pubmed/26628643 >.

89 LARSON, M. H. et al. CRISPR interference (CRISPRi) for sequence-specific control of gene expression. **Nature Protocols,** v. 8, n. 11, p. 2180-96, Nov 2013. ISSN 1750-2799. Disponível em: < https://www.ncbi.nlm.nih.gov/pubmed/24136345 >.

90 GILBERT, L. A. et al. Genome-Scale CRISPR-Mediated Control of Gene Repression and Activation. **Cell,** v. 159, n. 3, p. 647-61, Oct 23 2014. ISSN 1097-4172. Disponível em: < https://www.ncbi.nlm.nih.gov/pubmed/25307932 >.

91 ADLI, M. The CRISPR tool kit for genome editing and beyond. **Nature Communications,** v. 9, n. 1, p. 1911, 05 15 2018. ISSN 2041-1723. Disponível em: < https://www.ncbi.nlm.nih.gov/pubmed/29765029 >.

92 DOENCH, J. G. Am I ready for CRISPR? A user's guide to genetic screens. **Nature Reviews Genetics,** v. 19, n. 2, p. 67-80, 02 2018. ISSN 1471-0064. Disponível em: < https://www.ncbi.nlm.nih.gov/pubmed/29199283 >.

93 SCHUSTER, A. et al. RNAi/CRISPR Screens: from a Pool to a Valid Hit. **Trends in Biotechnology,** v. 37, n. 1, p. 38-55, 01 2019. ISSN 1879-3096. Disponível em: < https://www.ncbi.nlm.nih.gov/pubmed/30177380 >.

94 BARTHA, I. et al. Human gene essentiality. **Nature Reviews Genetics,** v. 19, n. 1, p. 51-62, Jan 2018. ISSN 1471-0064. Disponível em: < https://www.ncbi.nlm.nih.gov/pubmed/29082913 >.

95 WANG, T. et al. Genetic screens in human cells using the CRISPR-Cas9 system. **Science,** v. 343, n. 6166, p. 80-4, Jan 03 2014. ISSN 1095-9203. Disponível em: < https://www.ncbi.nlm.nih.gov/pubmed/24336569 >.

96 SHALEM, O. et al. Genome-scale CRISPR-Cas9 knockout screening in human cells. **Science,** v. 343, n. 6166, p. 84-87, Jan 03 2014. ISSN 1095-9203. Disponível em: < https://www.ncbi.nlm.nih.gov/pubmed/24336571 >.

97 DOENCH, J. G. et al. Rational design of highly active sgRNAs for CRISPR-Cas9-mediated gene inactivation. **Nature Biotechnology,** v. 32, n. 12, p. 1262-7, Dec 2014. ISSN 1546-1696. Disponível em: < https://www.ncbi.nlm.nih.gov/pubmed/25184501 >.

98 LI, W. et al. MAGeCK enables robust identification of essential genes from genome-scale CRISPR/Cas9 knockout screens. **Genome Biology,** v. 15, n. 12, p. 554, 2014. ISSN 1474-760X. Disponível em: < https://www.ncbi.nlm.nih.gov/pubmed/25476604 >.

99 HART, T.; MOFFAT, J. BAGEL: a computational framework for identifying essential genes from pooled library screens. **BMC Bioinformatics,** v. 17, p. 164, Apr 16 2016. ISSN 1471-2105. Disponível em: < https://www.ncbi.nlm.nih.gov/pubmed/27083490 >.

100 SANJANA, N. E. Genome-scale CRISPR pooled screens. **Analytical Biochemistry,** v. 532, p. 95-99, 09 01 2017. ISSN 1096-0309. Disponível em: < https://www.ncbi.nlm.nih.gov/pubmed/27261176 >.

[101] JOHANNESSEN, C. M. et al. A melanocyte lineage program confers resistance to MAP kinase pathway inhibition. **Nature,** v. 504, n. 7478, p. 138-42, Dec 05 2013. ISSN 1476-4687. Disponível em: < https://www.ncbi.nlm.nih.gov/pubmed/24185007 >.

[102] WANG, T. et al. Identification and characterization of essential genes in the human genome. **Science,** v. 350, n. 6264, p. 1096-101, Nov 27 2015. ISSN 1095-9203. Disponível em: < https://www.ncbi.nlm.nih.gov/pubmed/26472758 >.

[103] HART, T. et al. High-Resolution CRISPR Screens Reveal Fitness Genes and Genotype-Specific Cancer Liabilities. **Cell,** v. 163, n. 6, p. 1515-26, Dec 03 2015. ISSN 1097-4172. Disponível em: < https://www.ncbi.nlm.nih.gov/pubmed/26627737 >.

[104] DHOONMOON, A. et al. Genome-wide CRISPR synthetic lethality screen identifies a role for the ADP-ribosyltransferase PARP14 in DNA replication dynamics controlled by ATR. **Nucleic Acids Research,** v. 48, n. 13, p. 7252-7264, 07 27 2020. ISSN 1362-4962. Disponível em: < https://www.ncbi.nlm.nih.gov/pubmed/32542389 >.

[105] TOLEDO, C. M. et al. Genome-wide CRISPR-Cas9 Screens Reveal Loss of Redundancy between PKMYT1 and WEE1 in Glioblastoma Stem-like Cells. **Cell Reports,** v. 13, n. 11, p. 2425-2439, Dec 22 2015. ISSN 2211-1247. Disponível em: < https://www.ncbi.nlm.nih.gov/pubmed/26673326 >.

[106] LI, W. et al. Quality control, modeling, and visualization of CRISPR screens with MAGeCK-VISPR. **Genome Biology,** v. 16, p. 281, Dec 16 2015. ISSN 1474-760X. Disponível em: < https://www.ncbi.nlm.nih.gov/pubmed/26673418 >.

[107] DE WECK, A. et al. Correction of copy number induced false positives in CRISPR screens. **PLoS Computational Biology,** v. 14, n. 7, p. e1006279, 07 2018. ISSN 1553-7358. Disponível em: < https://www.ncbi.nlm.nih.gov/pubmed/30024886 >.

[108] STREZOSKA, Ž. et al. Optimized PCR conditions and increased shRNA fold representation improve reproducibility of pooled shRNA screens. **PLoS One,** v. 7, n. 8, p. e42341, 2012. ISSN 1932-6203. Disponível em: < https://www.ncbi.nlm.nih.gov/pubmed/22870320 >.

[109] STERNBERG, P. W. et al. Activation of the yeast HO gene by release from multiple negative controls. **Cell,** v. 48, n. 4, p. 567-577, Feb 1987. ISSN 0092-8674. Disponível em: < https://www.ncbi.nlm.nih.gov/pubmed/3545494 >.

[110] NASMYTH, K.; STILLMAN, D.; KIPLING, D. Both positive and negative regulators of HO transcription are required for mother-cell-specific mating-type switching in yeast. **Cell,** v. 48, n. 4, p. 579-587, Feb 1987. ISSN 0092-8674. Disponível em: < https://www.ncbi.nlm.nih.gov/pubmed/3028642 >.

[111] YOSHIMOTO, H.; OHMAE, M.; YAMASHITA, I. The Saccharomyces cerevisiae GAM2/SIN3 protein plays a role in both activation and repression of transcription. **Molecular and General Genetics,** v. 233, n. 1-2, p. 327-30, May 1992. ISSN 0026-8925. Disponível em: < https://www.ncbi.nlm.nih.gov/pubmed/1603074 >.

[112] SILVERSTEIN, R. A.; EKWALL, K. Sin3: a flexible regulator of global gene expression and genome stability. **Current Genetics,** v. 47, n. 1, p. 1-17, Jan 2005. ISSN 0172-8083. Disponível em: < https://www.ncbi.nlm.nih.gov/pubmed/15565322 >.

113 KADAMB, R. et al. Sin3: insight into its transcription regulatory functions. **European Journal of Cell Biology,** v. 92, n. 8-9, p. 237-46, 2013 Aug-Sep 2013. ISSN 1618-1298. Disponível em: < https://www.ncbi.nlm.nih.gov/pubmed/24189169 >.

114 ADAMS, M. K. et al. Differential Complex Formation via Paralogs in the Human Sin3 Protein Interaction Network. **Molecular and Cellular Proteomics,** v. 19, n. 9, p. 1468-1484, 09 2020. ISSN 1535-9484. Disponível em: < https://www.ncbi.nlm.nih.gov/pubmed/32467258 >.

115 AYER, D. E.; LAWRENCE, Q. A.; EISENMAN, R. N. Mad-Max transcriptional repression is mediated by ternary complex formation with mammalian homologs of yeast repressor Sin3. **Cell,** v. 80, n. 5, p. 767-76, Mar 10 1995. ISSN 0092-8674. Disponível em: < https://www.ncbi.nlm.nih.gov/pubmed/7889570 >.

116 ALLAND, L. et al. Role for N-CoR and histone deacetylase in Sin3-mediated transcriptional repression. **Nature,** v. 387, n. 6628, p. 49-55, May 01 1997. ISSN 0028-0836. Disponível em: < https://www.ncbi.nlm.nih.gov/pubmed/9139821 >.

117 HEINZEL, T. et al. A complex containing N-CoR, mSin3 and histone deacetylase mediates transcriptional repression. **Nature,** v. 387, n. 6628, p. 43-8, May 01 1997. ISSN 0028-0836. Disponível em: < https://www.ncbi.nlm.nih.gov/pubmed/9139820 >.

118 LAHERTY, C. D. et al. Histone deacetylases associated with the mSin3 corepressor mediate mad transcriptional repression. **Cell,** v. 89, n. 3, p. 349-56, May 02 1997. ISSN 0092-8674. Disponível em: < https://www.ncbi.nlm.nih.gov/pubmed/9150134 >.

119 ZHANG, Y. et al. The dermatomyositis-specific autoantigen Mi2 is a component of a complex containing histone deacetylase and nucleosome remodeling activities. **Cell,** v. 95, n. 2, p. 279-89, Oct 16 1998. ISSN 0092-8674. Disponível em: < https://www.ncbi.nlm.nih.gov/pubmed/9790534 >.

120 VERREAULT, A. et al. Nucleosomal DNA regulates the core-histone-binding subunit of the human Hat1 acetyltransferase. **Current Biology,** v. 8, n. 2, p. 96-108, Jan 15 1998. ISSN 0960-9822. Disponível em: < https://www.ncbi.nlm.nih.gov/pubmed/9427644 >.

121 FLEISCHER, T. C.; YUN, U. J.; AYER, D. E. Identification and characterization of three new components of the mSin3A corepressor complex. **Molecular and Cellular Biology,** v. 23, n. 10, p. 3456-67, May 2003. ISSN 0270-7306. Disponível em: < https://www.ncbi.nlm.nih.gov/pubmed/12724404 >.

122 BANSAL, N. et al. Targeting the SIN3A-PF1 interaction inhibits epithelial to mesenchymal transition and maintenance of a stem cell phenotype in triple negative breast cancer. **Oncotarget,** v. 6, n. 33, p. 34087-105, Oct 27 2015. ISSN 1949-2553. Disponível em: < https://www.ncbi.nlm.nih.gov/pubmed/26460951 >.

123 WANG, H. et al. The Saccharomyces cerevisiae SIN3 gene, a negative regulator of HO, contains four paired amphipathic helix motifs. **Molecular and Cellular Biology,** v. 10, n. 11, p. 5927-36, Nov 1990. ISSN 0270-7306. Disponível em: < https://www.ncbi.nlm.nih.gov/pubmed/2233725 >.

124 HE, Y.; RADHAKRISHNAN, I. Solution NMR studies of apo-mSin3A and -mSin3B reveal that the PAH1 and PAH2 domains are structurally independent. **Protein Science,** v. 17, n. 1, p. 171-5,

Jan 2008. ISSN 0961-8368. Disponível em: < https://www.ncbi.nlm.nih.gov/pubmed/18042683 >.

125 LE GUEZENNEC, X.; VERMEULEN, M.; STUNNENBERG, H. G. Molecular characterization of Sin3 PAH-domain interactor specificity and identification of PAH partners. **Nucleic Acids Research,** v. 34, n. 14, p. 3929-37, 2006. ISSN 1362-4962. Disponível em: < https://www.ncbi.nlm.nih.gov/pubmed/16914451 >.

126 GRZENDA, A. et al. Sin3: master scaffold and transcriptional corepressor. **Biochimica et Biophysica Acta,** v. 1789, n. 6-8, p. 443-50, 2009 Jun-Aug 2009. ISSN 0006-3002. Disponível em: < https://www.ncbi.nlm.nih.gov/pubmed/19505602 >.

127 BANSAL, N. et al. Emerging Roles of Epigenetic Regulator Sin3 in Cancer. **Advances Cancer Research,** v. 130, p. 113-135, 2016. ISSN 0065-230X. Disponível em: < https://www.ncbi.nlm.nih.gov/pubmed/27037752 >.

128 KADAMB, R. et al. Sin3: insight into its transcription regulatory functions. **European Journal of Cell Biology,** v. 92, n. 8-9, p. 237-246, 2013 Aug-Sep 2013. ISSN 1618-1298. Disponível em: < https://www.ncbi.nlm.nih.gov/pubmed/24189169 >.

129 XU, Y.; HARTON, J. A.; SMITH, B. D. CIITA mediates interferon-gamma repression of collagen transcription through phosphorylation-dependent interactions with co-repressor molecules. **The Journal of Biological Chemistry,** v. 283, n. 3, p. 1243-1256, Jan 2008. ISSN 0021-9258. Disponível em: < https://www.ncbi.nlm.nih.gov/pubmed/17991736 >.

130 VAN OEVELEN, C. et al. The mammalian Sin3 proteins are required for muscle development and sarcomere specification. **Molecular and Cellular Biology,** v. 30, n. 24, p. 5686-5697, Dec 2010. ISSN 1098-5549. Disponível em: < https://www.ncbi.nlm.nih.gov/pubmed/20956564 >.

131 FAHERTY, N. et al. Negative autoregulation of BMP dependent transcription by SIN3B splicing reveals a role for RBM39. **Scientific Reports,** v. 6, p. 28210, 06 2016. ISSN 2045-2322. Disponível em: < https://www.ncbi.nlm.nih.gov/pubmed/27324164 >.

132 GRANDINETTI, K. B. et al. Sin3B Expression Is Required for Cellular Senescence and Is Up-regulated upon Oncogenic Stress. **Cancer Research,** v. 69, n. 16, p. 6430, 2009. Disponível em: < http://cancerres.aacrjournals.org/content/69/16/6430.abstract >.

133 DIMAURO, T. et al. Transcriptional repression of Sin3B by Bmi-1 prevents cellular senescence and is relieved by oncogene activation. **Oncogene,** v. 34, n. 30, p. 4011-4017, Jul 2015. ISSN 1476-5594. Disponível em: < https://www.ncbi.nlm.nih.gov/pubmed/25263442 >.

134 RIELLAND, M. et al. Senescence-associated SIN3B promotes inflammation and pancreatic cancer progression. **The Journal of Clinical Investigation,** v. 124, n. 5, p. 2125-2135, May 2014. ISSN 1558-8238. Disponível em: < https://www.ncbi.nlm.nih.gov/pubmed/24691445 >.

135 RAYMAN, J. B. et al. E2F mediates cell cycle-dependent transcriptional repression in vivo by recruitment of an HDAC1/mSin3B corepressor complex. **Genes and Development,** v. 16, n. 8, p. 933-947, Apr 2002. ISSN 0890-9369. Disponível em: < https://www.ncbi.nlm.nih.gov/pubmed/11959842 >.

136 LEWIS, M. J. et al. SIN3A and SIN3B differentially regulate breast cancer metastasis. **Oncotarget,** v. 7, n. 48, p. 78713-78725, Nov 2016. ISSN 1949-2553. Disponível em: < https://www.ncbi.nlm.nih.gov/pubmed/27780928 >.

137 CANTOR, D. J.; DAVID, G. SIN3B, the SASP, and pancreatic cancer. **Molecular & Cellular Oncology,** v. 1, n. 4, p. e969167, 2014 Oct-Dec 2014. ISSN 2372-3556. Disponível em: < https://www.ncbi.nlm.nih.gov/pubmed/27308374 >.

138 OLIVEIRA, É. et al. Toxicogenomic and bioinformatics platforms to identify key molecular mechanisms of a curcumin-analogue DM-1 toxicity in melanoma cells. **Pharmacol Res,** v. 125, n. Pt B, p. 178-187, Nov 2017. ISSN 1096-1186. Disponível em: < https://www.ncbi.nlm.nih.gov/pubmed/28882690 >.

139 PENNACCHI, P. C. et al. Glycated Reconstructed Human Skin as a Platform to Study the Pathogenesis of Skin Aging. **Tissue Engineering Part A,** v. 21, n. 17-18, p. 2417-2425, Sep 2015. ISSN 1937-335X. Disponível em: < https://www.ncbi.nlm.nih.gov/pubmed/26132636 >.

140 FAIÃO-FLORES, F. et al. Targeting the hedgehog transcription factors GLI1 and GLI2 restores sensitivity to vemurafenib-resistant human melanoma cells. **Oncogene,** v. 36, n. 13, p. 1849-1861, Mar 2017. ISSN 1476-5594. Disponível em: < https://www.ncbi.nlm.nih.gov/pubmed/27748762 >.

141 Custom Primers - OligoPerfect™ Designer. Disponível em: < https://tools.thermofisher.com/content.cfm?pageid=9716 >. Acesso em: 28/09/2017.

142 SIEVERS, F. et al. Fast, scalable generation of high-quality protein multiple sequence alignments using Clustal Omega. **Mol Syst Biol,** v. 7, p. 539, Oct 2011. ISSN 1744-4292. Disponível em: < https://www.ncbi.nlm.nih.gov/pubmed/21988835 >.

143 GOUJON, M. et al. A new bioinformatics analysis tools framework at EMBL-EBI. **Nucleic Acids Res,** v. 38, n. Web Server issue, p. W695-9, Jul 2010. ISSN 1362-4962. Disponível em: < https://www.ncbi.nlm.nih.gov/pubmed/20439314 >.

144 SCHMITTGEN, T. D.; LIVAK, K. J. Analyzing real-time PCR data by the comparative C(T) method. **Nature Protocols,** v. 3, n. 6, p. 1101-8, 2008. ISSN 1750-2799. Disponível em: < https://www.ncbi.nlm.nih.gov/pubmed/18546601 >.

145 SANJANA, N. E.; SHALEM, O.; ZHANG, F. Improved vectors and genome-wide libraries for CRISPR screening. **Nature Methods,** v. 11, n. 8, p. 783-784, Aug 2014. ISSN 1548-7105. Disponível em: < https://www.ncbi.nlm.nih.gov/pubmed/25075903 >.

146 lentiCRISPRv2. Disponível em: < https://www.addgene.org/52961/ >. Acesso em: 29/11/2018.

147 JIN, Y. H. et al. Streamlined procedure for gene knockouts using all-in-one adenoviral CRISPR-Cas9. **Scientific Reports,** v. 9, n. 1, p. 277, 01 22 2019. ISSN 2045-2322. Disponível em: < https://www.ncbi.nlm.nih.gov/pubmed/30670765 >.

148 YANG, R. et al. Monoclonal Cell Line Generation and CRISPR/Cas9 Manipulation via Single-Cell Electroporation. **Small,** v. 14, n. 12, p. e1702495, 03 2018. ISSN 1613-6829. Disponível em: < https://www.ncbi.nlm.nih.gov/pubmed/29430869 >.

[149] FAJRIAL, A. K. et al. A review of emerging physical transfection methods for CRISPR/Cas9-mediated gene editing. **Theranostics,** v. 10, n. 12, p. 5532-5549, 2020. ISSN 1838-7640. Disponível em: < https://www.ncbi.nlm.nih.gov/pubmed/32373229 >.

[150] LINO, C. A. et al. Delivering CRISPR: a review of the challenges and approaches. **Drug Delivery,** v. 25, n. 1, p. 1234-1257, Nov 2018. ISSN 1521-0464. Disponível em: < https://www.ncbi.nlm.nih.gov/pubmed/29801422 >.

[151] GIULIANO, C. J. et al. Generating Single Cell-Derived Knockout Clones in Mammalian Cells with CRISPR/Cas9. **Current Protocols in Molecular Biology,** v. 128, n. 1, p. e100, 09 2019. ISSN 1934-3647. Disponível em: < https://www.ncbi.nlm.nih.gov/pubmed/31503414 >.

[152] KINGSTON, R. E.; CHEN, C. A.; ROSE, J. K. Calcium phosphate transfection. **Current Protocols in Molecular Biology,** v. Chapter 9, p. Unit 9.1, Aug 2003. ISSN 1934-3647. Disponível em: < https://www.ncbi.nlm.nih.gov/pubmed/18265332 >.

[153] FERRETTI, R. et al. BMI1 induces an invasive signature in melanoma that promotes metastasis and chemoresistance. **Genes and Development,** v. 30, n. 1, p. 18-33, Jan 2016. ISSN 1549-5477. Disponível em: < https://www.ncbi.nlm.nih.gov/pubmed/26679841 >.

[154] CERAMI, E. et al. The cBio cancer genomics portal: an open platform for exploring multidimensional cancer genomics data. **Cancer Discovery,** v. 2, n. 5, p. 401-404, May 2012. ISSN 2159-8290. Disponível em: < https://www.ncbi.nlm.nih.gov/pubmed/22588877 >.

[155] GOLDMAN, M. J. et al. Visualizing and interpreting cancer genomics data via the Xena platform. **Nat Biotechnol,** v. 38, n. 6, p. 675-678, 06 2020. ISSN 1546-1696. Disponível em: < https://www.ncbi.nlm.nih.gov/pubmed/32444850 >.

[156] DOBIN, A. et al. STAR: ultrafast universal RNA-seq aligner. **Bioinformatics,** v. 29, n. 1, p. 15-21, Jan 01 2013. ISSN 1367-4811. Disponível em: < https://www.ncbi.nlm.nih.gov/pubmed/23104886 >.

[157] LOVE, M. I.; HUBER, W.; ANDERS, S. Moderated estimation of fold change and dispersion for RNA-seq data with DESeq2. **Genome Biology,** v. 15, n. 12, p. 550, 2014. ISSN 1474-760X. Disponível em: < https://www.ncbi.nlm.nih.gov/pubmed/25516281 >.

[158] LUO, W.; BROUWER, C. Pathview: an R/Bioconductor package for pathway-based data integration and visualization. **Bioinformatics,** v. 29, n. 14, p. 1830-1, Jul 15 2013. ISSN 1367-4811. Disponível em: < https://www.ncbi.nlm.nih.gov/pubmed/23740750 >.

[159] JOUNG, J. et al. Genome-scale CRISPR-Cas9 knockout and transcriptional activation screening. **Nature Protocols,** v. 12, n. 4, p. 828-863, 04 2017. ISSN 1750-2799. Disponível em: < https://www.ncbi.nlm.nih.gov/pubmed/28333914 >.

[160] WEI, L. et al. Genome-wide CRISPR/Cas9 library screening identified PHGDH as a critical driver for Sorafenib resistance in HCC. **Nature Communications,** v. 10, n. 1, p. 4681, 10 15 2019. ISSN 2041-1723. Disponível em: < https://www.ncbi.nlm.nih.gov/pubmed/31615983 >.

[161] CHEN, S. et al. Genome-wide CRISPR screen in a mouse model of tumor growth and metastasis. **Cell,** v. 160, n. 6, p. 1246-60, Mar 12 2015. ISSN 1097-4172. Disponível em: < https://www.ncbi.nlm.nih.gov/pubmed/25748654 >.

[162] GOLDMAN, M. J. et al. Visualizing and interpreting cancer genomics data via the Xena platform. **Nature Biotechnology,** v. 38, n. 6, p. 675-678, 06 2020. ISSN 1546-1696. Disponível em: < https://www.ncbi.nlm.nih.gov/pubmed/32444850 >.

[163] EVANS, C.; HARDIN, J.; STOEBEL, D. M. Selecting between-sample RNA-Seq normalization methods from the perspective of their assumptions. **Briefings in Bioinformatics,** v. 19, n. 5, p. 776-792, 09 28 2018. ISSN 1477-4054. Disponível em: < https://www.ncbi.nlm.nih.gov/pubmed/28334202 >.

[164] UCSC Xena. Disponível em: < https://xenabrowser.net/ >. Acesso em: 14/12/2020.

[165] American Cancer Society. Disponível em: < https://www.cancer.org/ >. Acesso em: 14/12/2020.

[166] BALCH, C. M. et al. Final version of 2009 AJCC melanoma staging and classification. **J Clin Oncol,** v. 27, n. 36, p. 6199-206, Dec 2009. ISSN 1527-7755. Disponível em: < http://www.ncbi.nlm.nih.gov/pubmed/19917835 >.

[167] HAQQ, C. et al. The gene expression signatures of melanoma progression. **Proceedings of the National Academy of Sciences of the United States of America,** v. 102, n. 17, p. 6092-7, Apr 26 2005. ISSN 0027-8424. Disponível em: < https://www.ncbi.nlm.nih.gov/pubmed/15833814 >.

[168] SMITH, A. P.; HOEK, K.; BECKER, D. Whole-genome expression profiling of the melanoma progression pathway reveals marked molecular differences between nevi/melanoma in situ and advanced-stage melanomas. **Cancer Biology and Therapy,** v. 4, n. 9, p. 1018-29, Sep 2005. ISSN 1538-4047. Disponível em: < https://www.ncbi.nlm.nih.gov/pubmed/16251803 >.

[169] CANTOR, D. J.; DAVID, G. The potential of targeting Sin3B and its associated complexes for cancer therapy. **Expert Opin Ther Targets,** v. 21, n. 11, p. 1051-1061, 11 2017. ISSN 1744-7631. Disponível em: < https://www.ncbi.nlm.nih.gov/pubmed/28956957 >.

[170] WONG, M. L.; MEDRANO, J. F. Real-time PCR for mRNA quantitation. **Biotechniques,** v. 39, n. 1, p. 75-85, Jul 2005. ISSN 0736-6205. Disponível em: < https://www.ncbi.nlm.nih.gov/pubmed/16060372 >.

[171] LALONDE, S. et al. Frameshift indels introduced by genome editing can lead to in-frame exon skipping. **PLoS One,** v. 12, n. 6, p. e0178700, 2017. ISSN 1932-6203. Disponível em: < https://www.ncbi.nlm.nih.gov/pubmed/28570605 >.

[172] SHARPE, J. J.; COOPER, T. A. Unexpected consequences: exon skipping caused by CRISPR-generated mutations. **Genome Biology,** v. 18, n. 1, p. 109, 06 14 2017. ISSN 1474-760X. Disponível em: < https://www.ncbi.nlm.nih.gov/pubmed/28615035 >.

[173] DAVID, G. et al. Specific requirement of the chromatin modifier mSin3B in cell cycle exit and cellular differentiation. **Proceedings of the National Academy of Sciences of the United States of America,** v. 105, n. 11, p. 4168-72, Mar 18 2008. ISSN 1091-6490. Disponível em: < https://www.ncbi.nlm.nih.gov/pubmed/18332431 >.

[174] JU, R. J.; STEHBENS, S. J.; HAASS, N. K. The Role of Melanoma Cell-Stroma Interaction in Cell Motility, Invasion, and Metastasis. **Frontiers in Medicine (Lausanne),** v. 5, p. 307, 2018. ISSN 2296-858X. Disponível em: < https://www.ncbi.nlm.nih.gov/pubmed/30460237 >.

[175] VAN ZIJL, F.; KRUPITZA, G.; MIKULITS, W. Initial steps of metastasis: cell invasion and endothelial transmigration. **Mutational Research,** v. 728, n. 1-2, p. 23-34, 2011 Jul-Oct 2011. ISSN 0027-5107. Disponível em: < https://www.ncbi.nlm.nih.gov/pubmed/21605699 >.

[176] CLARK, W. H. et al. A study of tumor progression: the precursor lesions of superficial spreading and nodular melanoma. **Human Pathology,** v. 15, n. 12, p. 1147-65, Dec 1984. ISSN 0046-8177. Disponível em: < https://www.ncbi.nlm.nih.gov/pubmed/6500548 >.

[177] BENNETT, D. C. How to make a melanoma: what do we know of the primary clonal events? **Pigment Cell Melanoma Research,** v. 21, n. 1, p. 27-38, Feb 2008. ISSN 1755-1471. Disponível em: < https://www.ncbi.nlm.nih.gov/pubmed/18353141 >.

[178] LI, F. Z. et al. Phenotype switching in melanoma: implications for progression and therapy. **Frontiers in Oncology,** v. 5, p. 31, 2015. ISSN 2234-943X. Disponível em: < https://www.ncbi.nlm.nih.gov/pubmed/25763355 >.

[179] HARTMAN, M. L.; CZYZ, M. Pro-survival role of MITF in melanoma. **Journal of Investigative Dermatology,** v. 135, n. 2, p. 352-358, Feb 2015. ISSN 1523-1747. Disponível em: < https://www.ncbi.nlm.nih.gov/pubmed/25142731 >.

[180] TURLEY, E. A. et al. Mechanisms of disease: epithelial-mesenchymal transition--does cellular plasticity fuel neoplastic progression? **Nature Clinical Practice Oncology,** v. 5, n. 5, p. 280-90, May 2008. ISSN 1743-4262. Disponível em: < https://www.ncbi.nlm.nih.gov/pubmed/18349857 >.

[181] CARAMEL, J. et al. A switch in the expression of embryonic EMT-inducers drives the development of malignant melanoma. **Cancer Cell,** v. 24, n. 4, p. 466-80, Oct 14 2013. ISSN 1878-3686. Disponível em: < https://www.ncbi.nlm.nih.gov/pubmed/24075834 >.

[182] MÜLLER, J. et al. Low MITF/AXL ratio predicts early resistance to multiple targeted drugs in melanoma. **Nature Communications,** v. 5, p. 5712, Dec 2014. ISSN 2041-1723. Disponível em: < https://www.ncbi.nlm.nih.gov/pubmed/25502142 >.

[183] KONIECZKOWSKI, D. J. et al. A melanoma cell state distinction influences sensitivity to MAPK pathway inhibitors. **Cancer Discovery,** v. 4, n. 7, p. 816-27, Jul 2014. ISSN 2159-8290. Disponível em: < https://www.ncbi.nlm.nih.gov/pubmed/24771846 >.

[184] GJERDRUM, C. et al. Axl is an essential epithelial-to-mesenchymal transition-induced regulator of breast cancer metastasis and patient survival. **Proceedings of the National Academy of Sciences of the United States of America,** v. 107, n. 3, p. 1124-9, Jan 19 2010. ISSN 1091-6490. Disponível em: < https://www.ncbi.nlm.nih.gov/pubmed/20080645 >.

[185] RAMBOW, F.; MARINE, J. C.; GODING, C. R. Melanoma plasticity and phenotypic diversity: therapeutic barriers and opportunities. **Genes and Development,** v. 33, n. 19-20, p. 1295-1318, 10 2019. ISSN 1549-5477. Disponível em: < https://www.ncbi.nlm.nih.gov/pubmed/31575676 >.

[186] RODRÍGUEZ, M. I. et al. PARP-1 regulates metastatic melanoma through modulation of vimentin-induced malignant transformation. **PLoS Genetics,** v. 9, n. 6, p. e1003531, Jun 2013. ISSN 1553-7404. Disponível em: < https://www.ncbi.nlm.nih.gov/pubmed/23785295 >.

187 FATTORE, L. et al. Single cell analysis to dissect molecular heterogeneity and disease evolution in metastatic melanoma. **Cell Death Disease,** v. 10, n. 11, p. 827, 10 31 2019. ISSN 2041-4889. Disponível em: < https://www.ncbi.nlm.nih.gov/pubmed/31672982 >.

188 SU, Y. et al. Single-cell analysis resolves the cell state transition and signaling dynamics associated with melanoma drug-induced resistance. **Proceedings of the National Academy of Sciences of the United States of America,** v. 114, n. 52, p. 13679-13684, 12 26 2017. ISSN 1091-6490. Disponível em: < https://www.ncbi.nlm.nih.gov/pubmed/29229836 >.

189 SU, Y. et al. Phenotypic heterogeneity and evolution of melanoma cells associated with targeted therapy resistance. **PLoS Computational Biology,** v. 15, n. 6, p. e1007034, 06 2019. ISSN 1553-7358. Disponível em: < https://www.ncbi.nlm.nih.gov/pubmed/31166947 >.

190 ASHBURNER, M. et al. Gene ontology: tool for the unification of biology. The Gene Ontology Consortium. **Nature Genetics,** v. 25, n. 1, p. 25-9, May 2000. ISSN 1061-4036. Disponível em: < https://www.ncbi.nlm.nih.gov/pubmed/10802651 >.

191 BAO, Y. et al. Transcriptome profiling revealed multiple genes and ECM-receptor interaction pathways that may be associated with breast cancer. **Cellular and Molecular Biology Letters,** v. 24, p. 38, 2019. ISSN 1689-1392. Disponível em: < https://www.ncbi.nlm.nih.gov/pubmed/31182966 >.

192 MCGARY, E. C.; LEV, D. C.; BAR-ELI, M. Cellular adhesion pathways and metastatic potential of human melanoma. **Cancer Biology and Therapy,** v. 1, n. 5, p. 459-65, 2002 Sep-Oct 2002. ISSN 1538-4047. Disponível em: < https://www.ncbi.nlm.nih.gov/pubmed/12496470 >.

193 D'ARCY, C.; KIEL, C. Cell Adhesion Molecules in Normal Skin and Melanoma. **Biomolecules,** v. 11, n. 8, 08 15 2021. ISSN 2218-273X. Disponível em: < https://www.ncbi.nlm.nih.gov/pubmed/34439879 >.

194 HEUBERGER, J.; BIRCHMEIER, W. Interplay of cadherin-mediated cell adhesion and canonical Wnt signaling. **Cold Spring Harbor Perspectives in Biology,** v. 2, n. 2, p. a002915, Feb 2010. ISSN 1943-0264. Disponível em: < https://www.ncbi.nlm.nih.gov/pubmed/20182623 >.

195 KOVACS, D. et al. The role of Wnt/β-catenin signaling pathway in melanoma epithelial-to-mesenchymal-like switching: evidences from patients-derived cell lines. **Oncotarget,** v. 7, n. 28, p. 43295-43314, Jul 12 2016. ISSN 1949-2553. Disponível em: < https://www.ncbi.nlm.nih.gov/pubmed/27175588 >.

196 HODIS, E. et al. A landscape of driver mutations in melanoma. **Cell,** v. 150, n. 2, p. 251-63, Jul 20 2012. ISSN 1097-4172. Disponível em: < https://www.ncbi.nlm.nih.gov/pubmed/22817889 >.

197 SOSMAN, J. A. et al. Survival in BRAF V600-mutant advanced melanoma treated with vemurafenib. **New England Journal of Medicine,** v. 366, n. 8, p. 707-14, Feb 23 2012. ISSN 1533-4406. Disponível em: < https://www.ncbi.nlm.nih.gov/pubmed/22356324 >.

198 THOMPSON, N.; ADAMS, D. J.; RANZANI, M. Synthetic lethality: emerging targets and opportunities in melanoma. **Pigment Cell Melanoma Research,** v. 30, n. 2, p. 183-193, 03 2017. ISSN 1755-148X. Disponível em: < https://www.ncbi.nlm.nih.gov/pubmed/28097822 >.

199 ASHWORTH, A.; LORD, C. J. Synthetic lethal therapies for cancer: what's next after PARP inhibitors? **Nature Reviews Clinical Oncology,** v. 15, n. 9, p. 564-576, 09 2018. ISSN 1759-4782. Disponível em: < https://www.ncbi.nlm.nih.gov/pubmed/29955114 >.

200 GAO, L. et al. Proteome Analysis of USP7 Substrates Revealed Its Role in Melanoma Through PI3K/Akt/FOXO and AMPK Pathways. **Frontiers in Oncology,** v. 11, p. 650165, 2021. ISSN 2234-943X. Disponível em: < https://www.ncbi.nlm.nih.gov/pubmed/33869052 >.

201 VAN DER HORST, A. et al. FOXO4 transcriptional activity is regulated by monoubiquitination and USP7/HAUSP. **Nature Cell Biology,** v. 8, n. 10, p. 1064-73, Oct 2006. ISSN 1465-7392. Disponível em: < https://www.ncbi.nlm.nih.gov/pubmed/16964248 >.

202 XIANG, M. et al. Pharmacological inhibition of USP7 suppresses growth and metastasis of melanoma cells in vitro and in vivo. **Journal of Cellular and Molecular Medicine,** v. 25, n. 19, p. 9228-9240, Oct 2021. ISSN 1582-4934. Disponível em: < https://www.ncbi.nlm.nih.gov/pubmed/34469054 >.

203 FORBES, S. A. et al. COSMIC: mining complete cancer genomes in the Catalogue of Somatic Mutations in Cancer. **Nucleic Acids Research,** v. 39, n. Database issue, p. D945-50, Jan 2011. ISSN 1362-4962. Disponível em: < https://www.ncbi.nlm.nih.gov/pubmed/20952405 >.

204 ROWAN, A. et al. Somatic mutations in the Peutz-Jeghers (LKB1/STKII) gene in sporadic malignant melanomas. **Journal of Investigative Dermatology,** v. 112, n. 4, p. 509-11, Apr 1999. ISSN 0022-202X. Disponível em: < https://www.ncbi.nlm.nih.gov/pubmed/10201537 >.

205 SANCHEZ-CESPEDES, M. et al. Inactivation of LKB1/STK11 is a common event in adenocarcinomas of the lung. **Cancer Research,** v. 62, n. 13, p. 3659-62, Jul 01 2002. ISSN 0008-5472. Disponível em: < https://www.ncbi.nlm.nih.gov/pubmed/12097271 >.

206 MCCARTHY, A. et al. Conditional deletion of the Lkb1 gene in the mouse mammary gland induces tumour formation. **The Journal of Pathology,** v. 219, n. 3, p. 306-16, Nov 2009. ISSN 1096-9896. Disponível em: < https://www.ncbi.nlm.nih.gov/pubmed/19681070 >.

207 LIU, W. et al. LKB1/STK11 inactivation leads to expansion of a prometastatic tumor subpopulation in melanoma. **Cancer Cell,** v. 21, n. 6, p. 751-64, Jun 12 2012. ISSN 1878-3686. Disponível em: < https://www.ncbi.nlm.nih.gov/pubmed/22698401 >.

208 CHAUBAL, A.; PILE, L. A. Same agent, different messages: insight into transcriptional regulation by SIN3 isoforms. **Epigenetics Chromatin,** v. 11, n. 1, p. 17, 04 17 2018. ISSN 1756-8935. Disponível em: < https://www.ncbi.nlm.nih.gov/pubmed/29665841 >.

209 GAJAN, A. et al. The histone demethylase dKDM5/LID interacts with the SIN3 histone deacetylase complex and shares functional similarities with SIN3. **Epigenetics Chromatin,** v. 9, p. 4, 2016. ISSN 1756-8935. Disponível em: < https://www.ncbi.nlm.nih.gov/pubmed/26848313 >.

210 LIU, Z. et al. The histone H3K9 demethylase Kdm3b is required for somatic growth and female reproductive function. **International Journal of Biological Sciences,** v. 11, n. 5, p. 494-507, 2015. ISSN 1449-2288. Disponível em: < https://www.ncbi.nlm.nih.gov/pubmed/25892958 >.

211 HONDA, K.; TANIGUCHI, T. IRFs: master regulators of signalling by Toll-like receptors and cytosolic pattern-recognition receptors. **Nature Reviews Immunology,** v. 6, n. 9, p. 644-58, Sep 2006. ISSN 1474-1733. Disponível em: < https://www.ncbi.nlm.nih.gov/pubmed/16932750 >.

212 GUALCO, G.; WEISS, L. M.; BACCHI, C. E. MUM1/IRF4: A Review. **Applied Immunohistochemistry and Molecular Morphology,** v. 18, n. 4, p. 301-10, Jul 2010. ISSN 1533-4058. Disponível em: < https://www.ncbi.nlm.nih.gov/pubmed/20182347 >.

213 GUPTA, S. et al. Lineage-specific modulation of interleukin 4 signaling by interferon regulatory factor 4. **Journal of Experimental Medicine,** v. 190, n. 12, p. 1837-48, Dec 20 1999. ISSN 0022-1007. Disponível em: < https://www.ncbi.nlm.nih.gov/pubmed/10601358 >.

214 GRUMONT, R. J.; GERONDAKIS, S. Rel induces interferon regulatory factor 4 (IRF-4) expression in lymphocytes: modulation of interferon-regulated gene expression by rel/nuclear factor kappaB. **Journal of Experimental Medicine,** v. 191, n. 8, p. 1281-92, Apr 17 2000. ISSN 0022-1007. Disponível em: < https://www.ncbi.nlm.nih.gov/pubmed/10770796 >.

215 SCHMIDT, M. et al. Expression of interferon regulatory factor 4 in chronic myeloid leukemia: correlation with response to interferon alfa therapy. **Journal of Clinical Oncology,** v. 18, n. 19, p. 3331-8, Oct 01 2000. ISSN 0732-183X. Disponível em: < https://www.ncbi.nlm.nih.gov/pubmed/11013272 >.

216 SHAFFER, A. L. et al. IRF4: Immunity. Malignancy! Therapy? **Clinical Cancer Research,** v. 15, n. 9, p. 2954-61, May 01 2009. ISSN 1078-0432. Disponível em: < https://www.ncbi.nlm.nih.gov/pubmed/19383829 >.

217 _____. IRF4 addiction in multiple myeloma. **Nature,** v. 454, n. 7201, p. 226-31, Jul 10 2008. ISSN 1476-4687. Disponível em: < https://www.ncbi.nlm.nih.gov/pubmed/18568025 >.

218 NATKUNAM, Y. et al. Analysis of MUM1/IRF4 protein expression using tissue microarrays and immunohistochemistry. **Modern Pathology,** v. 14, n. 7, p. 686-94, Jul 2001. ISSN 0893-3952. Disponível em: < https://www.ncbi.nlm.nih.gov/pubmed/11455001 >.

219 BARRETINA, J. et al. The Cancer Cell Line Encyclopedia enables predictive modelling of anticancer drug sensitivity. **Nature,** v. 483, n. 7391, p. 603-7, Mar 28 2012. ISSN 1476-4687. Disponível em: < https://www.ncbi.nlm.nih.gov/pubmed/22460905 >.

220 MEYERS, R. M. et al. Computational correction of copy number effect improves specificity of CRISPR-Cas9 essentiality screens in cancer cells. **Nature Genetics,** v. 49, n. 12, p. 1779-1784, Dec 2017. ISSN 1546-1718. Disponível em: < https://www.ncbi.nlm.nih.gov/pubmed/29083409 >.

221 TSHERNIAK, A. et al. Defining a Cancer Dependency Map. **Cell,** v. 170, n. 3, p. 564-576.e16, Jul 27 2017. ISSN 1097-4172. Disponível em: < https://www.ncbi.nlm.nih.gov/pubmed/28753430 >.

222 RAHMAN, M. et al. Alternative preprocessing of RNA-Sequencing data in The Cancer Genome Atlas leads to improved analysis results. **Bioinformatics,** v. 31, n. 22, p. 3666-72, Nov 15 2015. ISSN 1367-4811. Disponível em: < https://www.ncbi.nlm.nih.gov/pubmed/26209429 >.

223 ALONSO, S. R. et al. Progression in cutaneous malignant melanoma is associated with distinct expression profiles: a tissue microarray-based study. **The American Journal of Pathology,** v.

164, n. 1, p. 193-203, Jan 2004. ISSN 0002-9440. Disponível em: < https://www.ncbi.nlm.nih.gov/pubmed/14695333 >.

224 LIN, X. et al. C-myc overexpression drives melanoma metastasis by promoting vasculogenic mimicry via c-myc/snail/Bax signaling. **Journal of Molecular Medicine (Berl),** v. 95, n. 1, p. 53-67, 01 2017. ISSN 1432-1440. Disponível em: < https://www.ncbi.nlm.nih.gov/pubmed/27543492 >.

225 PRAETORIUS, C. et al. A polymorphism in IRF4 affects human pigmentation through a tyrosinase-dependent MITF/TFAP2A pathway. **Cell,** v. 155, n. 5, p. 1022-33, Nov 21 2013. ISSN 1097-4172. Disponível em: < https://www.ncbi.nlm.nih.gov/pubmed/24267888 >.

APPENDIX

Appendix A.1. List of differentially expressed genes from RNA sequencing data

ENSEMBL ID	GENE	log2FoldChange	padj
ENSG00000157502	PWWP3B	5,58737109491246	6,06E-07
ENSG00000223870	NA	4,62223212804497	3,96E-09
ENSG00000204019	CT83	4,53766303995995	1,82E-05
ENSG00000176774	MAGEB18	4,48133912217909	1,76E-17
ENSG00000176746	MAGEB6	3,76126870827406	5,41E-15
ENSG00000124818	OPN5	3,69295124849149	0,000676956147648
ENSG00000169551	CT55	3,50254672184442	6,22E-13
ENSG00000182583	VCX	3,47941857072256	2,50E-14
ENSG00000154646	TMPRSS15	3,40785547307154	1,92E-14
ENSG00000141469	SLC14A1	3,40691250327962	2,73E-07
ENSG00000253189	NA	3,38194931488638	1,90E-08
ENSG00000259929	LOC107984893	3,37471090001581	9,13E-12
ENSG00000146938	NLGN4X	3,31558225087306	4,16E-07
ENSG00000182986	ZNF320	3,29440295067542	2,55E-06
ENSG00000286133	NA	3,2470390142754	0,005276692919528
ENSG00000213793	ZNF888	3,15068315792654	0,000509704838129
ENSG00000184731	FAM110C	3,13686748501993	1,56E-14
ENSG00000245719	LOC101929076	3,10390611539831	4,98E-06
ENSG00000169059	VCX3A	3,09215573013896	1,29E-12
ENSG00000269799	NA	3,07246495424133	9,42E-05
ENSG00000253853	NA	2,94967704906904	9,16E-07
ENSG00000179083	FAM133A	2,94243784025521	1,45E-13
ENSG00000205642	VCX3B	2,93286020844771	1,93E-06
ENSG00000260242	NA	2,92198507887956	1,62E-05
ENSG00000188039	NWD1	2,91980643470141	2,92E-07

ENSG00000228708	NA	2,88183169706385	9,14E-08
ENSG00000197632	SERPINB2	2,86911007683144	3,52E-14
ENSG00000248112	NA	2,86886856098748	8,93E-06
ENSG00000184860	SDR42E1	2,82710216750507	4,53E-14
ENSG00000261555	NA	2,78758852555	2,54E-07
ENSG00000180257	ZNF816	2,74644503957957	0,000258736637756
ENSG00000286134	NA	2,72050167827378	0,001171781989181
ENSG00000186487	MYT1L	2,71035056472577	9,15E-06
ENSG00000286544	NA	2,68308270854996	1,35E-06
ENSG00000111700	SLCO1B3	2,66407785025205	1,27E-06
ENSG00000140030	GPR65	2,66060002443206	0,001433991248486
ENSG00000235782	NA	2,61917844174838	0,006937924161989
ENSG00000282815	TEX13C	2,57079751433774	9,13E-12
ENSG00000187323	DCC	2,57059139741738	5,89E-09
ENSG00000249776	NA	2,55123342719978	0,003426021169781
ENSG00000287007	NA	2,54976758730574	3,05E-06
ENSG00000120279	MYCT1	2,54069674075901	0,000111789704801
ENSG00000168757	TSPY2	2,51170435881087	0,000296512386166
ENSG00000268758	ADGRE4P	2,51065596118332	8,89E-05
ENSG00000268460	LOC93429	2,49472433074672	0,000205025836656
ENSG00000231739	NA	2,49453887530509	0,000439306271932
ENSG00000135298	ADGRB3	2,48253979859883	0,001332511800238
ENSG00000254547	NA	2,47280128137797	0,000676956147648
ENSG00000286969	NA	2,39698945764296	0,008759169534731
ENSG00000108849	PPY	2,38069314750649	0,006206941925407
ENSG00000265766	CXADRP3	2,37581943837434	0,00135065742445
ENSG00000143851	PTPN7	2,37128044555289	0,000111789704801
ENSG00000259996	NA	2,35593656476315	2,42E-05
ENSG00000268879	NA	2,3396268283232	0,002961605452566

ENSG00000253775	NA	2,33349551743226	0,004578740094176
ENSG00000178776	C5orf46	2,31982785351011	0,001069983833753
ENSG00000109321	AREG	2,31642170392015	0,001680590816843
ENSG00000171033	PKIA	2,29780299440008	3,51E-05
ENSG00000148346	LCN2	2,2727548542229	0,003297150650776
ENSG00000136099	PCDH8	2,24186283465988	0,002934210453397
ENSG00000196628	TCF4	2,21348095133752	0,001090394776913
ENSG00000235300	THRA1/BTR	2,18725882538255	1,27E-06
ENSG00000165140	FBP1	2,1705061668314	8,28E-05
ENSG00000002726	AOC1	2,15058768339559	0,000370082011601
ENSG00000268621	IGFL2-AS1	2,14259369725781	0,000221638368416
ENSG00000156009	MAGEA8	2,13283983485276	0,005883862021004
ENSG00000170703	TTLL6	2,1137640252732	1,28E-05
ENSG00000187800	PEAR1	2,09178352195401	2,97E-06
ENSG00000144834	TAGLN3	2,06550847972967	0,001300209793674
ENSG00000229921	KIF25-AS1	2,06321652547315	0,001587556471858
ENSG00000267123	SCAT1	2,0550152112211	0,000156975773339
ENSG00000152092	ASTN1	2,04674760355301	0,003117411880194
ENSG00000286966	NA	2,02820529412503	0,003830822094063
ENSG00000122641	INHBA	1,98737490411263	0,008805054923862
ENSG00000249196	TMEM132D-AS1	1,97813518091786	0,000157560964886
ENSG00000121895	TMEM156	1,97216574271214	3,10E-06
ENSG00000134755	DSC2	1,96146687043874	0,006171698743114
ENSG00000121552	CSTA	1,9524220377212	0,001246862399049
ENSG00000182077	PTCHD3	1,93935222917952	0,002112000852807
ENSG00000279317	NA	1,90012352043049	0,001639636740767
ENSG00000196406	SPANXD	1,85977599508779	0,005183927037945
ENSG00000234948	LINC01524	1,85401950011445	0,000212779266327
ENSG00000162078	ZG16B	1,85057331166813	2,42E-05

ENSG00000184351	KRTAP19-1	1,81209056972227	0,005883862021004
ENSG00000238266	LINC00707	1,80977010647878	0,000515352529143
ENSG00000124102	PI3	1,7884911035007	0,005976580453834
ENSG00000118004	COLEC11	1,77962379048088	0,008805054923862
ENSG00000224063	NA	1,7021501458911	0,006697593121736
ENSG00000170458	CD14	1,70010048111706	0,008335789761293
ENSG00000288555	NA	1,69577163618769	0,004073305059657
ENSG00000258580	NA	1,69429009887811	0,000759985745044
ENSG00000204385	SLC44A4	1,69233079093007	0,003718549261923
ENSG00000165071	TMEM71	1,68936713960347	0,006171698743114
ENSG00000164199	ADGRV1	1,68185852979516	0,000111789704801
ENSG00000267107	PCAT19	1,663845864624	2,23E-06
ENSG00000164283	ESM1	1,6598804634488	0,000461324111747
ENSG00000125730	C3	1,65044400831962	0,000676956147648
ENSG00000287151	C2orf27A	1,63574311784324	0,009371045429318
ENSG00000139626	ITGB7	1,63397675725438	0,000461324111747
ENSG00000206199	ANKUB1	1,62764189109004	0,006939051540996
ENSG00000236719	OVAAL	1,61468178012193	0,000632065743793
ENSG00000198576	ARC	1,59594549962427	0,00996155147657
ENSG00000165449	SLC16A9	1,59452484954721	0,000218793486849
ENSG00000027869	SH2D2A	1,59191105535764	0,002034174774915
ENSG00000112238	PRDM13	1,5755517378683	0,006206941925407
ENSG00000047634	SCML1	1,56357968202678	0,001193654023072
ENSG00000069667	RORA	1,53418423204879	3,68E-06
ENSG00000225760	NA	1,52209435015151	0,002736704931799
ENSG00000239462	NA	1,47924462520151	6,74E-05
ENSG00000249631	NA	1,42598078015506	0,001031185386974
ENSG00000165029	ABCA1	1,41232971998081	0,00996155147657
ENSG00000240476	NA	1,40308488669513	0,005883862021004

ENSG00000127585	FBXL16	1,35780762601851	0,00629687750098
ENSG00000183154	LOC102723701	1,306965404849	0,006206941925407
ENSG00000197385	ZNF860	1,27595791053276	2,23E-05
ENSG00000253910	PCDHGB2	1,05532786564459	9,44E-05
ENSG00000165868	HSPA12A	-1,020660429121	0,001865709173689
ENSG00000140511	HAPLN3	-1,12510389924293	0,004572525923239
ENSG00000124785	NRN1	-1,16482564920843	0,000273085433661
ENSG00000008735	MAPK8IP2	-1,16952615646783	7,33E-05
ENSG00000288658	NA	-1,19940783504961	0,001434770503458
ENSG00000136531	SCN2A	-1,29470358387299	0,000227565483159
ENSG00000204291	COL15A1	-1,29754578707075	0,00996155147657
ENSG00000007062	PROM1	-1,30996067637885	0,00990762246077
ENSG00000080493	SLC4A4	-1,32926187744472	0,000691049732358
ENSG00000168505	GBX2	-1,34289953716349	0,000196538571915
ENSG00000110042	DTX4	-1,36326330163174	0,001371376934423
ENSG00000083290	ULK2	-1,3724686587495	0,006206941925407
ENSG00000173320	STOX2	-1,38761172156865	0,001181765211736
ENSG00000101230	ISM1	-1,39270579048976	0,008985754530244
ENSG00000100302	RASD2	-1,39977604304729	0,001985366944611
ENSG00000162804	SNED1	-1,40436309596967	0,000187466844819
ENSG00000144857	BOC	-1,41054805112489	1,06E-05
ENSG00000198846	TOX	-1,46070786291879	0,00261428574111
ENSG00000227051	C14orf132	-1,46381923419878	0,00674972155906
ENSG00000131378	RFTN1	-1,49257010951693	1,15E-06
ENSG00000188613	NANOS1	-1,49819753080793	0,000641549190286
ENSG00000162591	MEGF6	-1,50622421016161	0,008759169534731
ENSG00000130762	ARHGEF16	-1,50964365285807	0,006022287641608
ENSG00000104321	TRPA1	-1,51902366600195	0,001963017711528
ENSG00000171812	COL8A2	-1,52215718709783	0,000853554613413

ENSG00000153246	PLA2R1	-1,53616478738847	0,001587556471858
ENSG00000225492	GBP1P1	-1,53737827323601	0,001757129562909
ENSG00000143341	HMCN1	-1,54420101039376	0,008759169534731
ENSG00000257335	MGAM	-1,55841922608986	0,007685759716661
ENSG00000147100	SLC16A2	-1,57035585070494	8,53E-08
ENSG00000111341	MGP	-1,58355758645314	0,000141676960519
ENSG00000107731	UNC5B	-1,61008867178398	0,002911646144316
ENSG00000156113	KCNMA1	-1,61478267088152	0,00261428574111
ENSG00000108821	COL1A1	-1,62943556017675	0,001963017711528
ENSG00000115594	IL1R1	-1,6315423774409	0,00135065742445
ENSG00000105894	PTN	-1,6365653633036	0,003807916873294
ENSG00000144619	CNTN4	-1,63783652986226	0,008444147437284
ENSG00000130600	H19	-1,6536818831561	0,000882902382098
ENSG00000130881	LRP3	-1,65742608214317	0,009471114743385
ENSG00000126217	MCF2L	-1,66133726074105	0,003363514827585
ENSG00000112655	PTK7	-1,66567872339056	0,000370719831138
ENSG00000280135	NA	-1,67130531550981	0,002635670532987
ENSG00000144668	ITGA9	-1,6799533516191	0,000225931949836
ENSG00000101096	NFATC2	-1,69379921472251	6,10E-09
ENSG00000115290	GRB14	-1,70003530912002	0,000653942411154
ENSG00000235770	LINC00607	-1,70615200636204	0,007178926247247
ENSG00000249306	LINC01411	-1,709436812169	0,001121072765282
ENSG00000169083	AR	-1,70998891938115	0,009526633784965
ENSG00000167912	LOC100505501	-1,72111068623669	0,000461324111747
ENSG00000286447	NA	-1,72287934917717	5,38E-06
ENSG00000144152	FBLN7	-1,72471246618895	9,89E-06
ENSG00000019549	SNAI2	-1,72839136401238	0,000779952239945
ENSG00000186998	EMID1	-1,73205253102476	0,00996155147657
ENSG00000077063	CTTNBP2	-1,73760985726108	3,86E-05

ENSG00000189108	IL1RAPL2	-1,78155703504092	0,003876523717321
ENSG00000278962	NA	-1,79004221770599	1,31E-10
ENSG00000163958	ZDHHC19	-1,83964625380189	0,005265813167178
ENSG00000007171	NOS2	-1,84075093045837	0,000218793486849
ENSG00000148600	CDHR1	-1,84286943727768	0,000515352529143
ENSG00000103175	WFDC1	-1,84732604605823	0,008901295388816
ENSG00000188883	KLRG2	-1,85023576459851	0,008047416079561
ENSG00000168824	NSG1	-1,86389339863344	0,000284428367563
ENSG00000132561	MATN2	-1,88370033310027	1,20E-09
ENSG00000162624	LHX8	-1,89274328119608	0,003520882673364
ENSG00000170498	KISS1	-1,89616033269695	0,00996155147657
ENSG00000167751	KLK2	-1,89863637588423	0,00145038050652
ENSG00000111452	ADGRD1	-1,90562873930791	0,002832767700199
ENSG00000155754	C2CD6	-1,92238625448545	1,02E-07
ENSG00000233535	NA	-1,92667870144347	1,15E-06
ENSG00000170370	EMX2	-1,92896739285678	6,62E-06
ENSG00000162482	AKR7A3	-1,93445198345335	0,001347939634823
ENSG00000171596	NMUR1	-1,93785425088396	6,21E-05
ENSG00000127743	IL17B	-1,94022931061193	0,00158326803501
ENSG00000103489	XYLT1	-1,95002621287444	0,000294377145953
ENSG00000154928	EPHB1	-1,95199547043437	0,001007621577153
ENSG00000137573	SULF1	-1,96610874771175	3,11E-05
ENSG00000235280	NA	-1,97102417532424	0,005976580453834
ENSG00000149243	KLHL35	-1,9736105000688	2,50E-05
ENSG00000126838	PZP	-1,9852462146127	0,005976580453834
ENSG00000165905	LARGE2	-1,98859212989843	0,00030327458468
ENSG00000213626	LBH	-2,01520950993157	1,89E-05
ENSG00000131477	RAMP2	-2,01787928135954	0,00720327221151
ENSG00000163331	DAPL1	-2,02342238483068	0,009955822405437

ENSG00000170153	RNF150	-2,02952010990113	6,45E-06
ENSG00000169436	COL22A1	-2,03851461195446	0,004996944570862
ENSG00000170542	SERPINB9	-2,04449775483199	0,002961605452566
ENSG00000198108	CHSY3	-2,04927745677813	4,57E-05
ENSG00000162849	KIF26B	-2,07796381562379	1,27E-06
ENSG00000005513	SOX8	-2,08465389919565	0,000839361503486
ENSG00000130592	LSP1	-2,09607931087369	0,001129663697661
ENSG00000259417	CTXND1	-2,10410749865291	2,71E-05
ENSG00000080224	EPHA6	-2,12135862242162	2,16E-14
ENSG00000273706	LHX1	-2,12886692999751	3,55E-05
ENSG00000113749	HRH2	-2,13928251848326	0,001648175914983
ENSG00000116157	GPX7	-2,15314749500994	1,13E-13
ENSG00000179855	GIPC3	-2,15539247101136	0,001246862399049
ENSG00000117791	MTARC2	-2,15810018390537	0,000127070974976
ENSG00000183798	EMILIN3	-2,16659191932365	0,000271682990707
ENSG00000176641	RNF152	-2,17659377700088	2,94E-14
ENSG00000130303	BST2	-2,18460282827114	1,07E-07
ENSG00000170516	COX7B2	-2,20039433064532	0,000461324111747
ENSG00000236078	LINC01447	-2,22282438452821	7,55E-06
ENSG00000048740	CELF2	-2,25213583087063	0,000461324111747
ENSG00000197705	KLHL14	-2,26052841705623	0,001144097905842
ENSG00000185155	MIXL1	-2,28854482747406	2,12E-05
ENSG00000184613	NELL2	-2,30437235688224	2,19E-06
ENSG00000122145	TBX22	-2,30591698561575	0,001628525932609
ENSG00000142173	COL6A2	-2,31796309808468	1,13E-13
ENSG00000162706	CADM3	-2,35020286297275	0,00996155147657
ENSG00000234842	MTCO2P16	-2,35728263611517	6,22E-10
ENSG00000179314	WSCD1	-2,35864301107954	0,001060577421794
ENSG00000240694	PNMA2	-2,36235263483677	1,22E-15

ENSG00000279415	NA	-2,37765517613668	0,000271682990707
ENSG00000170579	DLGAP1	-2,39602750880091	1,46E-05
ENSG00000180176	TH	-2,40343896339175	6,19E-05
ENSG00000186377	CYP4X1	-2,41159097015244	9,16E-07
ENSG00000062038	CDH3	-2,41629101013115	6,07E-05
ENSG00000159263	SIM2	-2,41944221239015	2,23E-06
ENSG00000204655	MOG	-2,42411882716486	3,51E-05
ENSG00000077984	CST7	-2,42453914889403	6,41E-15
ENSG00000228835	NA	-2,45843688325421	0,000127070974976
ENSG00000198125	MB	-2,48759728230141	1,07E-08
ENSG00000254585	MAGEL2	-2,50756542475408	0,000294568310949
ENSG00000162692	VCAM1	-2,51815729680052	0,003117411880194
ENSG00000154856	APCDD1	-2,51861007192952	3,76E-07
ENSG00000224299	MTATP6P16	-2,58478496929827	1,07E-07
ENSG00000167157	PRRX2	-2,6064416515333	0,000334405009313
ENSG00000198739	LRRTM3	-2,62769685438372	0,004578740094176
ENSG00000140557	ST8SIA2	-2,65929325331476	0,000337488868514
ENSG00000111371	SLC38A1	-2,66929615865063	5,87E-06
ENSG00000185860	CCDC190	-2,77693739082313	0,001748710480841
ENSG00000113494	PRLR	-2,78102851317619	5,04E-07
ENSG00000157570	TSPAN18	-2,78227921891441	4,57E-05
ENSG00000213694	S1PR3	-2,91603137252617	1,86E-06
ENSG00000101977	MCF2	-2,96275857406187	0,000111789704801
ENSG00000173198	CYSLTR1	-2,98785263137899	2,85E-06
ENSG00000102109	PCSK1N	-2,99310605657826	6,74E-05
ENSG00000133110	POSTN	-3,12451081686571	8,26E-12
ENSG00000178726	THBD	-3,15812908416461	5,20E-13
ENSG00000150594	ADRA2A	-3,21152290755716	6,32E-17
ENSG00000149256	TENM4	-3,46434246626505	2,94E-14

ENSG00000125851	PCSK2	-3,4797546359332	5,37E-15
ENSG00000067445	TRO	-3,51098611582985	8,23E-15
ENSG00000197462	NA	-3,69390205097805	9,44E-05
ENSG00000135821	GLUL	-3,75624466860649	8,26E-49
ENSG00000136928	GABBR2	-4,03253254071322	3,66E-10
ENSG00000133488	SEC14L4	-4,42533753863011	1,76E-17
ENSG00000174600	CMKLR1	-4,5257400797057	2,85E-12

Appendix A.2. List of enriched and depleted genes from genome-wide CRISPR screening data

Control Clone	Classification	num_clones	num_genes	genes
C4	depleted	3	2	USP7,STK11
C4	depleted	2	14	FEN1,GINS2,RFC3,THOC2,RPA1,MRPL47,MED16,PRPF6,RAD51C,PCID2,POLE4,CCNB1,RBM33,CSK
C4	depleted	1	34	MCM2,CPSF3L,ACTL6A,GINS4,PPIL1,PSMA7,PLK1,SNRNP27,MRPS18A,SKA1,PCBP1,HIRA,COPB1,COPS5,PPP1CC,MED11,DDX24,TADA2B,CHMP4B,FLCN,NAE1,MAP3K4,MDM2,KDM1A,PIBF1,RAD54L2,TRIP12,SIK2,GRID2,RREB1,CDK8,SBNO2,KCTD10,RUNX1
C4	enriched	3	1	KDM3B
C4	enriched	1	2	GNAS,TP53

Appendix A.3. Biosafety committee approval for work using lentivirus

UNVERSIDADE DE SÃO PAULO
FACULDADE DE CIÊNCIAS FARMACÊUTICAS
Comissão Interna de Biossegurança

Of.CIBio/0172020/FCF

São Paulo, 16 de outubro de 2020.

Senhora Professora,

Conforme parecer favorável emitido pela Comissão Técnica de Biossegurança, através Extrato de nº 7.175/20, publicado no Diário Oficial de União em 14 de outubro p.p. (em anexo), vimos informar a Vossa Senhoria que o Projeto *"Gene SIN3B: possível alvo na quimiorresistência e progressão do melanoma"*, sob sua responsabilidade foi **aprovado**.

Atenciosamente,

Prof. Dr. JOÃO CARLOS MONTEIRO DE CARVALHO
Presidente da CIBio

Ilma. Sra.
Profa. Dra. SILVYA STUCCHI MARIA ENGLER
Departamento de Análises Clínicas e Toxicológicas da FCF-USP
NESTA

Av. Prof. Lineu Prestes, nº 580, Bloco 13 A - Cidade Universitária - CEP 05508-900 - São Paulo - SP
Fone (011) 3091-3042 - e-mail: atadfcf.usp.br